Supplementary Information for

Electron-rich phenanthroline bearing N-heterocyclic imine substituents: synthesis, optical properties, metal coordination

Jonas H. Franzen,[a] Xuequan Zhou,[b] Kelly Biv,[c] Alessandro Ajò,[b] Austin Mencke,[c] Lukas F. B. Wilm,[d] Michael Seidl,[a] Thomas S. Hofer,[a] Luisa De Cola,[b,e] Peter Brüggeller,[a] Mark E. Thompson,[c,*] Fabian Dielmann[a,*]

[a] Institut für Allgemeine, Anorganische und Theoretische Chemie, Leopold-Franzens-Universität Innsbruck, Innrain 80-82, 6020 Innsbruck (Austria)
e-mail: fabian.dielmann@uibk.ac.at

[b] Department of Biochemistry and Molecular Pharmacology, Istituto di Ricerche Farmacologiche Mario Negri, IRCCS, 20156 Milano, Italy.
E-Mail: luisa.decola@unimi.it

[c] Department of Chemistry, University of Southern California, Los Angeles, CA 90089, USA.
E-Mail: met@usc.edu

[d] Institut für Allgemeine und Anorganische Chemie, Universität Münster, Corrensstraße 28/30, 48149 Münster (Germany)

[e] *Department of Pharmaceutical Science, DISFARM. Università degli Studi di Milano, Via C. Golgi 19, 20133 Milan, Italy.*

Contents:

Synthetic Details 4

Preparation of the Phenanthroline Ligand **1** 5

Preparation of 2,9-diamino-1,10-phenanthroline: 5

Preparation of **1**, **1**·HBF_4, **1**·$2HBF_4$ and **1**·$2HB(C_6F_5)_4$ 11

Preparation of the Zn(II) complex **2**·2MeCN 20

NMR studies of **1**·HBF_4 24

Synthesis of the HBF_4-salts for the assessment of the $\mathrm{pKBH^+}$ value for **1** 27

Electrochemical Investigations 38

Cyclic voltammetry studies of 1,10-phenanthroline 40

Cyclic voltammetry studies of **1** 41

Cyclic voltammetry studies of **1**·$HB(C_6F_5)_4$ 45

Cyclic voltammetry studies of **2**·2MeCN 47

Photophysical Investigation 49

Compound **1** 50

Compound **1**·HBF_4 55

Compound **2**·2MeCN 58

Jablonski Diagrams of **1**, **1**·HBF_4 and **2**·2MeCN 61

Protonation Experiments of **1** 63

Protonation of **1** and assessment of the $\mathrm{pKBH^+}$ value for **1** 64

Protonation of 1 64

pKBH +(ACN) value of 1 65

Experimental procedures 67

Computational Details 75

UV/Vis Spectrum 76

XYZ Coordinates 78

X-ray Diffraction Studies 90

References 96

Synthetic Details

General remarks: If not mentioned otherwise, all manipulations were performed under an inert atmosphere of dry argon, using standard Schlenk and drybox techniques. Dry and oxygen-free solvents were employed. ^{1}H, ^{11}B, ^{13}C and ^{15}N spectra were recorded at 300 K in the solvent indicated on Bruker AVANCE I 400, Bruker AVANCE III 400, Bruker AVANCE II 200, Bruker AVANCE NEO 500 or Bruker AVANCE IV 400 spectrometers. Chemical shifts are given in parts per million (ppm) relative to $SiMe_4$ (TMS) in $CDCl_3$ (^{1}H, ^{13}C), 15% $BF_3 \bullet Et_2O$ in $CDCl_3$ (^{11}B) or NH_3 (^{15}N) and were referenced internally to the residual solvent signals. NMR multiplicities are abbreviated as follows: s = singlet, d = doublet, t = triplet, q = quartet, m = multiplet, br = broad signal. IR spectra were obtained on a Bruker ALPHA II FT-IR Spectrometer. Intensities of the signals are abbreviated as follows: w = weak, m = medium, s = strong, vs = very strong. Mass spectra were obtained with an Orbitrap Q Exactive (Thermo Scientific) spectrometer.

Reagents and Handling: 1,3-Di-*tert*-butylchloroimidazolinium tetrafluoroborate,[1,2] $[H(OEt_2)_2][B(C_6F_5)_4]$,[3] $NEt_3 \cdot HBF_4$[4] and P(NI*i*Pr)$_2$(*i*Pr)[5] were prepared according to literature procedures. All other compounds were purchased from commercial sources and used as received (NI*i*Pr = 4,5-dimethyl-*N*,*N*'-diisopropylimidazolin-2-ylidenamino).

Preparation of the Phenanthroline Ligand **1**

Preparation of 2,9-diamino-1,10-phenanthroline:

The synthesis of 2,9-diamino-1,10-phenanthroline was carried out following a modified literature procedure that describes the synthetic approach of the analogous bipyridine compound.[6]

Synthesis of 2,9-dihydrazino-1,10-phenanthroline:

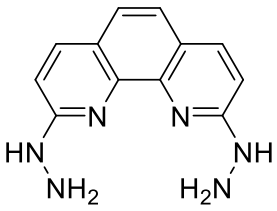

2,9-dihydrazino-1,10-phenanthroline was prepared using a modified literature procedure.[7]

2,9-Dichloro-1,10-phenanthroline (25.0 g, 100 mmol, 1.0 eq.) was suspended in hydrazine (250 mL, 80% solution in water) and heated to reflux for four hours. The resulting red suspension was allowed to cool to ambient temperatures and stored at +4 °C for 16 hours leading to the precipitation of the product as a yellow solid. After filtration and washing of the solid with a copious amount of distilled water, the product was dried *in vacuo* and obtained in 99% yield (24.0 g, 99.9 mmol).

^{1}H NMR (400 MHz, DMSO-d_6): δ = 7.9 (d, $^{3}J_{HH}$ = 8.8 Hz, 2H, H_{aryl}), 7.3 (d, $^{4}J_{HH}$ = 1.1 Hz, 2H, H_{aryl}), 7.0 (d, $^{3}J_{HH}$ = 8.8 Hz, 2H, H_{aryl}), 5.9 (s, br, 6H, –N**H**N**H**$_2$) ppm.

^{13}C{^{1}H} NMR (101 MHz, DMSO-d_6): δ = 158.5 (s, C_{aryl}), 142.3 (s, C_{aryl}), 136.6 (s, C_{aryl}), 122.6 (s, C_{aryl}), 120.9 (s, C_{aryl}), 111.0 (s, C_{aryl}) ppm.

HRMS (ESI): m/z calculated for $[C_{12}H_{13}N_6]^+$ (**M**+H)$^+$ 241.11962, found 241.11928.

IR (neat): $\tilde{\nu}$ = 3307 (w), 3180 (ν(NH_2), m), 3071 (m), 2217 (w), 2170 (w), 2117 (m), 2004 (w), 1680 (s), 1618 (s), 1585 (s), 1557 (m), 1530 (m), 1509 (s), 1498 (s), 1457 (m), 1438 (m), 1379 (s), 1344 (m), 1280 (s), 1259 (m), 1238 (m), 1225 (m), 1208 (m), 1175 (m), 1143 (m), 1131 (m), 1088 (m), 1075 (m) cm^{-1}.

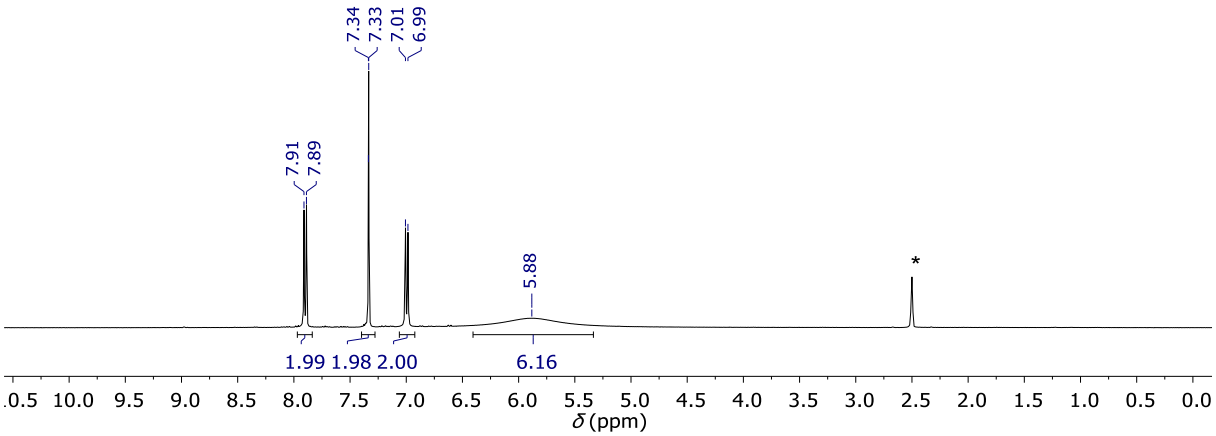

Figure S1: ^{1}H NMR spectrum of 2,9-dihydrazino-1,10-phenanthroline in DMSO-d_6 (* = solvent residual signal).

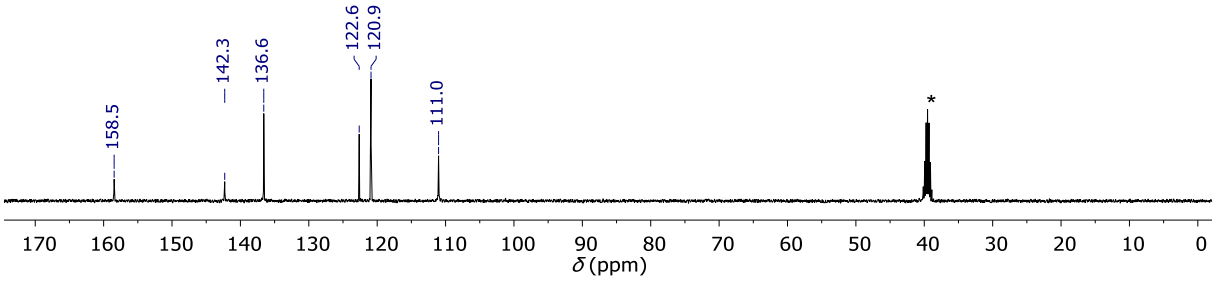

Figure S2: $^{13}C\{^{1}H\}$ NMR spectrum of 2,9-dihydrazino-1,10-phenanthroline in DMSO-d_6 (* = solvent signal).

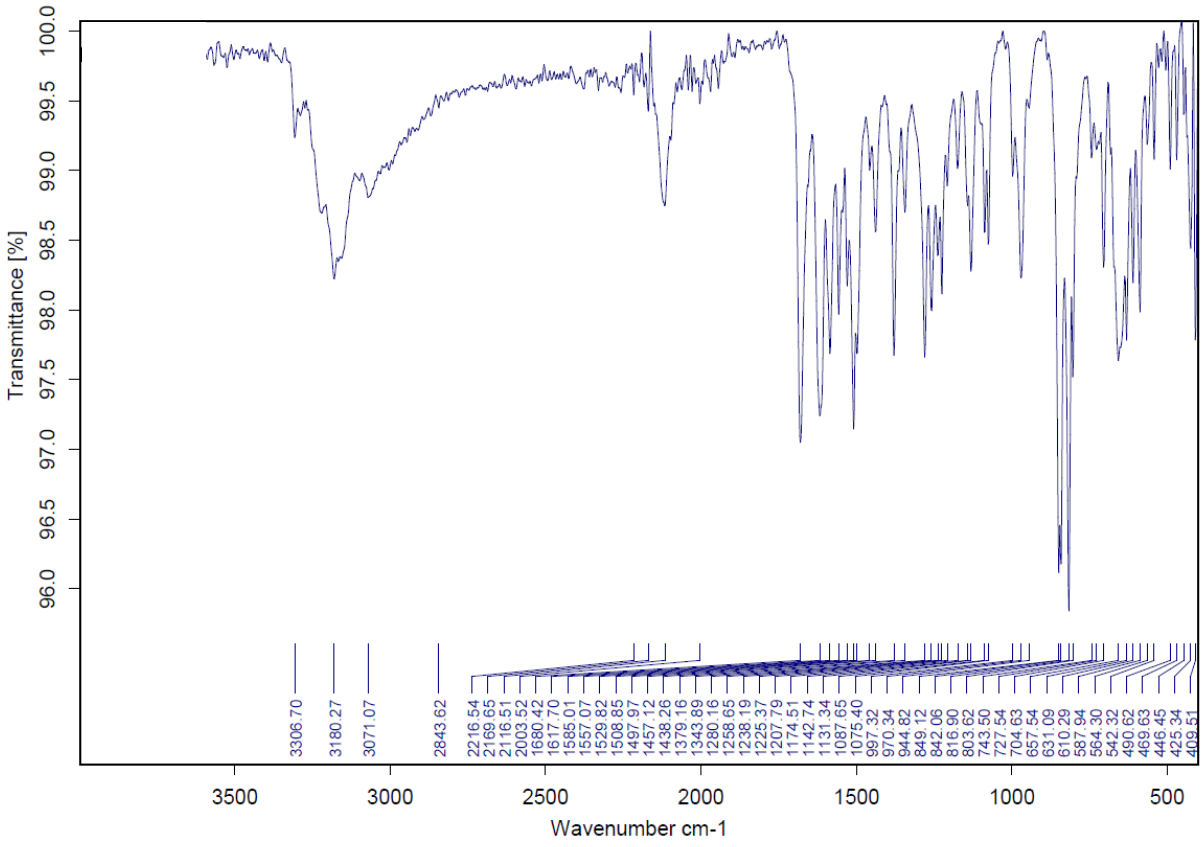

Figure S3: IR spectrum of 2,9-dihydrazino-1,10-phenanthroline (neat).

Synthesis of 2,9-diazido-1,10-phenanthroline:

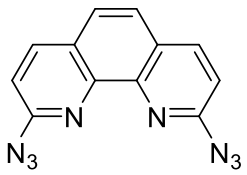

2,9-dihydrazino-1,10-phenanthroline (24.0 g, 99.9 mmol, 1.0 eq.) was suspended in concentrated hydrochloric acid (220 mL) and cooled to 0 °C using an ice bath. Using a dropping funnel, a solution of $NaNO_2$ (68.9 g, 999 mmol, 10 eq.) in distilled water (250 mL) was slowly added to the suspension. **CAUTION**: A large volume of nitrous gases is released during the process. The resulting orange suspension was stirred at ambient temperature for 16 hours and then basified (pH≈14) using an aqueous solution of NaOH (30%) causing the product to precipitate. The product was isolated by filtration followed by washing with a copious amount of water until the filtrate was neutral. The product was dried *in vacuo* for 16 hours and 2,9-diazido-1,10-phenanthroline was obtained as a light-brown solid in 95% yield. (25.0 g, 95.3 mmol).

^{1}H NMR (400 MHz, DMSO-d_6): δ = 8.55 (d, $^3J_{HH}$ = 8.7 Hz, 1H, H_{aryl}), 8.38 (d, $^3J_{HH}$ = 9.3 Hz, 1H), 8.32 (d, $^3J_{HH}$ = 9.3 Hz, 1H), 8.14 (d, $^3J_{HH}$ = 8.7 Hz, 1H), 8.11 (d, $^3J_{HH}$ = 8.7 Hz, 1H) 7.32 (d, $^3J_{HH}$ = 8.7 Hz) ppm.

^{13}C{^{1}H} NMR (126 MHz, DMSO-d_6): δ = 155.3 (s, C_{aryl}), 148.2 (s, C_{aryl}), 140.2 (s, C_{aryl}), 137.2 (s, C_{aryl}), 134.2 (s, C_{aryl}), 127.7 (s, C_{aryl}), 127.1(s, C_{aryl}), 126.1 (s, C_{aryl}), 125.8 (s, C_{aryl}), 125.4 (s, C_{aryl}), 115.8 (s, C_{aryl}), 114.9 (s, C_{aryl}) ppm.

HRMS (ESI): m/z calculated for $[C_{12}H_7N_8]^+$ (**M**+H)$^+$ 263.07882, found 263.07873; m/z calculated for $[C_{12}H_6N_8Na]^+$ (**M**+Na)$^+$ 285.06076, found 285.06064; m/z calculated for $[C_{24}H_{12}N_{16}Na]^+$ (2**M**+Na)$^+$ 547.13231, found 547.13263.

IR (neat)**:** $\tilde{\nu}$ = 3440 (w), 3058 (w), 2167 (w), 2117 ($\nu_{as}(N_3)$, s), 1665 (w), 1630 (m), 1594 (m), 1557 (w), 1530 (s), 1498 (s), 1466 (w), 1435 (m), 1394 (m), 1362 (m), 1344 (s), 1282 ($\nu(N_3)$,s), 1259 (s), 1238 (s), 1146 (m), 1133 (s), 1088 (m), 1019 (w) cm^{-1}.

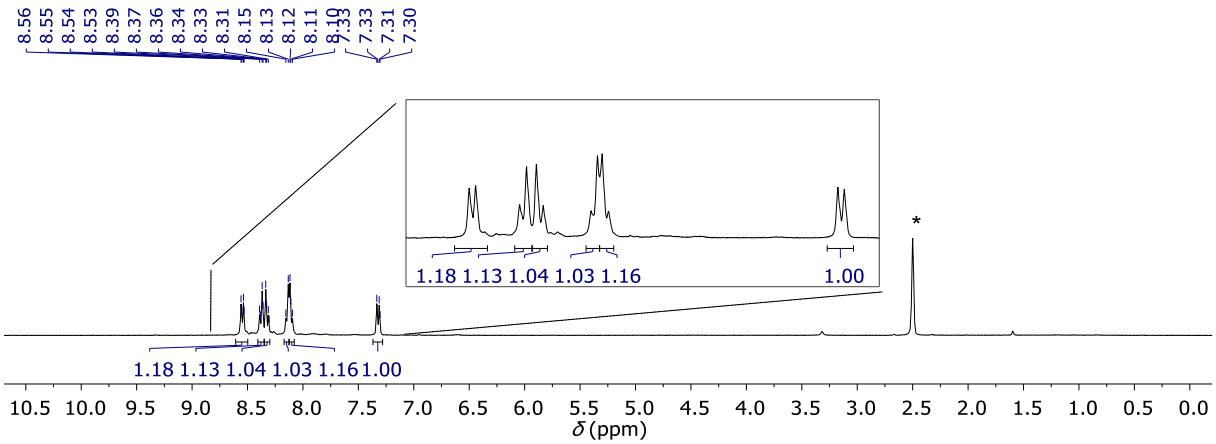

Figure S4: ^{1}H NMR spectrum of 2,9-diazido-1,10-phenanthroline in DMSO-d_6 (* = residual solvent signal).

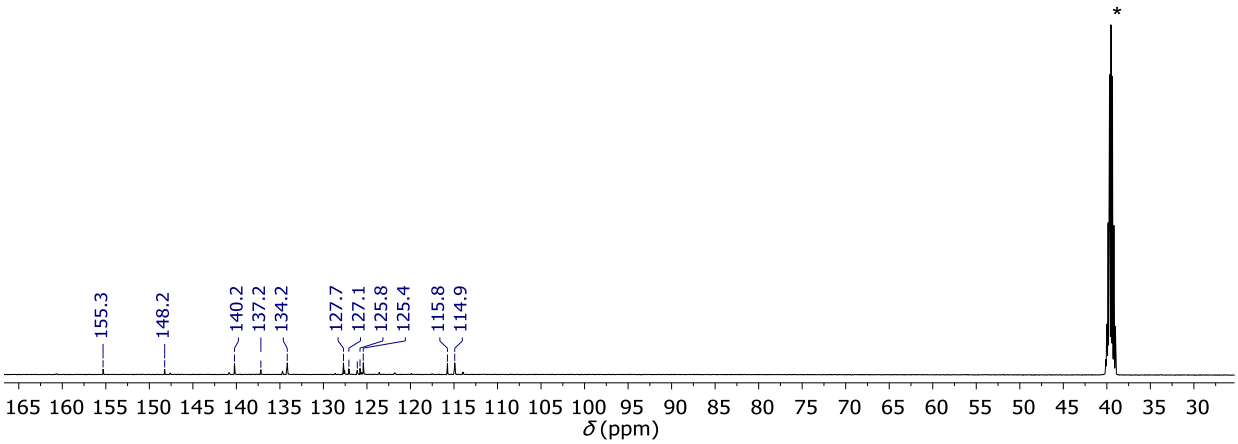

Figure S5: $^{13}C\{^{1}H\}$ NMR spectrum of 2,9-diazido-1,10-phenanthroline in DMSO-d_6 (* = solvent signal).

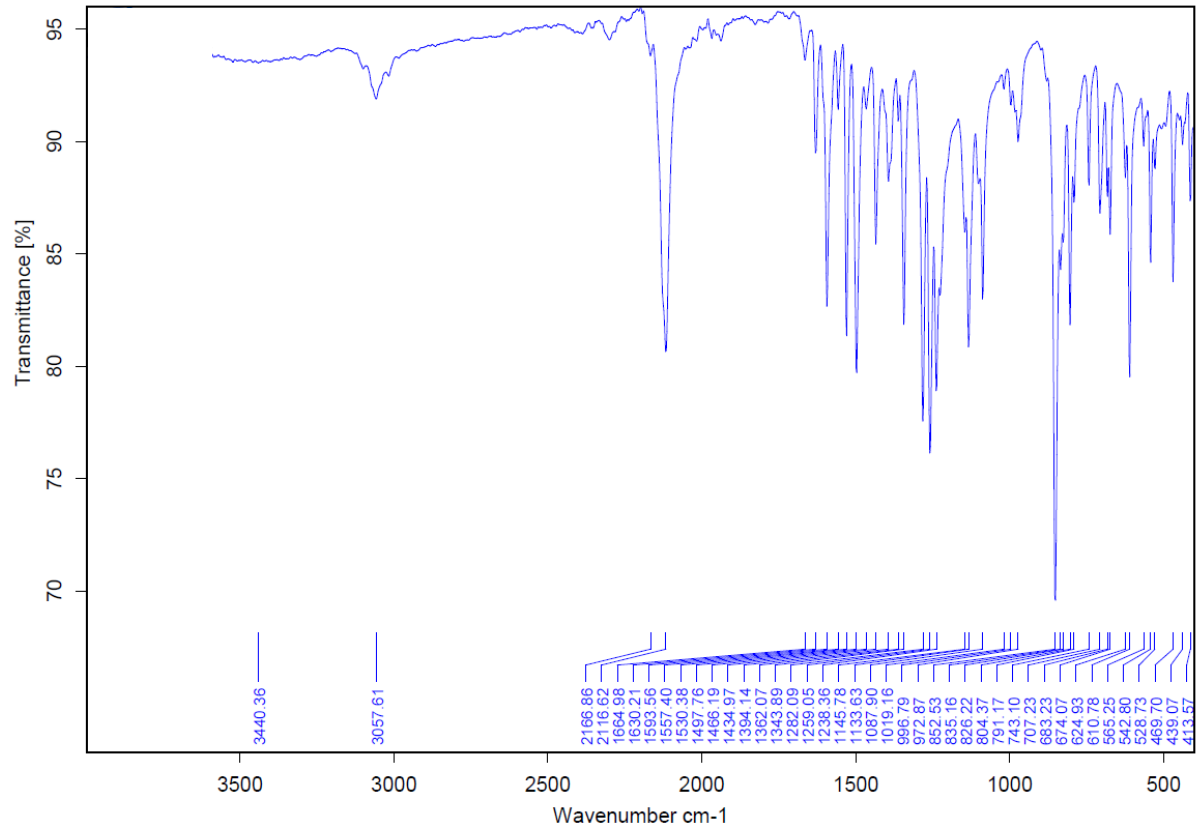

Figure S6: IR spectrum of 2,9-diazido-1,10-phenanthroline (neat).

Synthesis of 2,9-diamino-1,10-phenanthroline:

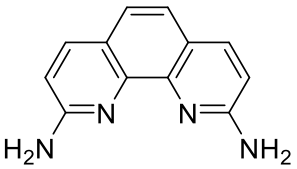

2,9-Diazido-1,10-phenanthroline (5.00 g, 19.1 mmol, 1.0 eq.) was suspended in a degassed solution of MeOH/H_2O (ratio 5:2, 80 mL) and stirred at ambient temperature for 20 min. Tri-*n*-butylphosphine (14.1 mL, 57.2 mmol, 3.0 eq.) was added dropwise. The Schlenk tube was equipped with a bubbler to release N_2 which was formed during the reaction and the suspension was stirred at ambient temperatures for 16 hours. The resulting dark red suspension was filtrated and the residue was first washed with toluene (2x15 mL) and *n*-hexane (2x15 mL) and then extracted with MeOH (3x15 mL). The combined MeOH fractions were concentrated to ~20% of the original volume and stored at –20 °C for 16 hours to precipitate the product as light-red solid.
To maximize the yield, the mother liquor of the dark red suspension was also concentrated to ~20% of its original volume and stored at +4 °C for 16 hours to precipitate the product. After filtration, the solids were washed with toluene and *n*-hexane until no tri-*n*-butylphosphine oxide was detected in the ^{31}P NMR spectrum.

2,9-Diamino-1,10-phenanthroline was isolated as light-red solid in 56% yield (2.27 g, 10.8 mmol).

The ^{1}H NMR shifts are in agreement with previous reports.[8]

^{1}H NMR (500 MHz, DMSO-d_6): δ = 7.88 (d, $^3J_{HH}$ = 8.6 Hz, 2H, H_{aryl}), 7.29 (s, 2H, H_{aryl}), 6.82 (d, $^3J_{HH}$ = 8.6 Hz, 2H, H_{aryl}), 6.31 (s, 4H, NH_2) ppm.

^{13}C{^{1}H} NMR (126 MHz, DMSO-d_6): δ = 157.9 (s, C_{aryl}), 144.2 (s, C_{aryl}), 137.1 (s, C_{aryl}), 122.3 (s, C_{aryl}), 120.8 (s, C_{aryl}), 111.6 (s, C_{aryl}) ppm.

HRMS (ESI): m/z calculated for $[C_{12}H_{11}N_4]^+$ (**M**+H)$^+$ 211.09782, found 211.09771.

IR (neat): $\tilde{\nu}$ = 3428 (w), 3168 (w), 1618 (m), 1600 (m), 1557 (m), 1519 (m), 1490 (m), 1430 (m), 1378 (m), 1355 (m), 1312 (m), 1222 (w), 1197 (w), 1140 (m), 1081 (w), 1052 (w) cm^{-1}.

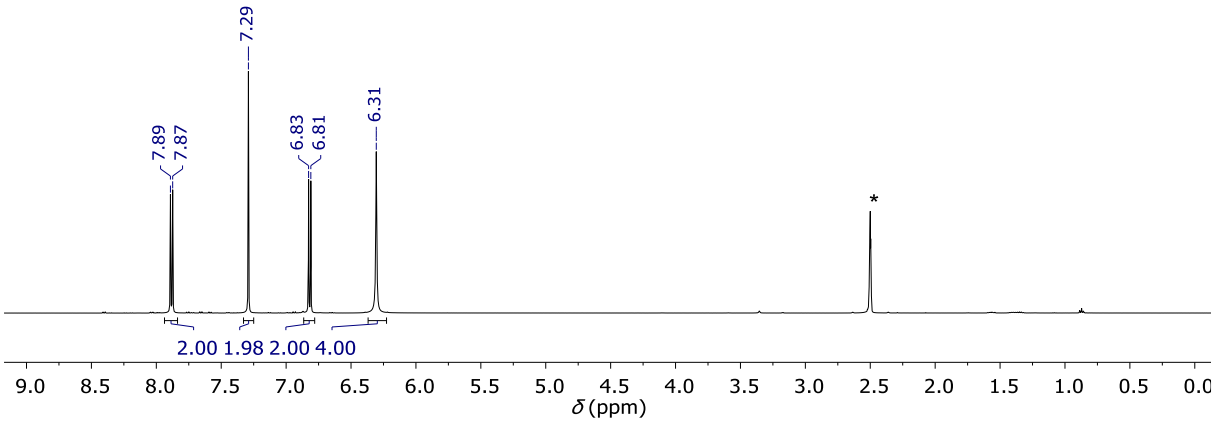

Figure S7: ^{1}H NMR spectrum of 2,9-diamino-1,10-phenantholine in DMSO-d_6 (* = residual solvent signal).

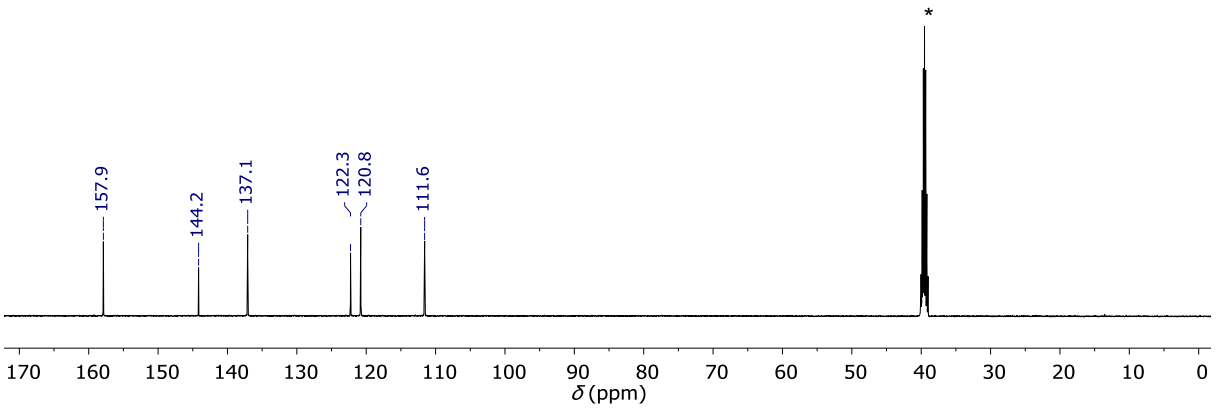

Figure S8: ^{13}C{^{1}H} NMR spectrum of 2,9-diamino-1,10-phenantholine in DMSO-d_6 (* = solvent signal).

Preparation of **1**, **1**·HBF_4, **1**·$2HBF_4$ and **1**·$2HB(C_6F_5)_4$

Synthesis of 1·HBF_4:

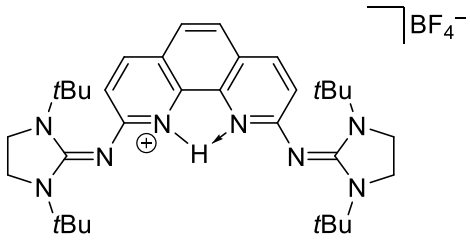

2,9-Diamino-1,10-phenanthroline (3.00 g, 14.2 mmol, 1.0 eq.), *N*,*N*'-di-*tert*-butyl-2-chloroimidazolinium tetrafluoroborate (8.69 g, 28.5 mmol, 2.0 eq.) and KF (4.97 g, 85.6 mmol, 6.0 eq.) were suspended in MeCN (25 mL) in a PTFE-sealed Schlenk tube. The suspension was heated at 90 °C for three days and the resulting yellow suspension was filtrated at ambient temperature. The solids were washed with distilled water (3x10 mL) to remove KF and then Et_2O (3x10 mL). The bright-yellow product was dried *in vacuo* at 140 °C for 16 hours and isolated in 98% yield (9.20 g, 13.8 mmol).

NMR analysis for **1**·HBF_4 is discussed in more detail below.

^{1}H NMR (400 MHz, DCM-d_2): δ = 10.61 (s, br, 1H, N–H), 7.81 (d, $^{3}J_{HH}$ = 9.1 Hz, 2H, H_{aryl}), 7.25 (s, 2H, H_{aryl}), 6.60 (d, $^{3}J_{HH}$ = 9.1 Hz, 2H, H_{aryl}), 3.72 (s, 8H, CH_2), 1.35 (s, 36H, CH_2) ppm.

^{11}B{} NMR (128 MHz, DCM-d_2): δ = –1.1 (s) ppm.

^{11}B{^{1}H} NMR (128 MHz, DCM-d_2): δ = –1.1 (s) ppm.

^{19}F{} NMR (377 MHz, DCM-d_2) δ = –153.2 (s) ppm.

^{19}F{^{1}H} NMR (377 MHz, DCM-d_2) δ = –153.2 (s) ppm.

Due to signal broadening, most of the aromatic ^{13}C resonances are not visible in the ^{13}C{^{1}H} NMR spectrum (Figure S10).

HRMS (ESI): m/z calculated for $[C_{34}H_{51}N_8]^+$ (**M**–BF_4)$^+$ 571.4236, found 571.4231; m/z calculated for $[C_{34}H_{52}N_8]^{2+}$ (**M**+H–BF_4)$^{2+}$ 286.2154, found: 286.2152.

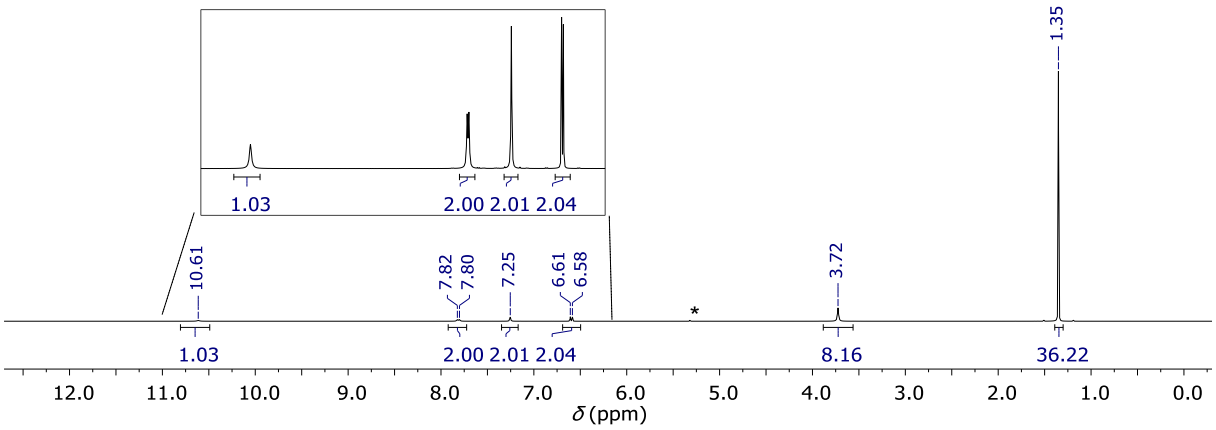

Figure S9: ^{1}H NMR spectrum of **1**·HBF_4 in DCM-d_2 (* = residual solvent signal).

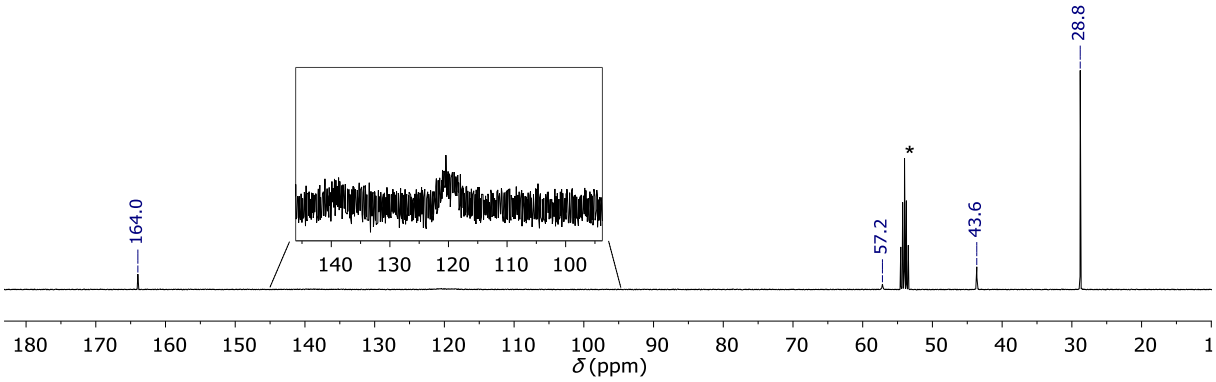

Figure S10: $^{13}C\{^{1}H\}$ NMR spectrum of **1**·HBF_4 in DCM-d_2 (* = solvent signal).

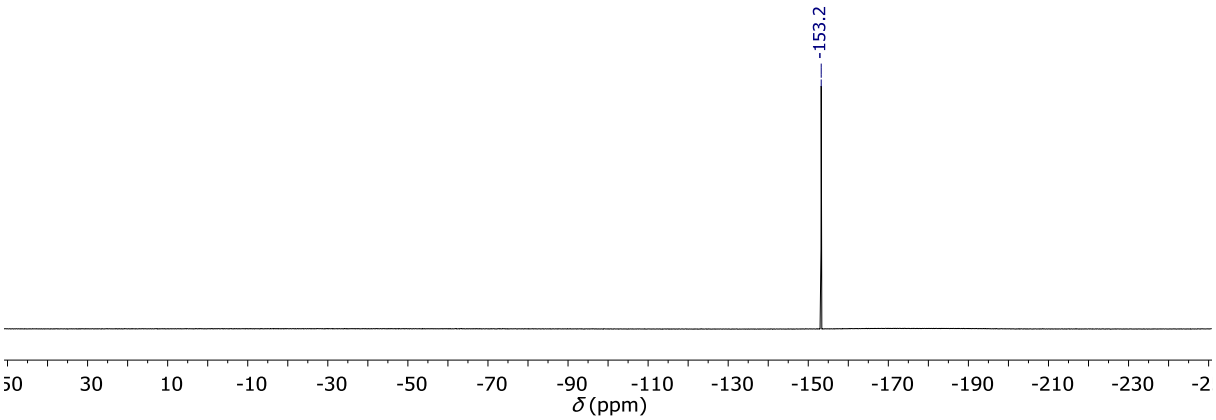

Figure S11: $^{19}F\{\}$ NMR spectrum of **1**·HBF_4 in DCM-d_2.

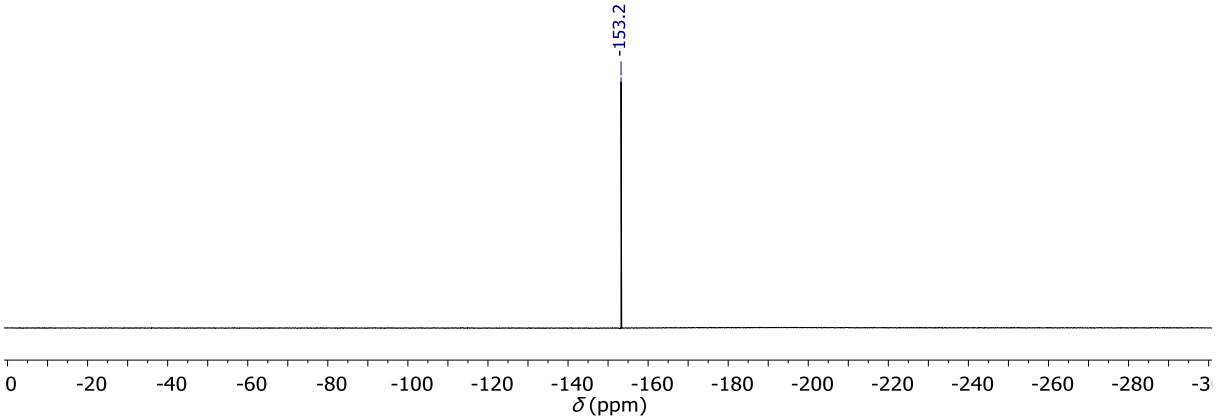

Figure S12: $^{19}F\{^{1}H\}$ NMR spectrum of **1**·HBF_4 in DCM-d_2.

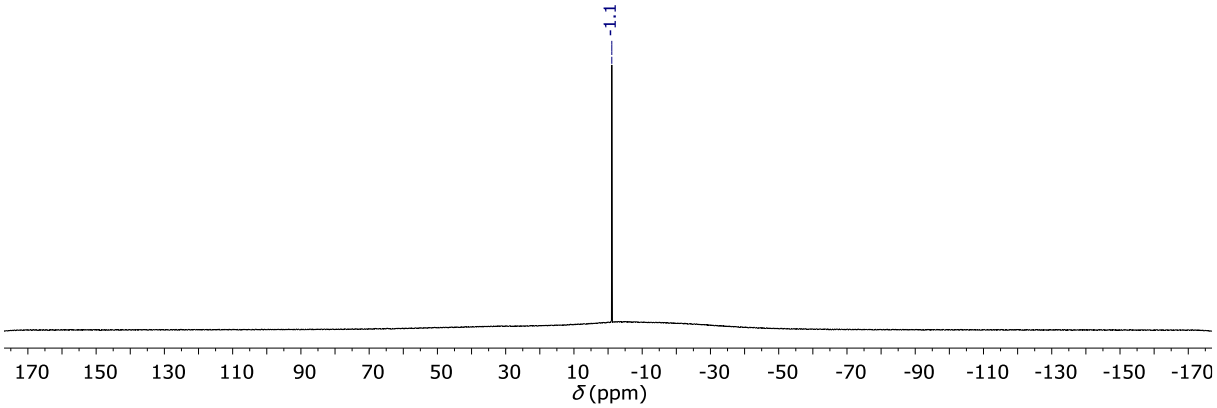

Figure S13: $^{11}B\{\}$ NMR spectrum of **1**·HBF_4 in DCM-d_2.

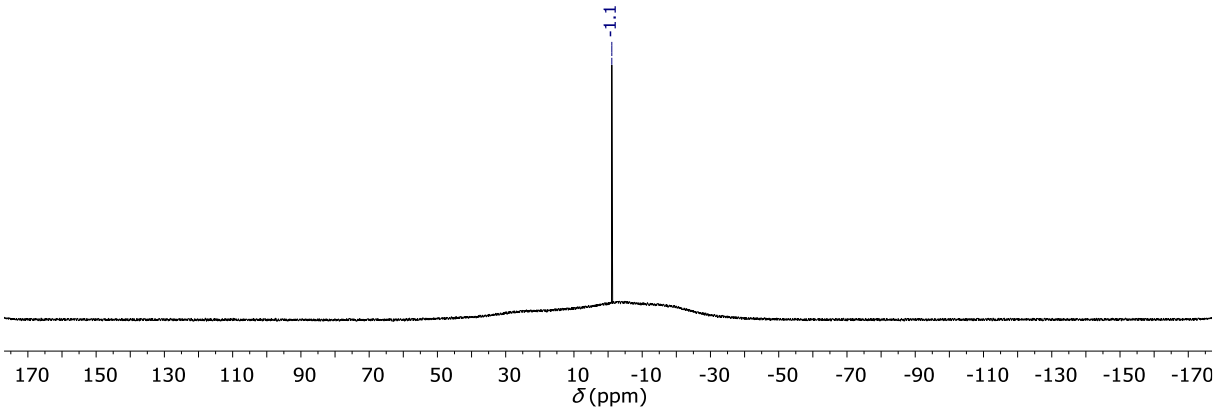

Figure S14: $^{11}B\{^1H\}$ NMR spectrum of **1**·HBF_4 in DCM-d_2.

Synthesis of 1:

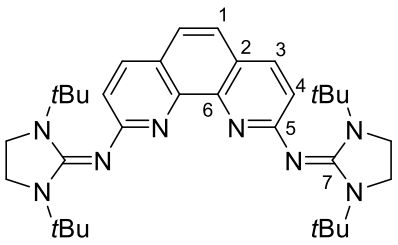

1·HBF_4 (2.00 g, 3.04 mmol, 1.0 eq.) and KO*t*Bu (1.36 g, 12.2 mmol, 4.0 eq.) were suspended in THF (25 mL) in a PTFE-sealed Schlenk tube and heated at 60 °C for 2 days. The prolonged heating was necessary due to the low solubility of 1·HBF_4. The solvent of the resulting orange suspension was removed under reduced pressure and the solids were washed first with distilled water (3x15 mL) and then *n*-hexane (3x5 mL) to remove excess KO*t*Bu and HO*t*Bu. The solids were dried *in vacuo* and subsequently extracted with toluene (3x40 mL) at 60 °C. The combined organic phases were concentrated using a rotary evaporator. The resulting product was dried *in vacuo* at 100 °C for 16 hours and **1** was obtained in 83% yield (1.44 g, 2.52 mmol).

2D NMR analysis was performed to exactly assign all resonances.

^{1}H-NMR (400 MHz, C_6D_6): δ = 7.65 (d, $^3J_{HH}$ = 8.6 Hz, 2H, H-3), 7.21 (s, 2H, H-1), 6.93 (d, $^3J_{HH}$ = 8.6 Hz, 2H, H-4), 3.05 (s, 8H, CH_2), 1.33 (s, 36H, CH_3) ppm.

$^{13}C\{^1H\}$-NMR (101 MHz, C_6D_6): δ = 160.9 (s, C-5), 159.6 (s, C-7), 146.8 (s, C-6), 136.8 (s, C-3), 123.0 (s, C-2), 121.0 (s, C-1), 117.9 (s, C-4), 55.5 (s, **C**$(CH_3)_3$), 42.5 (s, CH_2), 28.7 (s, C(**C**$H_3)_3$) ppm.

HRMS (ESI): m/z calculated for $[C_{34}H_{51}N_8]^+$ (**1**+H)$^+$ 571.4236, found 571.4232; m/z calculated for $[C_{34}H_{52}N_8]^{2+}$ (**1**+2H)$^{2+}$ 286.2152 found 286.2153.

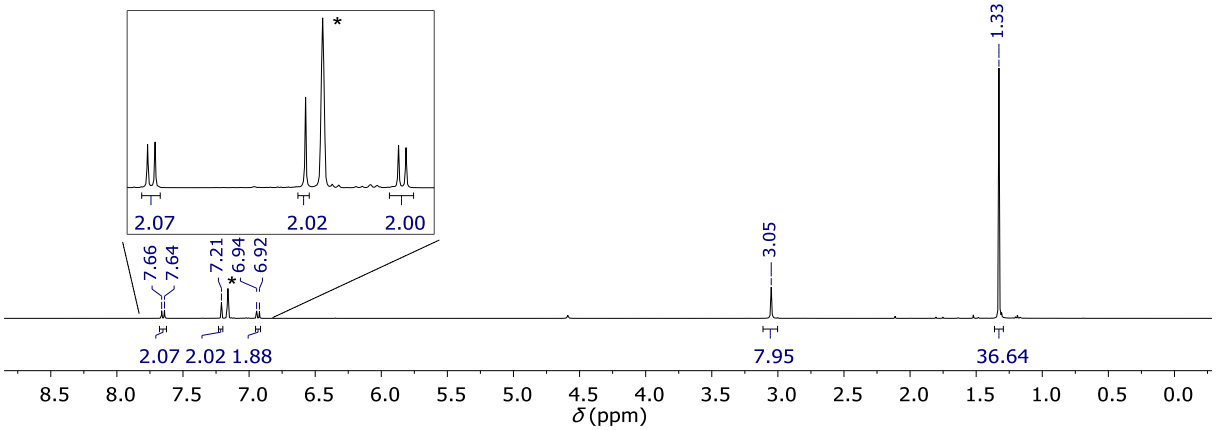

Figure S15: ^1H NMR spectrum of **1** in C_6D_6 (* = residual solvent signal).

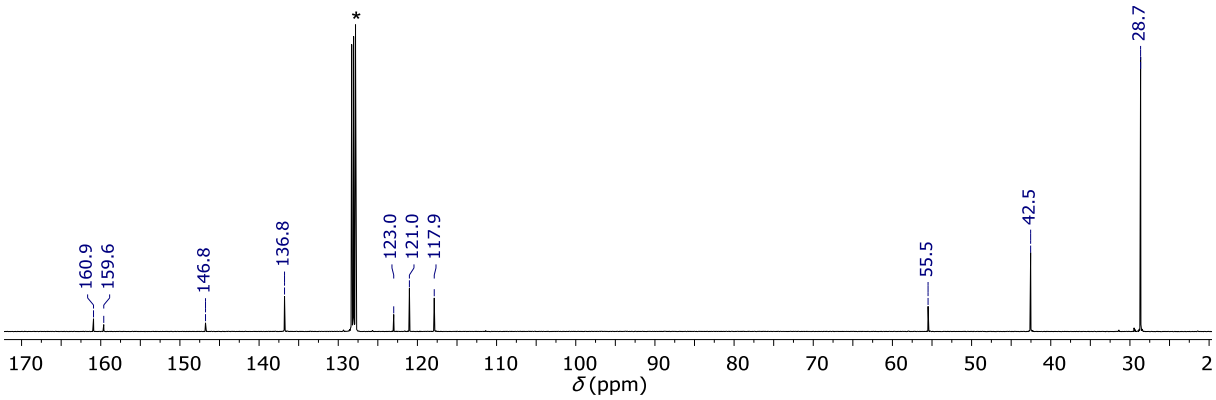

Figure S16: $^{13}C\{^1H\}$ NMR spectrum of **1** in C_6D_6 (* = solvent signal).

Synthesis of 1·2HBF$_4$ and 1·2HB(C$_6$F$_5$)$_4$:

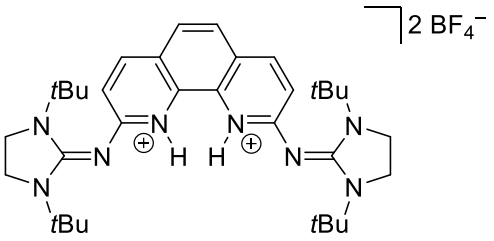

1·HBF$_4$ (250 mg, 379 µmol, 1.0 eq.) was dissolved in MeCN (4 mL) and HBF$_4$·OEt$_2$ (51 µL, 379 µmol, 1.0 eq.) was added. After stirring at ambient temperatures for 4 hours, Et$_2$O (10 mL) was added to precipitate the product as off-white solid. The supernatant was filtered off via canula filtration and the residue was washed with Et$_2$O (2x5 mL) and then dried *in vacuo* at 70 °C for 1 hour. **1**·2HBF$_4$ was obtained as off-white solid in 50% yield (110 mg, 192 µmol).

For the NMR analysis, single-crystals of **1**·2HBF$_4$ were dried *in vacuo* and redissolved in MeCN-d_3. Note that in the ^{1}H NMR spectrum, multiple resonances are significantly broadened and thus integration of the signals can be ambiguous (Figure S24).

The position of the protons in the solid state was confirmed by SCXRD studies (Figure S108).

^{1}H NMR (400 MHz, MeCN-d_3): δ = 10.33 (s, br, N–H), 8.14 (s, br, 2H, H$_{aryl}$), 7.63 (s, 2H, H$_{aryl}$), 6.87 (s, br, 2H, H$_{aryl}$), 3.90 (s, 8H, CH$_2$), 1.36 (s, 36H, C(CH$_3$)$_3$) ppm.

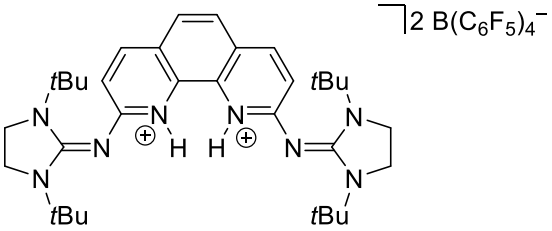

In an NMR tube, **1** (25.0 mg, 43.8 µmol, 1.0 eq.) was dissolved in DCM-d_2 and [H(OEt$_2$)$_2$][B(C$_6$F$_5$)$_4$] (72.6 mg, 87.6 µmol, 2.0 eq.) was added. Immediately, the orange solution turned pale yellow. NMR experiments confirmed the full conversion of the starting material and the NMR characterization was carried out using the same sample without further workup.

^{1}H NMR (400 MHz, CD$_2$Cl$_2$): δ = 11.50 (s, br, 2H, N–H), 7.94 (s, br, 2H, H$_{aryl}$), 7.52 (s, br, 2H, H$_{aryl}$), 6.56 (s, br, 2H, H$_{aryl}$), 3.84 (s, 8H, CH$_2$), 1.38 (s, 36H, C(CH$_3$)$_3$) ppm.

^{13}C{^{1}H} NMR (101 MHz, CD$_2$Cl$_2$): δ = 164.0 (s, C$_{q,aryl}$), 153.4 (s, C$_{q,aryl}$), 150.0 (s, br, B(C$_6$F$_5$)$_4$), 147.6 (s, br, B(C$_6$F$_5$)$_4$), 142.4 (s, CH$_{aryl}$), 140.0 (t, br, J_{CF} = 14 Hz, B(C$_6$F$_5$)$_4$), 138.1 (t, br, B(C$_6$F$_5$)$_4$), 137.6 (t, J_{CF} = 14 Hz, B(C$_6$F$_5$)$_4$), 135.7 (t, br, B(C$_6$F$_5$)$_4$), 125.9 (s, C$_{q,aryl}$), 124.5 (s, CH$_{aryl}$), 122.8 (s, C$_{q,aryl}$), 118.1 (s, CH$_{aryl}$), 58.5 (s, **C**(CH$_3$)$_3$), 44.2 (s, CH$_2$), 28.8 (s, C(**C**H$_3$)$_3$) ppm.

^{19}F{} NMR (376 MHz, CD$_2$Cl$_2$): δ = –132.9 (s, br, *o*-C$_6$F$_5$), –163.6 (t, $^3J_{FF}$ = 20 Hz), –167.5 (t, $^3J_{FF}$ = 20 Hz) ppm.

^{19}F{^{1}H} NMR (376 MHz, CD$_2$Cl$_2$): δ = –132.9 (s, br, *o*-C$_6$F$_5$), –163.6 (t, $^3J_{FF}$ = 20 Hz, *p*-C$_6$F$_5$), –167.5 (t, $^3J_{FF}$ = 20 Hz, *m*-C$_6$F$_5$) ppm.

^{11}B NMR (128 MHz, CD$_2$Cl$_2$): δ = –16.6 (s) ppm.

^{11}B{^{1}H} NMR (128 MHz, CD$_2$Cl$_2$): δ = –16.6 (s) ppm.

HRMS (ESI): m/z calculated for $[C_{34}H_{52}N_8]^{2+}$ (**M**–2BF_4)$^{2+}$ 286.2154, found 286.2155; m/z calculated for $[C_{34}H_{52}N_8]^{2+}$ (**M**–H–2BF_4)$^{+}$ 571.4231, found 571.4237.

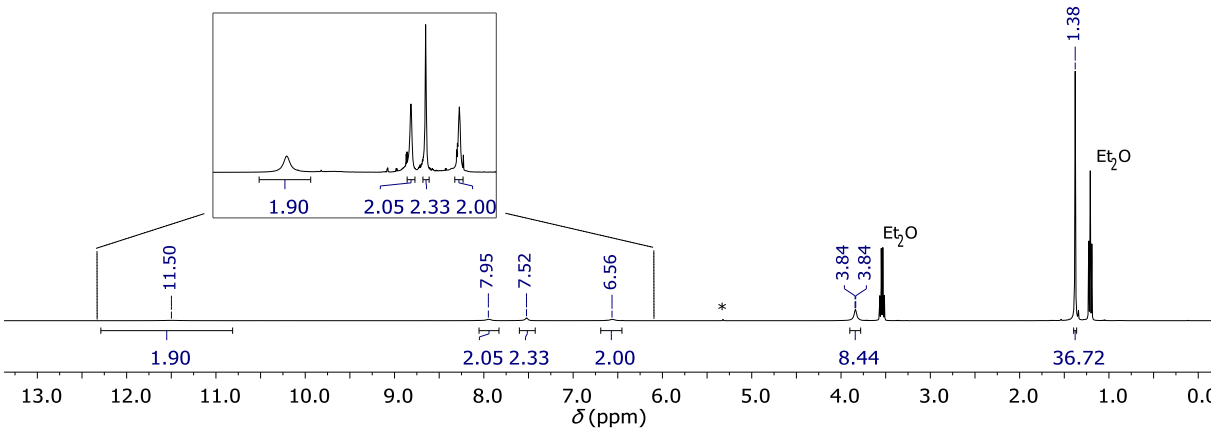

Figure S17: ^{1}H NMR spectrum of **1**·2HB(C_6F_5)$_4$ in DCM-d_2 (* = residual solvent signal).

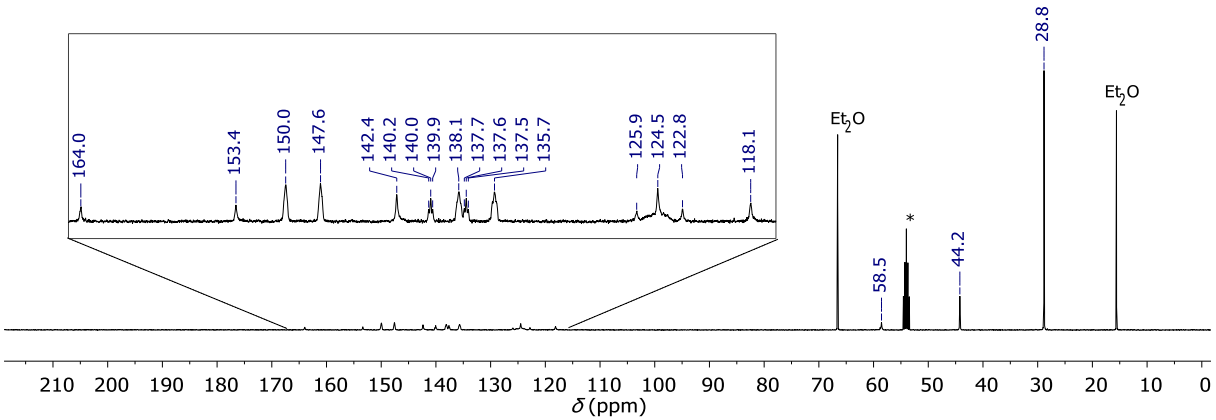

Figure S18: ^{13}C{^{1}H} NMR spectrum of **1**·2HB(C_6F_5)$_4$ in DCM-d_2 (* = solvent signal).

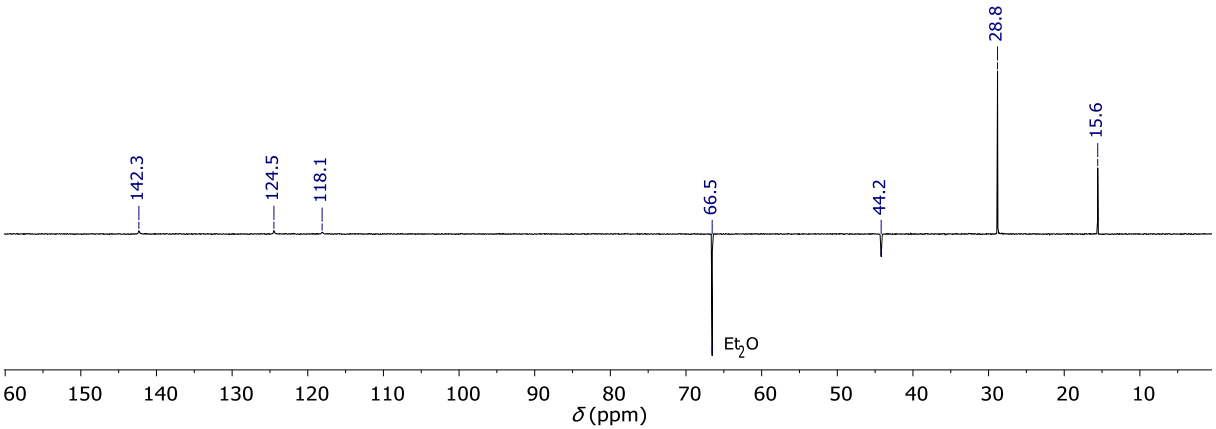

Figure S19: ^{13}C{^{1}H} DEPT135 NMR spectrum of **1**·2HB(C_6F_5)$_4$ in DCM-d_2.

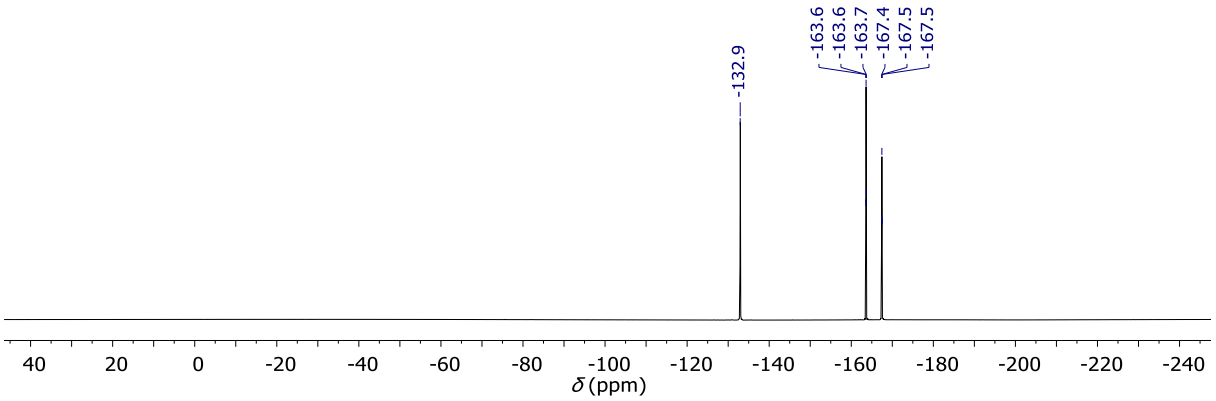

Figure S20: $^{19}F\{\}$ NMR spectrum of **1**·2HB(C_6F_5)$_4$ in DCM-d_2.

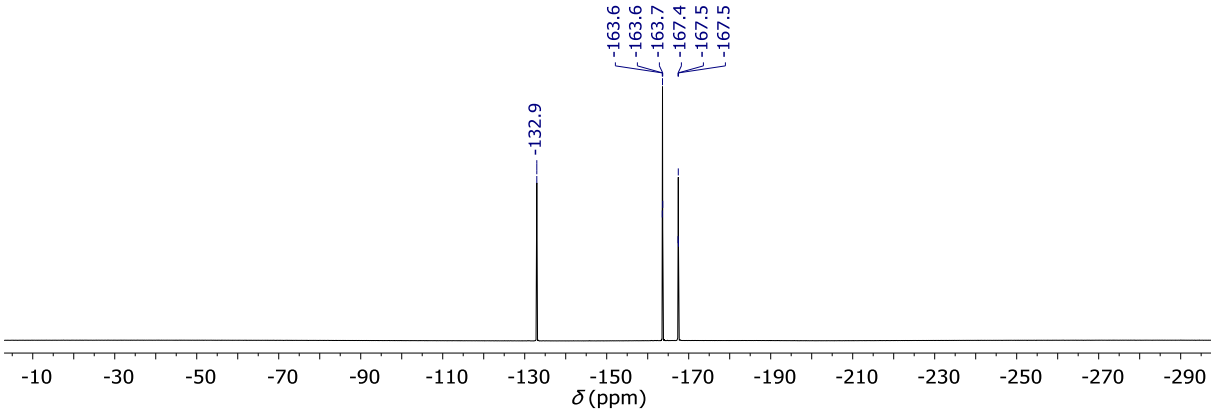

Figure S21: $^{19}F\{^1H\}$ NMR spectrum of **1**·2HB(C_6F_5)$_4$ in DCM-d_2.

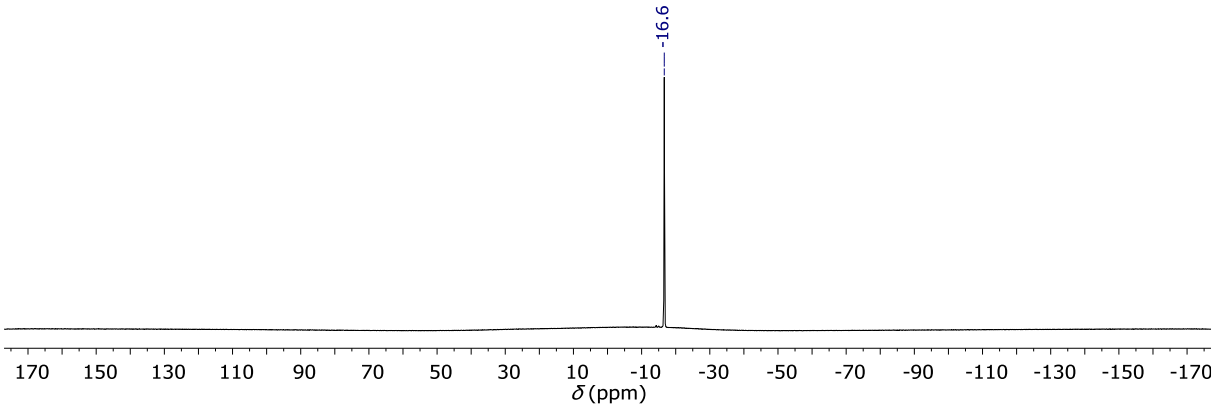

Figure S22: $^{11}B\{\}$ NMR spectrum of **1**·2HB(C_6F_5)$_4$ in DCM-d_2.

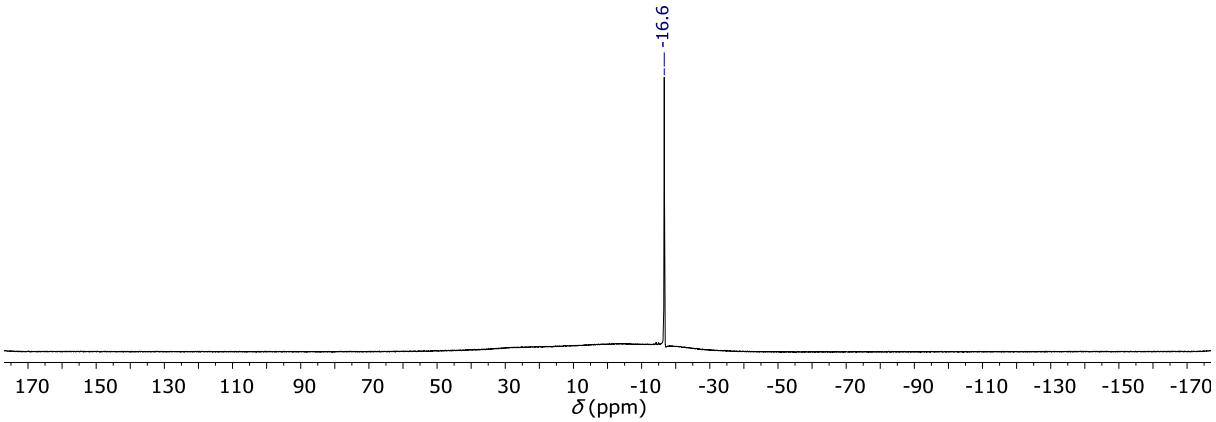

Figure S23: $^{11}B\{^{1}H\}$ NMR spectrum of **1**·2HB$(C_6F_5)_4$ in DCM-d_2.

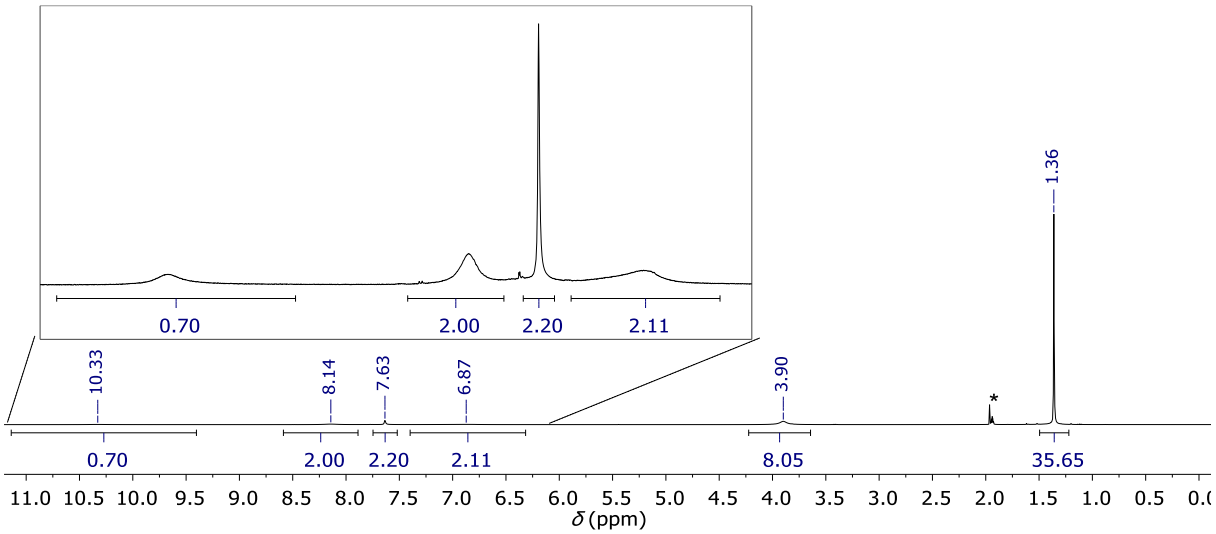

Figure S24: ^{1}H NMR spectrum of **1**·2HBF_4 in MeCN-d_3 (* = residual solvent signal).

Protonation experiments of 1·2HB(C_6F_5)$_4$:

In an NMR tube, **1** was dissolved in CD_2Cl_2 and protonated stepwise with [H(OEt_2)$_2$][B(C_6F_5)$_4$] until the resonances of **1**·2HB(C_6F_5)$_4$ were observed in the respective ^{1}H NMR spectrum (*vide supra*, Figure S17). A third equivalent of the acid was added in attempts to generate the trication [**1**·3H]$^{3+}$. Yet, in the ^{1}H NMR spectrum (Figure S25), only the resonances of the starting material, i.e. **1**·2HB(C_6F_5)$_4$ and [H(OEt_2)$_2$][B(C_6F_5)$_4$], are visible. Also, the addition of a fourth equivalent of acid led to the same results. This indicates that a third protonation does not occur using this acid and that the dication [**1**·2H]$^{2+}$ possesses a lower basicity than Et_2O.

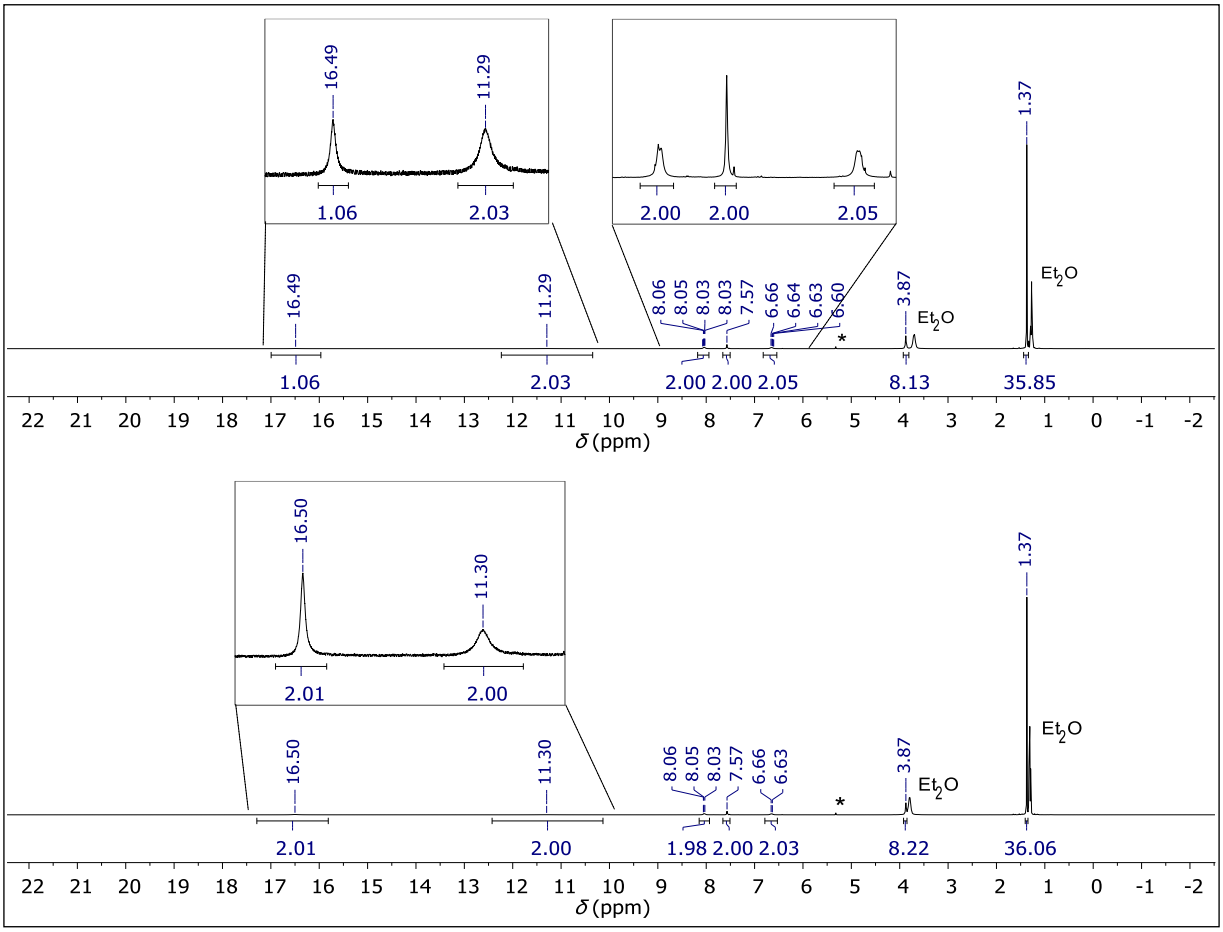

Figure S25: ^{1}H NMR spectrum of **1**·2HB(C_6F_5)$_4$ in presence of 1 eq. of [H(OEt_2)$_2$)][B(C_6F_5)$_4$] (top) and of 2 eq. of [H(OEt_2)$_2$)][B(C_6F_5)$_4$] (bottom) in DCM-d_2 (* = residual solvent signal).

Preparation of the Zn(II) complex **2**·2MeCN

Synthesis of 2·2MeCN**:**

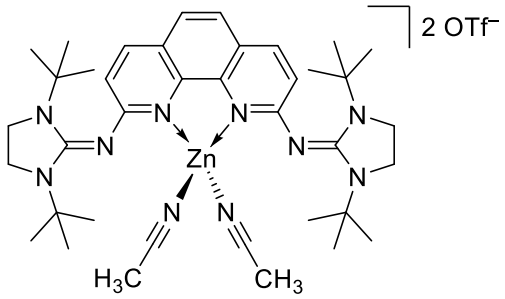

1 (200 mg, 350 µmol, 1.0 eq.) was dissolved in MeCN (4 mL) and $Zn(OTf)_2$ (127 mg, 350 µmol, 1.0 eq.) was added. The orange suspension was stirred at ambient temperature for 16 hours. To the resulting yellow solution, Et_2O (10 mL) was added to precipitate a yellow solid. The supernatant was removed via cannula filtration and the residue was washed with Et_2O (2x5 mL). The SCXRD analysis of **2**·2MeCN revealed that two MeCN molecules coordinate to the Zn^{II} metal center (see below). Drying the product *in vacuo* at 80 °C for 16 h removes the ligating MeCN and complex **2** is obtained as yellow solid in 66% yield (234 mg, 230 µmol). The absence of MeCN in the ^{1}H NMR analysis confirms the complete removal of solvent molecules. To analyze compound **2**·2MeCN, the resulting yellow precipitate obtained after the addition of Et_2O (10 mL) was dried in an argon stream and then subjected to NMR analysis.

NMR analysis of **2**·2MeCN:

^{1}H NMR (400 MHz, DMSO-*d*6): δ = 7.94 (d, $^3J_{HH}$ = 9.0 Hz, 2H, H_{aryl}), 7.33 (s, 2H, H_{aryl}), 6.62 (d, $^3J_{HH}$ = 9.0 Hz, 2H, H_{aryl}), 3.73 (s, 8H, CH_2), 2.1 (s, 6H, CH_3CN), 1.33 (s, 36H, $C(CH_3)_3$) ppm.

^{19}F{} NMR (377 MHz, DMSO-d_6): δ = –77.74 ppm.

^{19}F{^{1}H} NMR (377 MHz, DMSO-d_6): δ = –77.74 ppm.

^{13}C{^{1}H} NMR (101 MHz, DMSO-d_6): δ = 163.8 (s, N=CNN), 157.1 (s, $C_{q,\ aryl}$), 138.1 (s, CH_{aryl}), 137.6 (s, $C_{q,aryl}$), 120.7 (d, $^1J_{CF}$ = 322 Hz, $CF_3SO_3^-$)†, 119.8 (s, C_{aryl}), 119.7 (s, C_{aryl}), 118.1 (s, C_{aryl}), 117.7 (s, CH_3**C**N), 56.3 (s, **C**$(CH_3)_3$), 42.6 (s, CH_2), 28.3 (s, C(**C**$H_3)_3$) ppm, 1.1 (s, **C**H_3CN).

† For the $CF_3SO_3^-$ anion, the coupling caused by the three F atoms of the ^{13}C resonance is expected to be a quartet. The signal is not fully resolved due to the signal to noise ratio.

NMR analysis of **2**

^{1}H NMR (400 MHz, DMSO-*d*6): δ = 7.94 (d, $^3J_{HH}$ = 9.0 Hz, 2H, H_{aryl}), 7.33 (s, 2H, H_{aryl}), 6.62 (d, $^3J_{HH}$ = 9.0 Hz, 2H, H_{aryl}), 3.73 (s, 8H, CH_2), 1.33 (s, 36H, $C(CH_3)_3$) ppm.

^{19}F{} NMR (377 MHz, DMSO-d_6): δ = –77.74 ppm.

^{19}F{^{1}H} NMR (377 MHz, DMSO-d_6): δ = –77.74 ppm.

^{13}C{^{1}H} NMR (101 MHz, DMSO-d_6): δ = 163.8 (s, N=CNN), 157.1 (s, $C_{q,\ aryl}$), 138.1(s, CH_{aryl}), 137.6 (s, $C_{q,aryl}$), 119.8 (s, C_{aryl}), 119.7 (s, C_{aryl}), 117.7 (s, C_{aryl}), 56.3 (s, **C**$(CH_3)_3$), 42.6 (s, CH_2), 28.3 (s, C(**C**$H_3)_3$) ppm.

The ^{13}C resonances of the $CF_3SO_3^-$ anion are not visible in the $^{13}C\{^1H\}$ NMR spectrum due to the signal to noise ratio.

HRMS (ESI): m/z calculated for $[C_{35}H_{50}N_8SO_3F_3Zn]^+$ (**M**–OTf)$^+$ 783.2976, found 783.2974; m/z calculated for $[C_{36}H_{53}N_9Zn]^{2+}$ (**M**–2OTf+MeCN)$^{2+}$ 337.6852, found 337.6857; m/z calculated for $[C_{34}H_{52}N_8OZn]^+$ (**M**–2OTf+H_2O)$^{2+}$ 326.1772, found 326.1778.

NMR spectra of **2**·2MeCN:

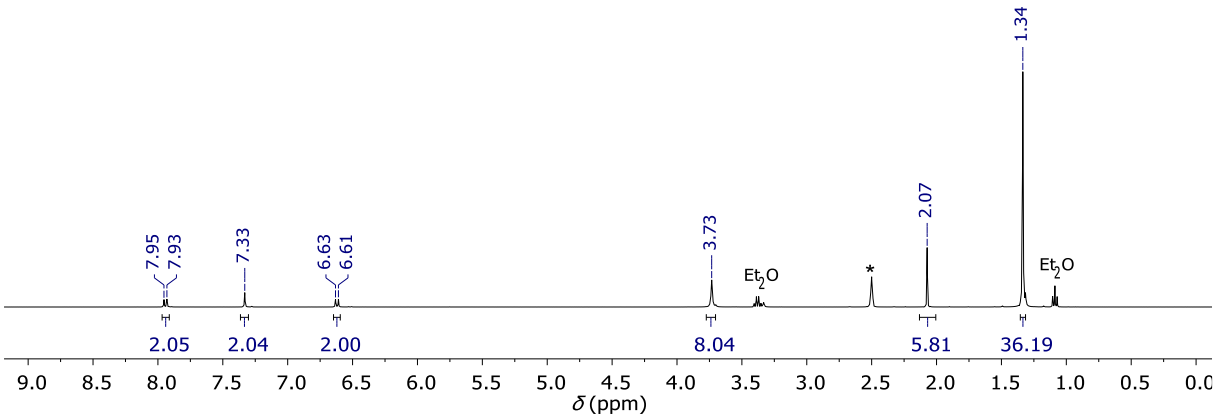

Figure S26: ^1H NMR spectrum of **2**·2MeCN in DMSO-d_6 (* = residual solvent signal).

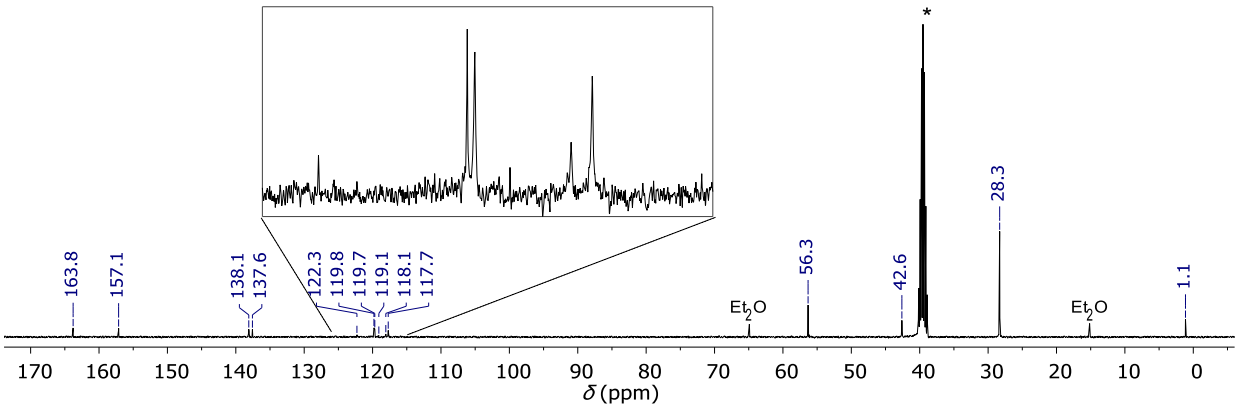

Figure S27: $^{13}C\{^1H\}$ NMR spectrum of **2**·2MeCN in DMSO-d_6 (* = solvent signal).

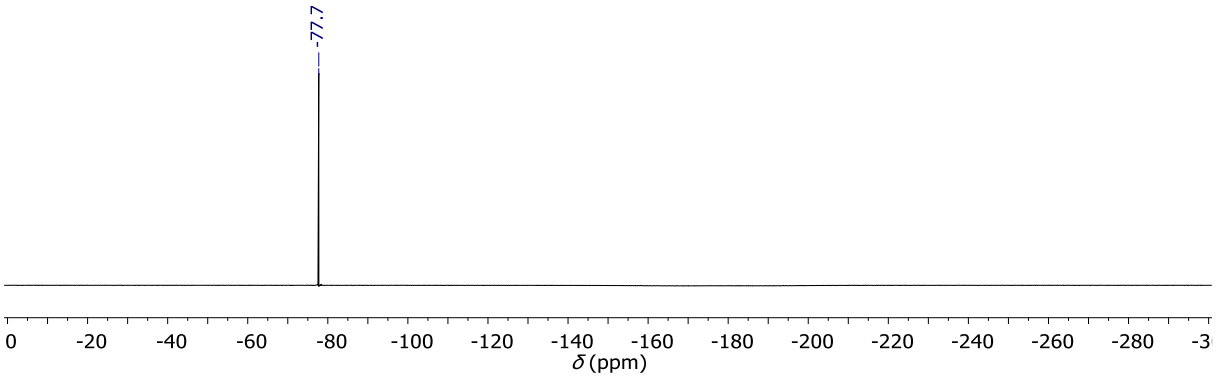

Figure S28: $^{19}F\{\}$ NMR spectrum of **2**·2MeCN in DMSO-d_6.

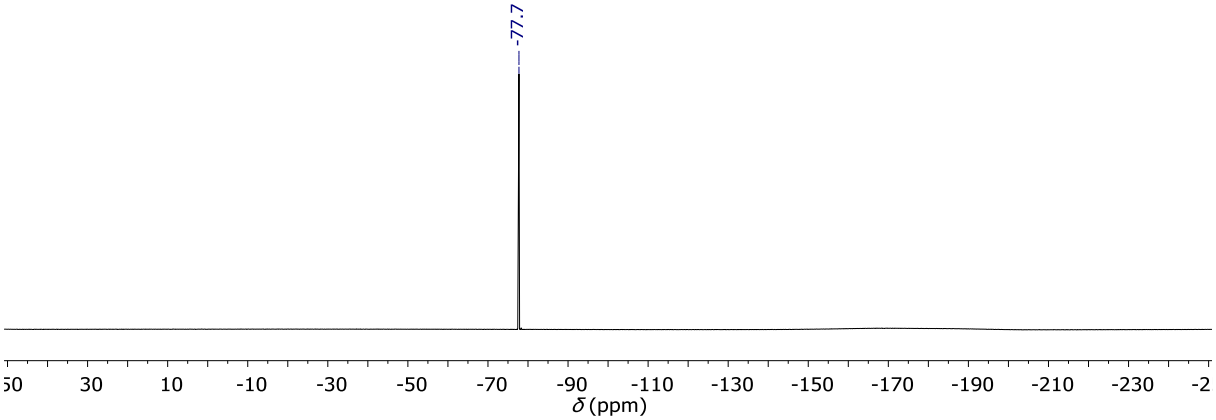

Figure S29: $^{19}F\{^1H\}$ NMR spectrum of **2**·2MeCN in DMSO-d_6.

NMR spectra of **2**:

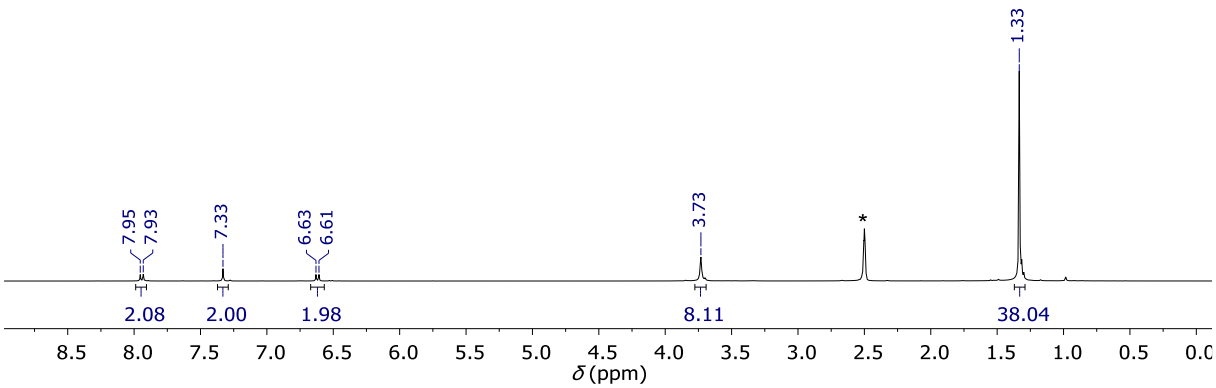

Figure S30: ^1H NMR spectrum of **2** in DMSO-d_6 (* = residual solvent signal).

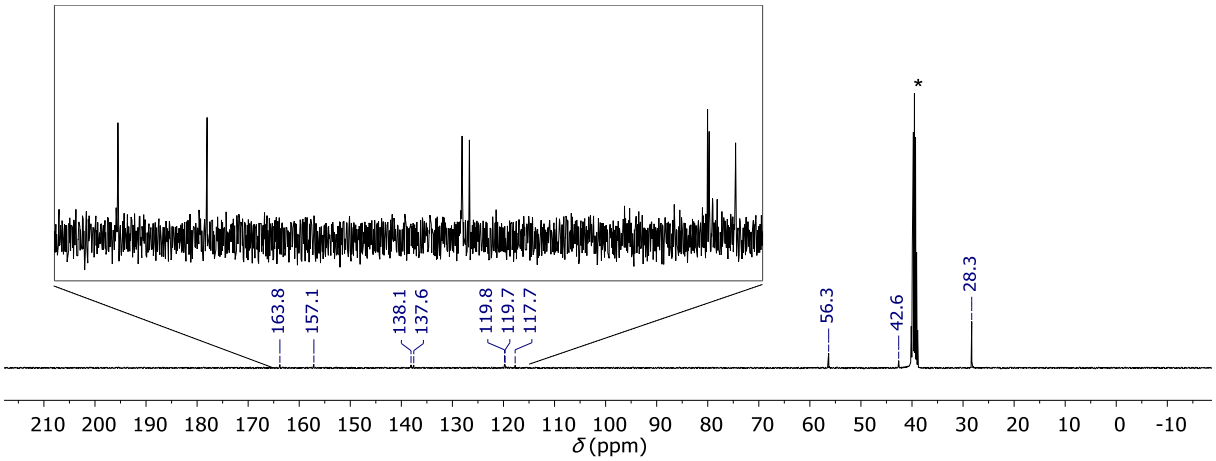

Figure S31: $^{13}C\{^{1}H\}$ NMR spectrum of **2** in DMSO-d_6 (* = solvent signal).

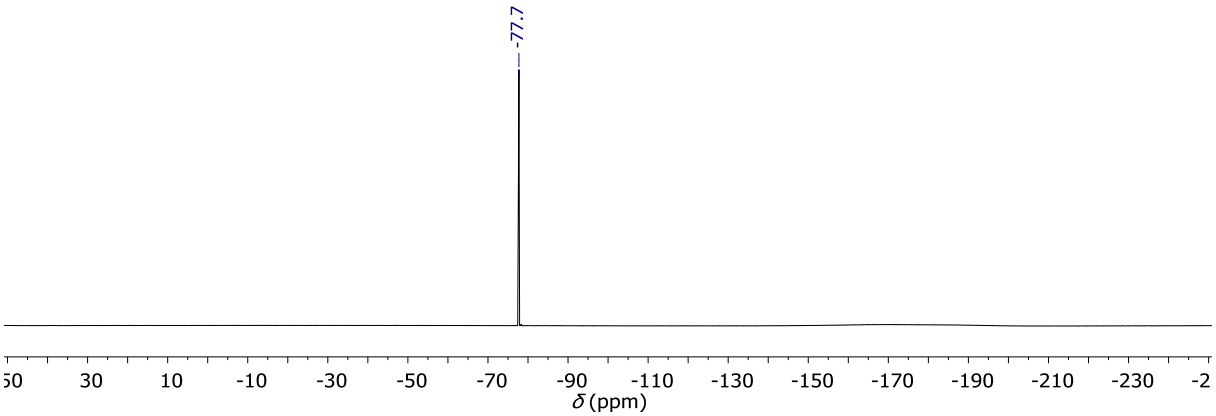

Figure S32: $^{19}F\{\}$ NMR spectrum of **2** in DMSO-d_6.

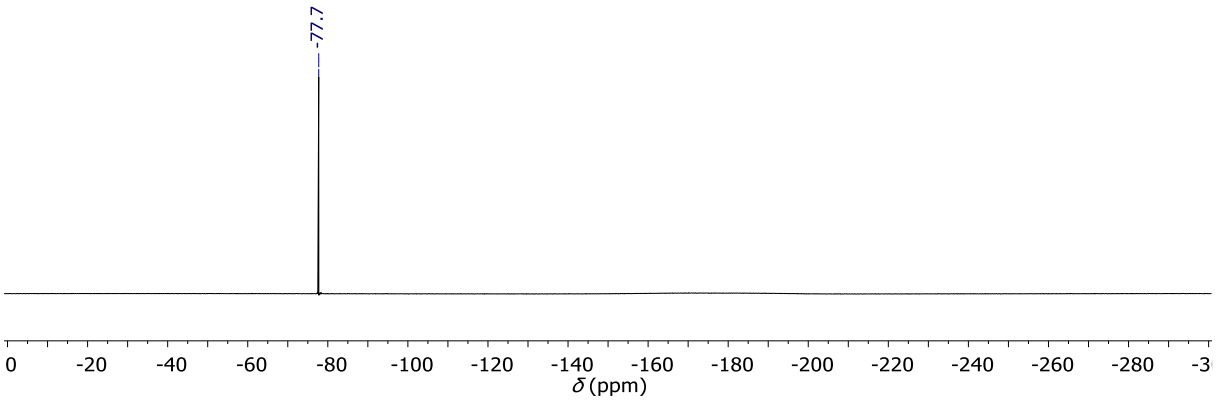

Figure S33: $^{19}F\{\}$ NMR spectrum of **2** in DMSO-d_6.

NMR studies of **1**·HBF_4

2D-NMR, i.e. NH-HMBC, NH-HSQC, CH-HSQC, CH-HMBC and HH-NOESY, experiments were conducted in attempts to determine the position of the acidic proton. **1**·HBF_4 was dissolved in either DCM-d_2 or DMSO-d_6.

The NMR experiments in DMSO-d_6 were carried out at 25 °C, 75 °C and 120 °C. Unfortunately, in all resulting spectra of the above-mentioned experiments, no N–H-, C–H- or H–H-coupling was observed that would allow the assignment of the [**1**·H]$^+$ proton to a specific N atom. At 120 °C, the postulated dynamic process involving shuttling of the proton is accelerated and sharp signals are observed in the resulting $^{13}C\{^1H\}$ NMR spectrum which were not observed at ambient temperatures in DCM-d_2 or DMSO-d_6 (Figure S35).

Thus, the following NMR shifts are reported for DMSO-d_6 at 120 °C:

^{1}H NMR (400 MHz, **393.2 K**, DMSO-d_6): δ = 10.35 (s, 1H, N–H), 7.96 (d, $^3J_{HH}$ = 9.1 Hz, 2H, H_{aryl}), 7.34 (s, 2H, H_{aryl}), 6.74 (d, $^3J_{HH}$ = 9.1 Hz, 2H, H_{aryl}), 3.76 (s, 8H, CH_2), 1.35 (s, 36H, $C(CH_3)_3$).

$^{13}C\{^1H\}$ NMR (101 MHz, **393.2 K**, DMSO-d_6): δ = 162.1 (s, $C_{q,aryl}$), 154.4 (s, $C_{q,aryl}$), 138.0 (s, CH_{aryl}), 133.1 (s, $C_{q,aryl}$), 119.2 (s, $C_{q,aryl}$), 119.8 (s, CH_{aryl}), 118.3 (s, CH_{aryl}), 55.7 (s, **C**$(CH_3)_3$), 42.3 (s, CH_2), 27.4 ($C(\mathbf{C}H_3)_3$).

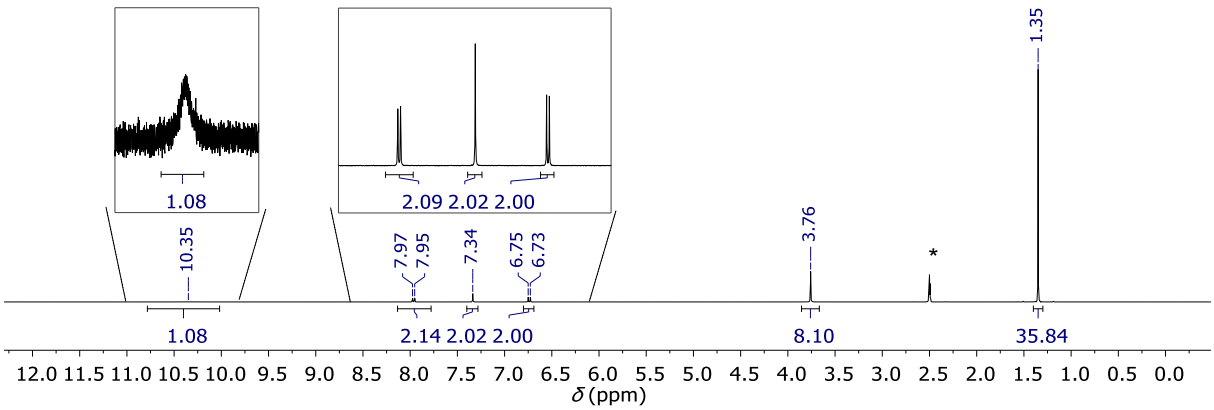

Figure S34: ^{1}H NMR spectrum of **1**·HBF_4 in DMSO-d_6 measured at 120 °C (* = residual solvent signal).

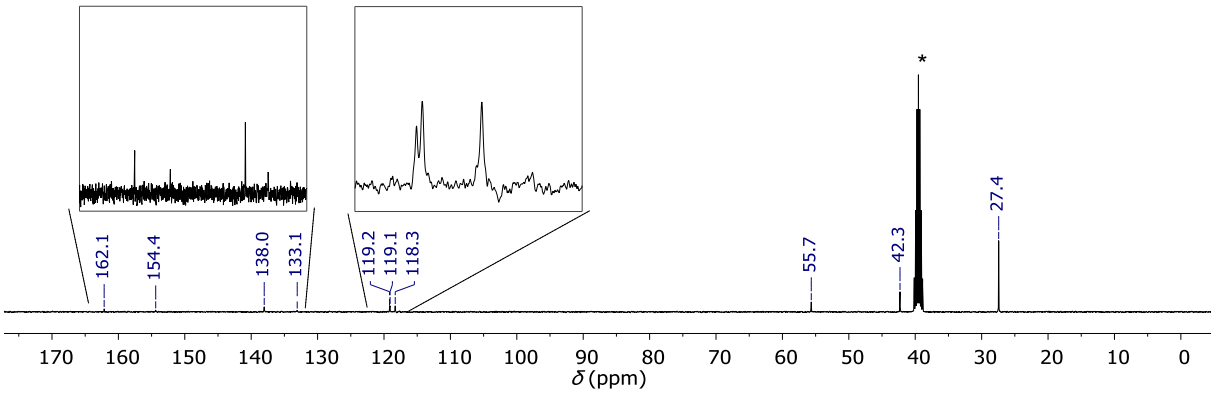

Figure S35: $^{13}C\{^{1}H\}$ NMR spectrum of **1**·HBF_4 in DMSO-d_6 measured at 120 °C (* = solvent signal).

The NMR experiments in CD_2Cl_2 were carried out at –50 °C. Similarly to the experiments in DMSO-d_6, no N–H-, C–H- or H–H-coupling was observed that would allow the assignment of the [**1**·H]$^+$ proton to a specific N atom. At –50 °C, the postulated dynamic process involving shuttling of the proton is decelerated and the resonances are slightly broadened in relation to the measurement of **1**·HBF_4 at ambient temperatures. In the $^{13}C\{^{1}H\}$ NMR spectrum, only one aromatic signal is detected which was also observed in the spectrum recorded at ambient temperatures.

^{1}H NMR (400 MHz, **<u>223.1 K</u>**, DCM-d_2): δ = 10.65 (s, 1H, N–H), 7.78 (d, J_{HH} = 9.1 Hz, 2H), 7.23 (s, 2H), 6.47 (d, J_{HH} = 9.1 Hz, 2H), 3.65 (s, 8H, CH_2), 1.28 (s, 36H, $C(CH_3)_3$) ppm.

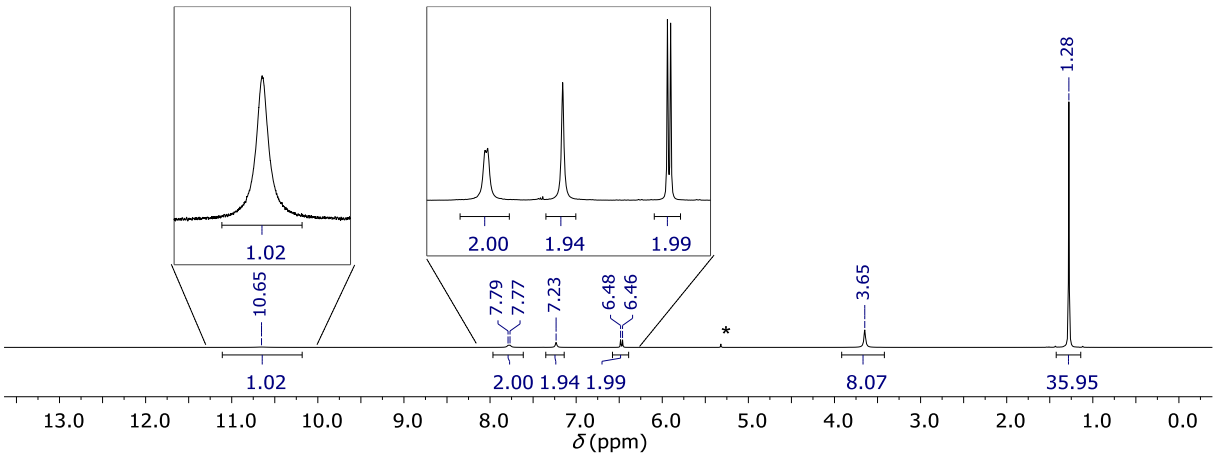

Figure S36: ^{1}H NMR spectrum of **1**·HBF_4 in DCM-d_2 measured at –50 °C (* = residual solvent signal).

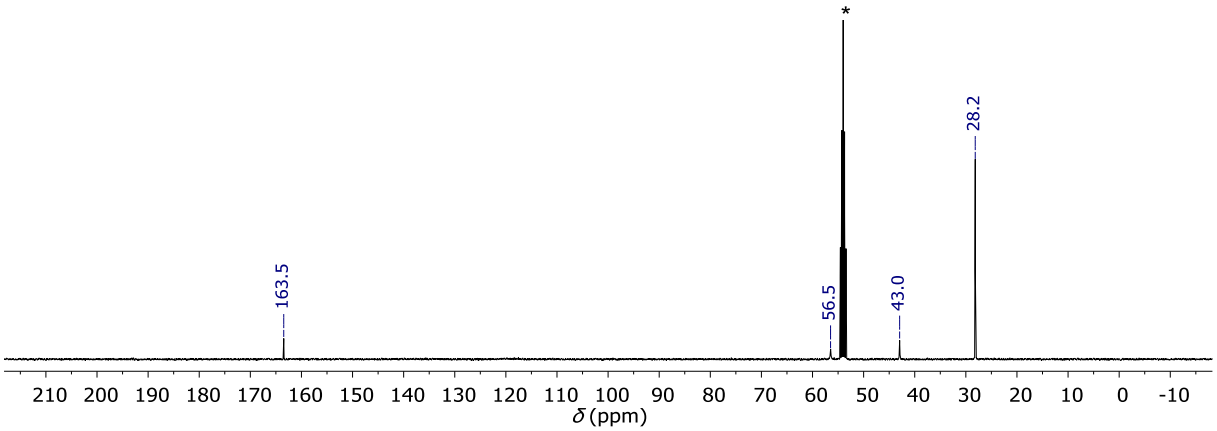

Figure S37: $^{13}C\{^{1}H\}$ NMR spectrum of **1**·HBF_4 in DCM-d_2 measured at –50 °C (* = solvent signal).

In summary, the NMR experiments disallow to conclude to which N atom the proton in **1**·HBF_4 is bound. Yet, in the solid state, the SCXRD analysis revealed that the proton is located at the phenanthroline N atoms. Therefore, the Lewis structures of **1**·HBF_4 and **1**·$2HBF_4$ / **1**·$2HB(C_6F_5)_4$ represent this conformation.

Synthesis of the HBF_4-salts for the assessment of the pK_{BH^+} value for **1**

Synthesis of $PPh_3 \cdot HBF_4$:

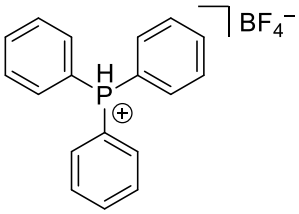

The synthesis was modified from literature.[9]
PPh_3 (1.01 g, 3.81 mmol, 1.0 eq.) was dissolved in toluene (15 mL) and $HBF_4 \cdot Et_2O$ (0.522 mL, 3.81 mmol, 1.0 eq.) was added slowly. The product immediately precipitates as white solid and the resulting suspension was stirred at ambient temperature for 30 min. $PPh_3 \cdot HBF_4$ was isolated by filtration, washed with Et_2O (3x10 mL) and dried *in vacuo* at 120 °C for 3 h. Yield: 0.784 g (2.24 mmol, 58%).

^{1}H NMR (400 MHz, MeCN-d_3): δ = 8.72 (d, $^{1}J_{PH}$ = 527.5 Hz, 1H), 7.95–7.86 (m, 3H, $H_{phenyl,para}$), 7.86–7.57 (m, 12H, $H_{phenyl,meta,ortho}$) ppm.

^{31}P{} NMR (162 MHz, MeCN-d_3): δ = 4.9 (d, $^{1}J_{PH}$ = 528 Hz).

^{31}P{^{1}H} NMR (162 MHz, MeCN-d_3): δ = 4.9 (s) ppm.

^{11}B{} NMR (128 MHz, MeCN-d_3): δ = –1.2 (s) ppm.

^{11}B{^{1}H} NMR (128 MHz, MeCN-d_3): δ = –1.2 (s) ppm.

^{19}F{} NMR (377 MHz, MeCN-d_3) δ = –151.6 (s) ppm.

^{19}F{^{1}H} NMR (377 MHz, MeCN-d_3) δ = –151.6 (s) ppm.

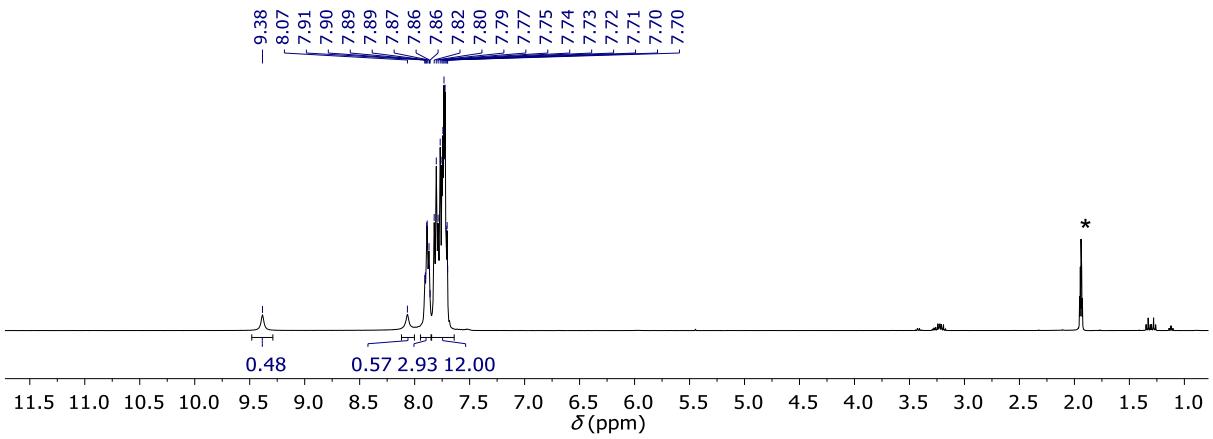

Figure S38: ^{1}H NMR spectrum of $PPh_3 \cdot HBF_4$ in MeCN-d_3 (* = residual solvent signal).

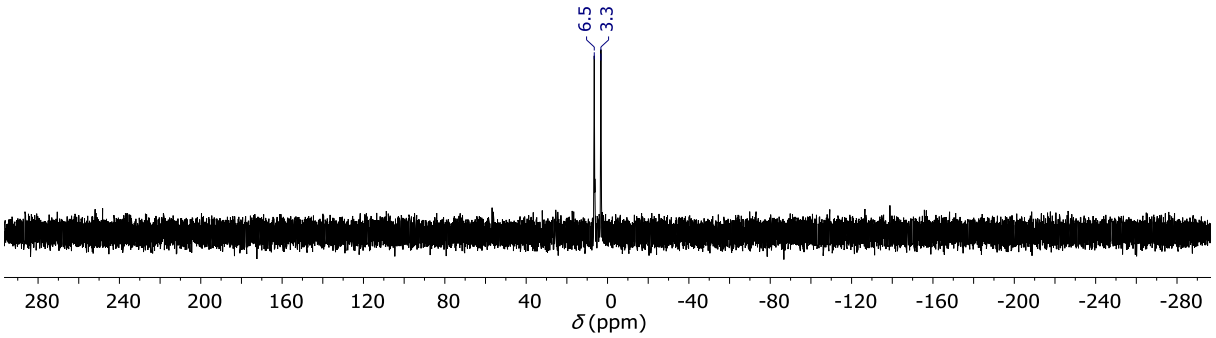

Figure S39: $^{31}P\{\}$ NMR spectrum of $PPh_3 \cdot HBF_4$ in MeCN-d_3.

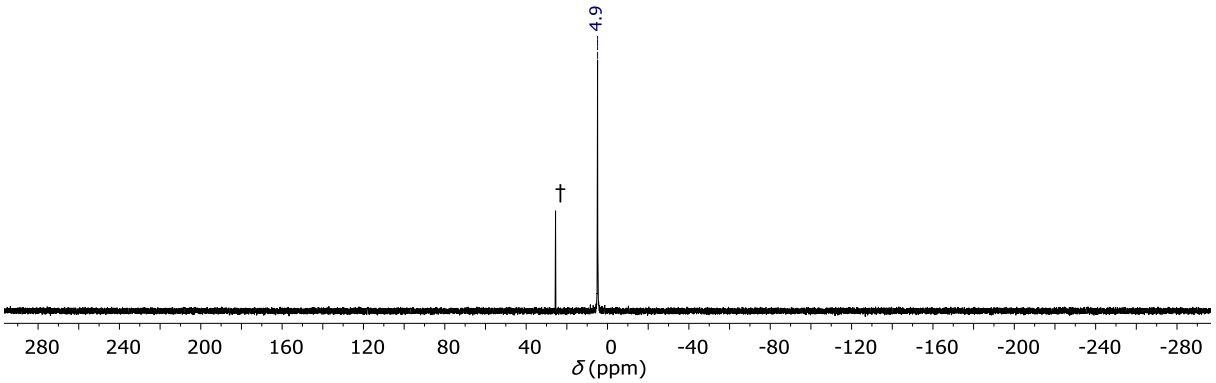

Figure S40: $^{31}P\{^1H\}$ NMR spectrum of $PPh_3 \cdot HBF_4$ in MeCN-d_3 († = 3% hydrolysis).

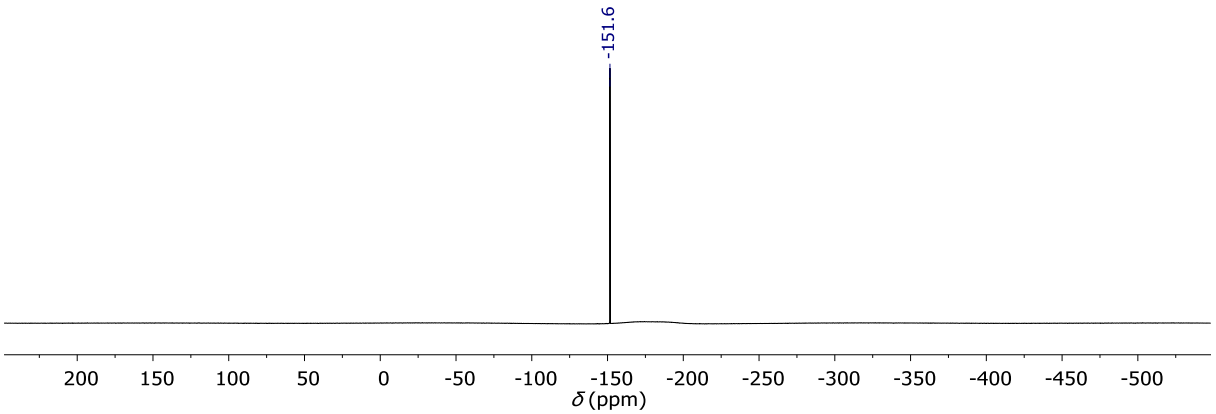

Figure S41: $^{19}F\{\}$ NMR spectrum of $PPh_3 \cdot HBF_4$ in MeCN-d_3.

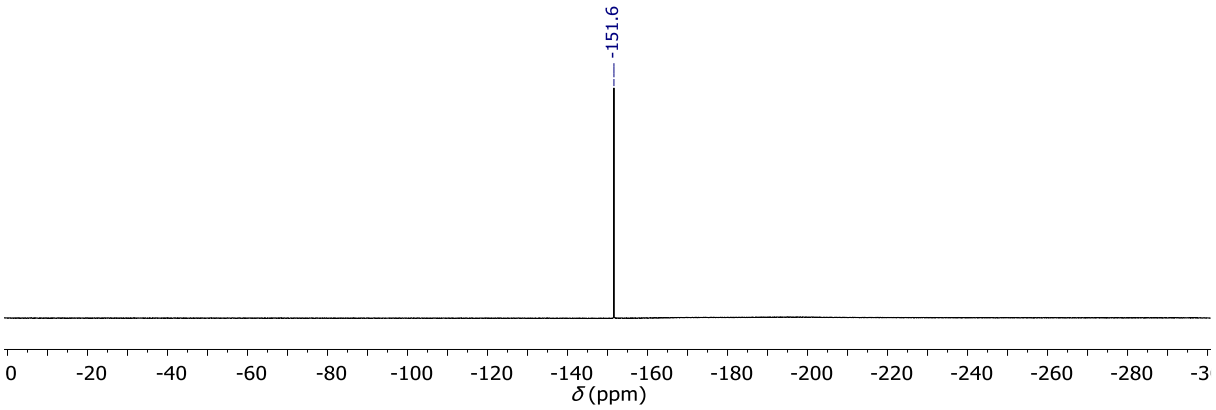

Figure S42: $^{19}F\{^{1}H\}$ NMR spectrum of $PPh_3 \cdot HBF_4$ in MeCN-d_3.

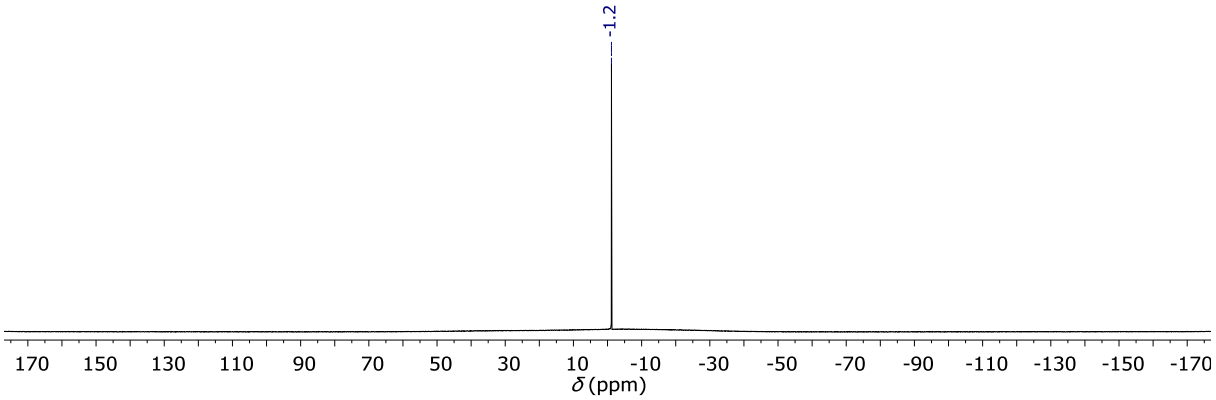

Figure S43: $^{11}B\{\}$ NMR spectrum of $PPh_3 \cdot HBF_4$ in MeCN-d_3.

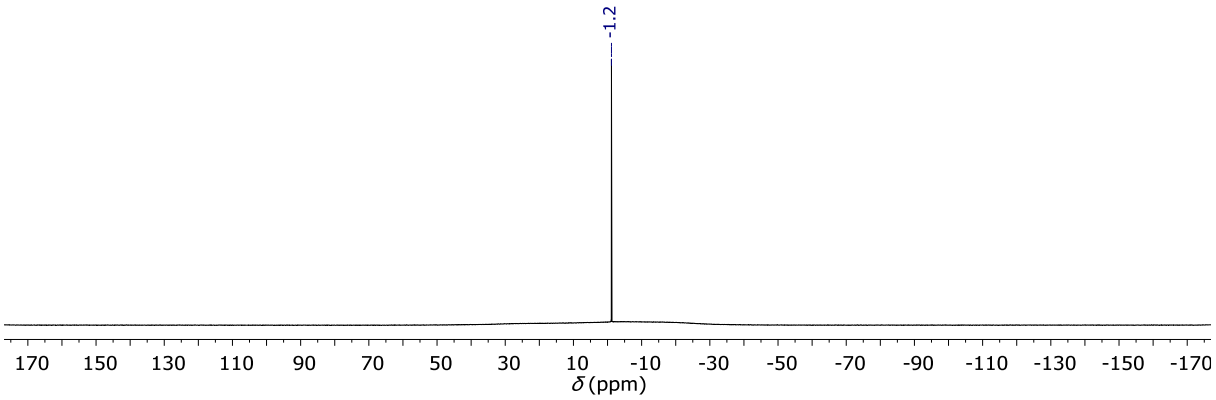

Figure S44: $^{11}B\{^{1}H\}$ NMR spectrum of $PPh_3 \cdot HBF_4$ in MeCN-d_3.

Synthesis of DBU·HBF$_4$:

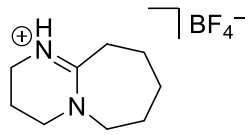

The synthesis was modified from literature.[10]

DBU (5.0 ml, 33.5 mmol 1.0 eq.) was dissolved in H_2O (5 mL) and a solution of 50 w% HBF_4 in H_2O (4.17 mL, 33.5 mmol, 1.0 eq.) was added slowly to the stirring solution. After 1 h at ambient temperature, the solvent was removed under reduced pressure and the crude product was dissolved in DCM (20 mL). *n*-Hexane was added until no further precipitation was observed and DBU·HBF$_4$ was isolated by filtration as white solid and washed with Et_2O (3x15 mL). The product was dried *in vacuo* for 5 h at 120 °C and obtained in 86% yield (6.91 g, 28.8 mmol).

^{1}H NMR (400 MHz, MeCN-d_3): δ = 7.49 (s, 1H, NH), 3.59–3.49 (m, 2H, CH_2), 3.49–3.41 (m, 2H, CH_2), 3.27 (td, J_{HH} = 5.9, 1.2 Hz, 2H, CH_2), 2.68–2.43 (m, 2H, CH_2), 2.01–1.95 (m, 2H, CH_2), 1.80–1.60 (m, 6H, 3xCH_2) ppm.

^{11}B{} NMR (128 MHz, MeCN-d_3): δ = –1.2 (s) ppm.

^{11}B{^{1}H} NMR (128 MHz, MeCN-d_3): δ = –1.2 (s) ppm.

^{19}F{} NMR (377 MHz, MeCN-d_3) δ = –151.8 (s) ppm.

^{19}F{^{1}H} NMR (377 MHz, MeCN-d_3) δ = –151.8 (s) ppm.

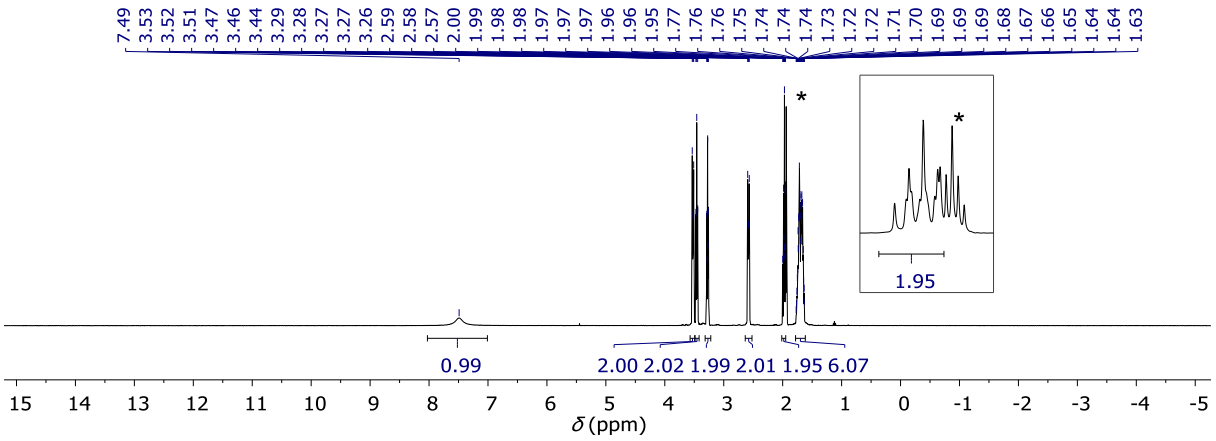

Figure S45: ^{1}H NMR spectrum of DBU·HBF$_4$ in MeCN-d_3 (* = residual solvent signal, overlapping with resonance of product).

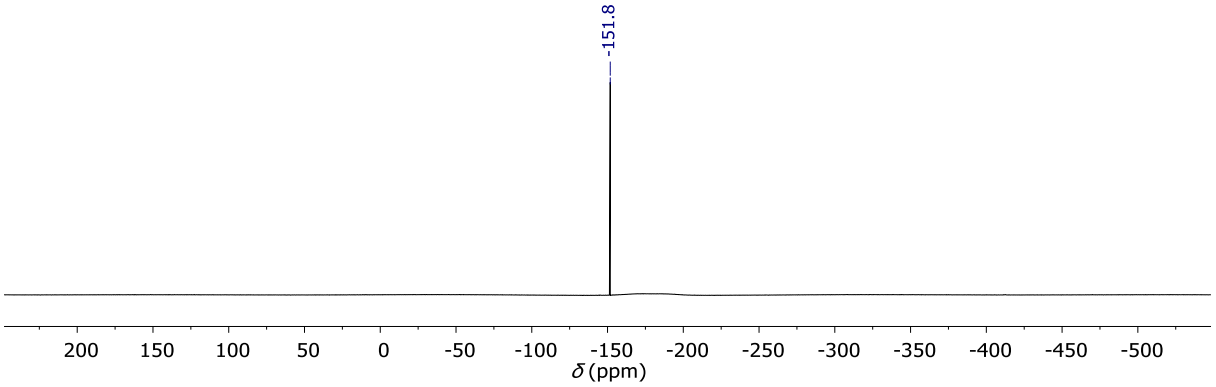

Figure S46: $^{19}F\{^{1}H\}$ NMR spectrum of DBU·HBF_4 in MeCN-d_3.

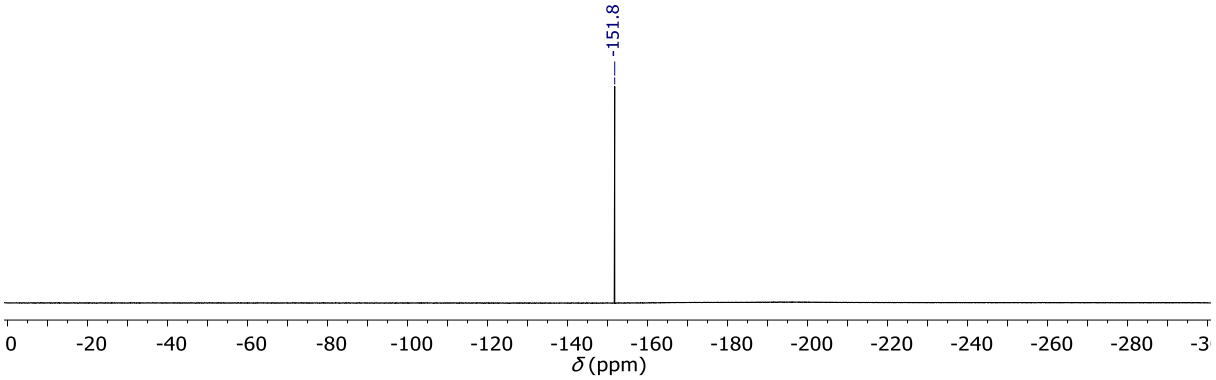

Figure S47: $^{19}F\{\}$ NMR spectrum of DBU·HBF_4 in MeCN-d_3.

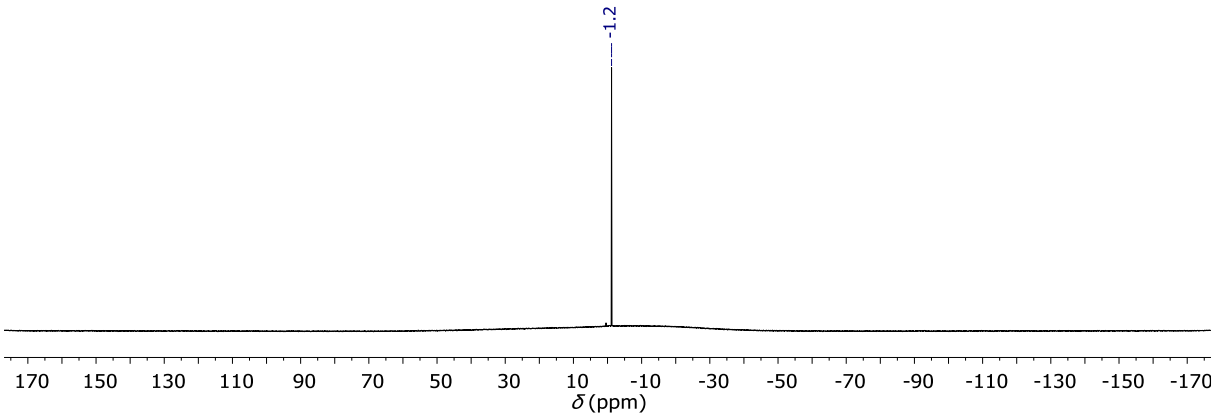

Figure S48: $^{11}B\{\}$ NMR spectrum of DBU·HBF_4 in MeCN-d_3.

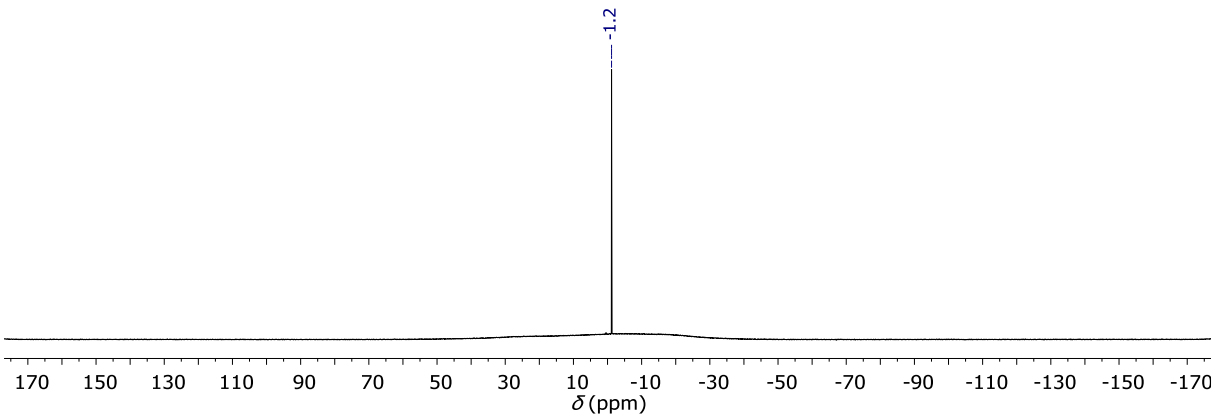

Figure S49: $^{11}B\{^{1}H\}$ NMR spectrum of DBU·HBF_4 in MeCN-d_3.

Synthesis of TBD·HBF_4:

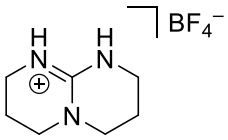

The synthesis was modified from literature.[11]
TBD (306 mg, 2.2 mmol, 1.0 eq.) was dissolved in toluene (5 mL) and HBF_4·Et_2O (0.3 mL, 2.2 mmol, 1.0 eq.) was added slowly. After stirring at ambient temperature for 1 h, the solvent was removed under reduced pressure and the resulting yellow oil was washed with *n*-hexane (3x10 mL). The oil was dried *in vacuo* at 120 °C for 5 h and solidified upon cooling to ambient temperature after 1 h. TBD·HBF_4 was obtained as off-white solid in 86% yield (1.9 mmol, 431 mg).

Some resonances overlap with the solvent residual signal of MeCN-d_3.

^{1}H NMR (400 MHz, MeCN-d_3): δ = 5.99 (s, 2H, NH), 3.27 (t, J_{HH} = 6.0 Hz, 4H, N–CH_2), 3.26–3.19 (m, 4H, N–CH_2), 1.96–1.91 (m, 4H, CH_2–CH_2–CH_2).

^{11}B{} NMR (128 MHz, MeCN-d_3): δ = –1.2 (s) ppm.

^{11}B{^{1}H} NMR (128 MHz, MeCN-d_3): δ = –1.2 (s) ppm.

^{19}F{} NMR (377 MHz, MeCN-d_3) δ = –151.6 (s) ppm.

^{19}F{^{1}H} NMR (377 MHz, MeCN-d_3) δ = –151.6 (s) ppm.

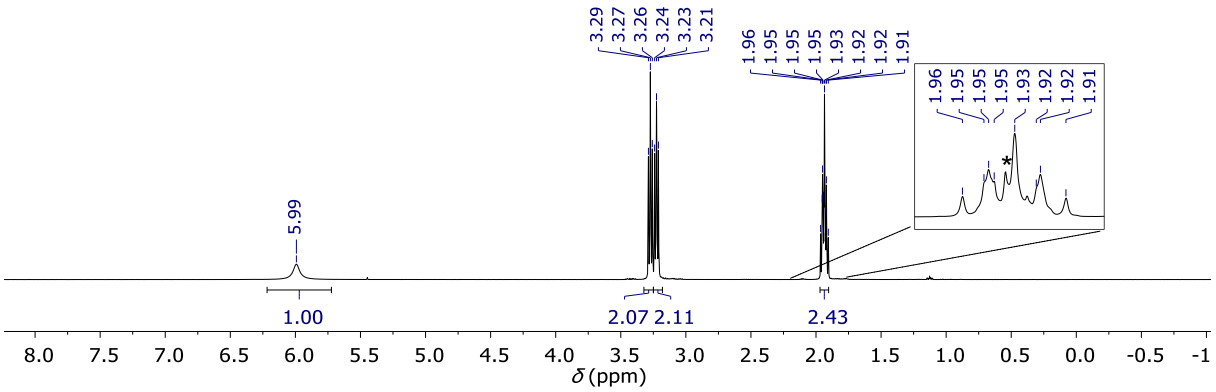

Figure S50: ^{1}H NMR spectrum of TBD·HBF$_4$ in MeCN-d_3 (* = residual solvent signal, overlapping with resonance of product).

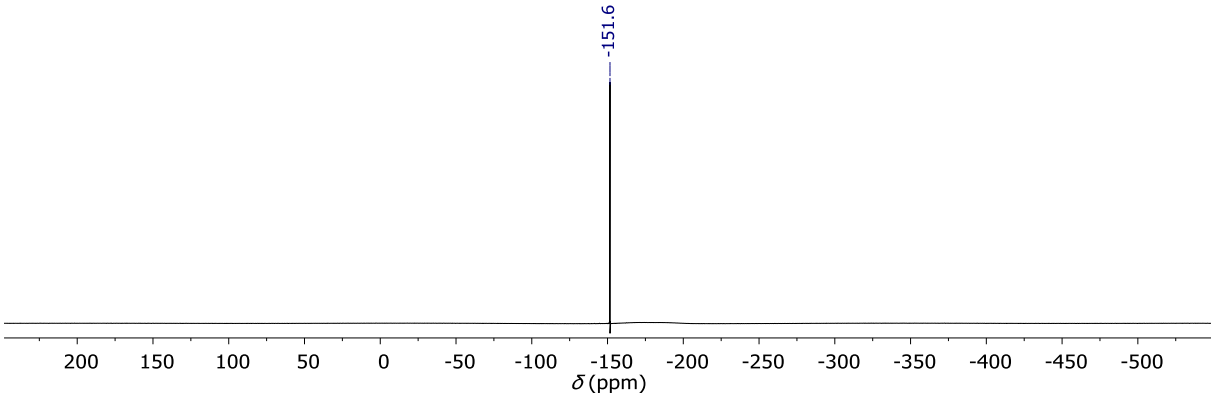

Figure S51: ^{19}F{} NMR spectrum of TBD·HBF$_4$ in MeCN-d_3.

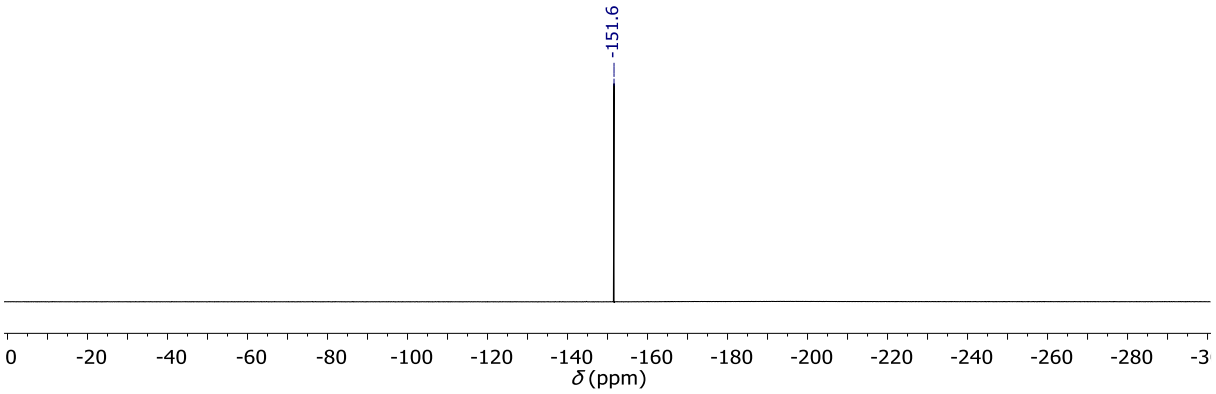

Figure S52: ^{19}F{^{1}H} NMR spectrum of TBD·HBF$_4$ in MeCN-d_3.

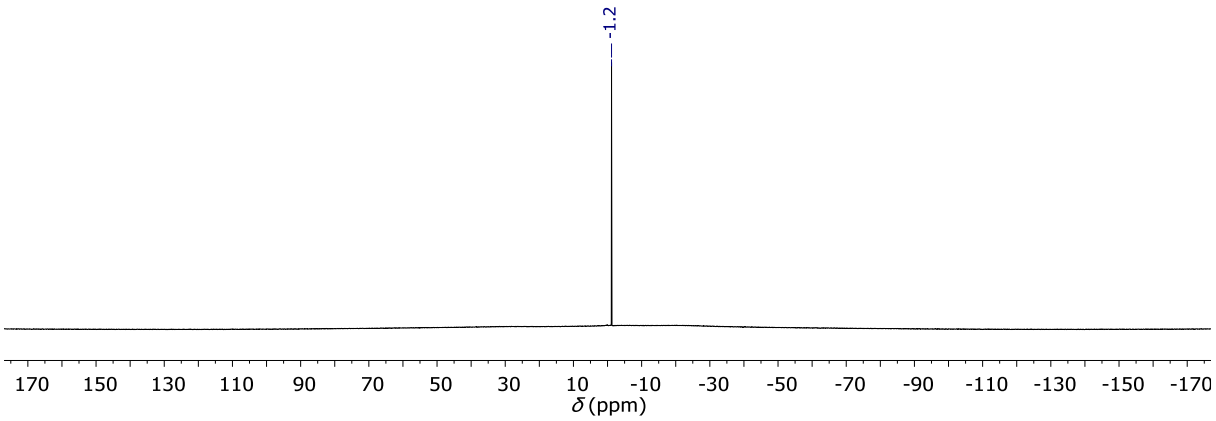

Figure S53: $^{11}B\{\}$ NMR spectrum of TBD·HBF_4 in MeCN-d_3.

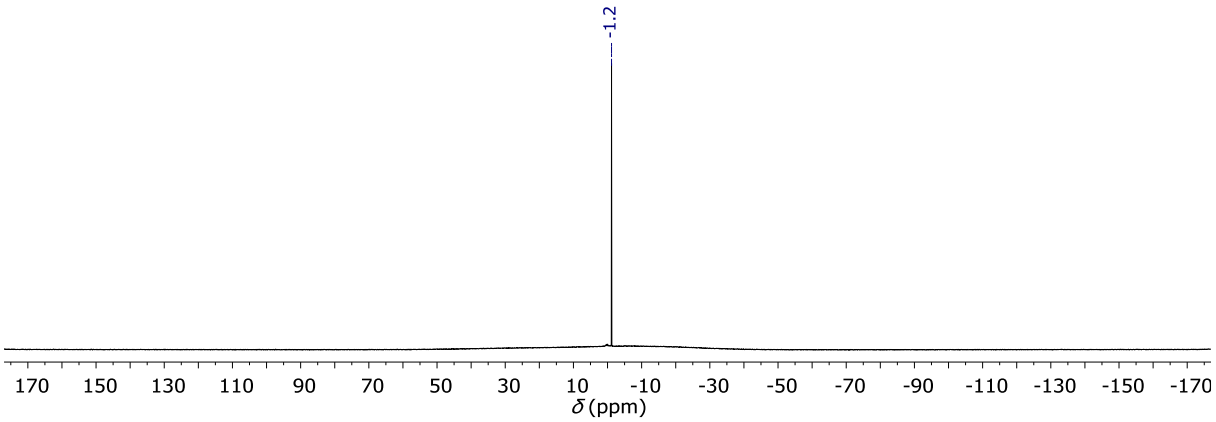

Figure S54: $^{11}B\{^1H\}$ NMR spectrum of TBD·HBF_4 in MeCN-d_3.

Synthesis of $P(tmg)_3 \cdot HBF_4$:

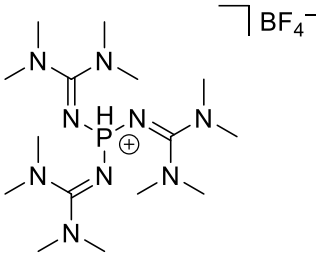

The chloride salt $P(tmg)_3 \cdot HCl$ was prepared according to literature procedure.[12] $P(tmg)_3 \cdot HCl$ (1.00 g, 2.44 mmol, 1.0 eq.) was dissolved in DCM (10 mL), $NaBF_4$ (295 mg, 2.68 mmol, 1.1 eq.) was added and the suspension was stirred at ambient temperature for 16 h. The solids were filtrated off and the solvent of the filtrate was removed under reduced pressure. $P(tmg)_3 \cdot HBF_4$ was dried *in vacuo* at 110 °C for 3 h and obtained in 53% yield (596 mg, 1.29 mmol).

^{1}H NMR (400 MHz, MeCN-d_3): δ = 7.83 (d, $^{1}J_{PH}$ = 539.4 Hz, 1H, PH), 2.85 (d, J = 1.0 Hz, 36H, CH_3) ppm.

^{31}P{} NMR (162 MHz, MeCN-d_3): δ = –16.7 (d, $^{1}J_{PH}$ = 539 Hz).

^{31}P{^{1}H} NMR (162 MHz, MeCN-d_3): δ = –16.7 (s) ppm.

^{11}B{} NMR (128 MHz, MeCN-d_3): δ = –1.2 (s) ppm.

^{11}B{^{1}H} NMR (128 MHz, MeCN-d_3): δ = –1.2 (s) ppm.

^{19}F{} NMR (377 MHz, MeCN-d_3) δ = –151.9 (s) ppm.

^{19}F{^{1}H} NMR (377 MHz, MeCN-d_3) δ = –151.9 (s) ppm.

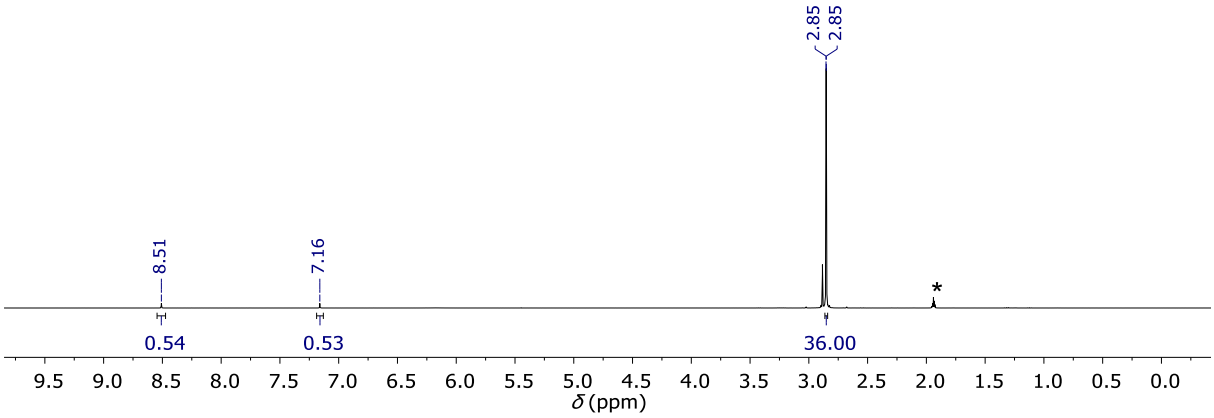

Figure S55: ^{1}H NMR spectrum of $P(tmg)_3 \cdot HBF_4$ in MeCN-d_3 (* = residual solvent signal).

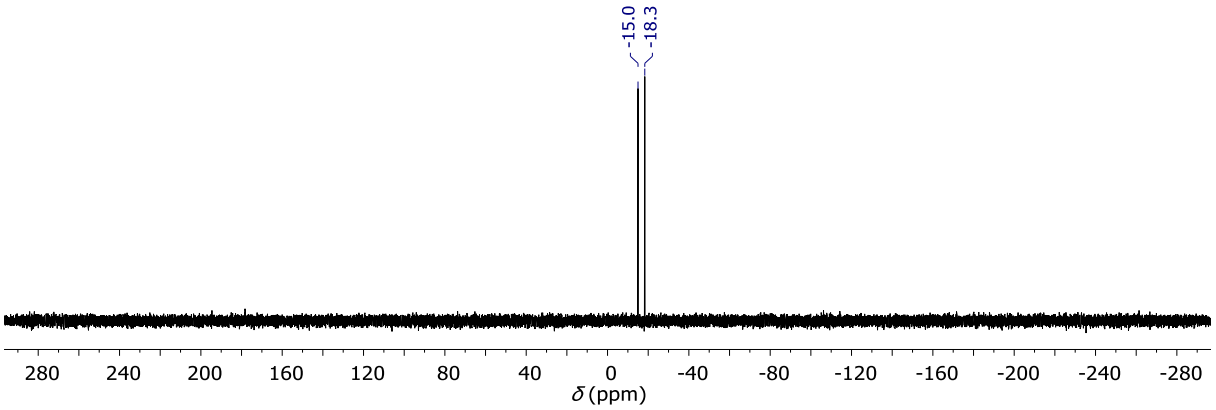

Figure S56: ^{31}P{} NMR spectrum of P(tmg)$_3$·HBF$_4$ in MeCN-d_3.

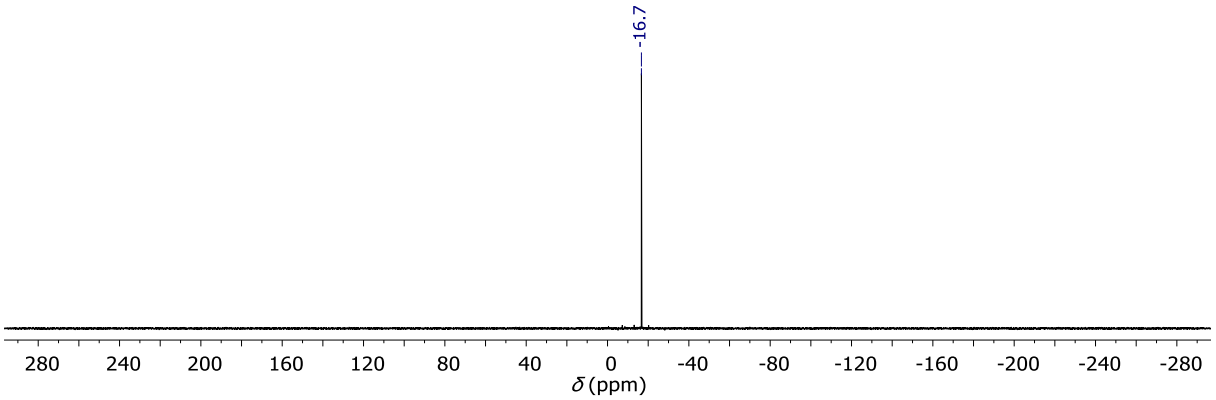

Figure S57: ^{31}P{} NMR spectrum of P(tmg)$_3$·HBF$_4$ in MeCN-d_3.

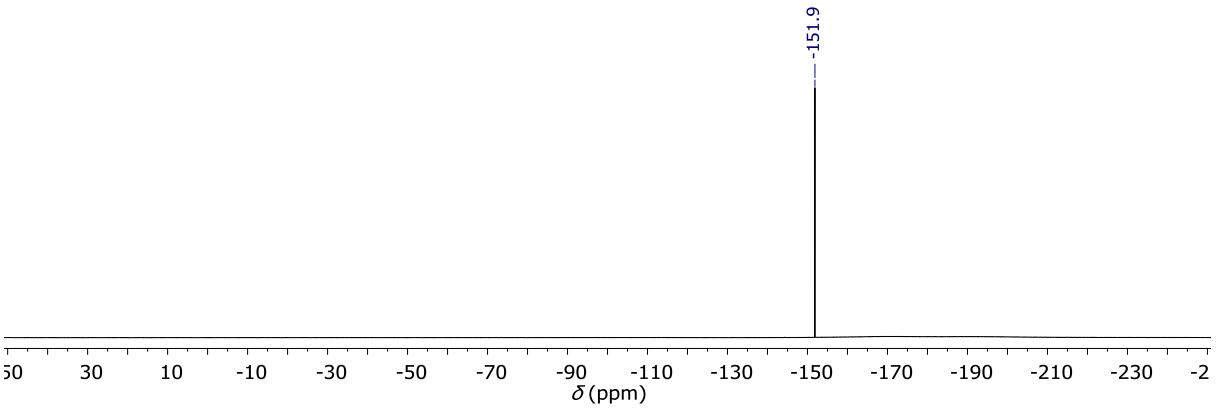

Figure S58: ^{19}F{} NMR spectrum of P(tmg)$_3$·HBF$_4$ in MeCN-d_3.

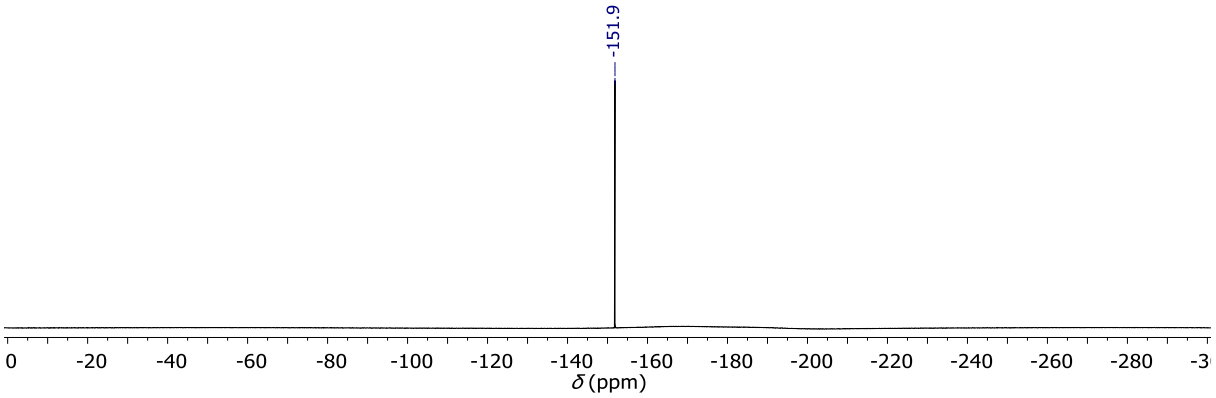

Figure S59: $^{19}F\{^{1}H\}$ NMR spectrum of $P(tmg)_3{\cdot}HBF_4$ in MeCN-d_3.

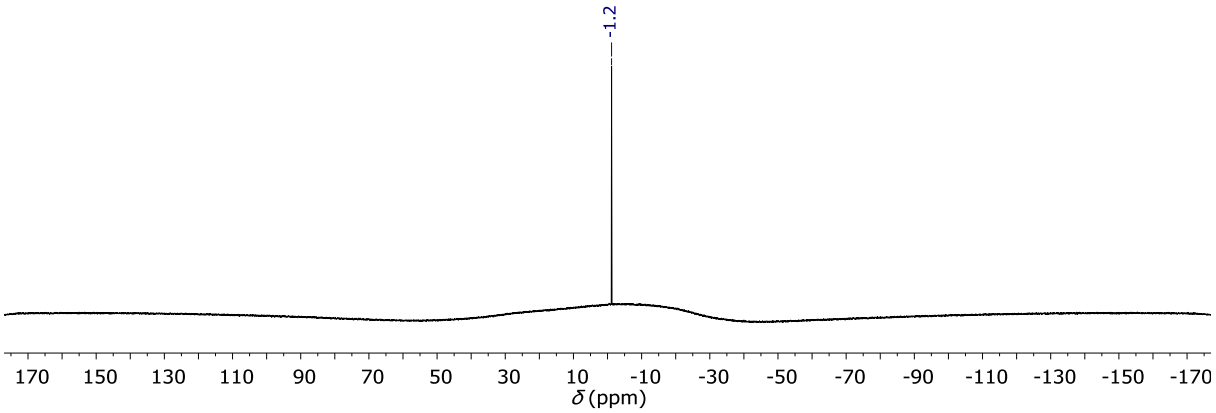

Figure S60: $^{11}B\{\}$ NMR spectrum of $P(tmg)_3{\cdot}HBF_4$ in MeCN-d_3.

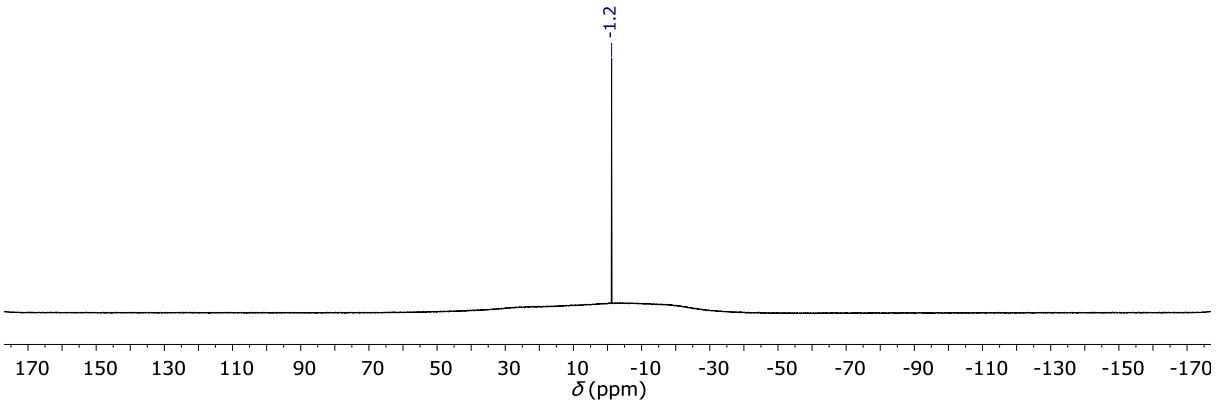

Figure S61: $^{11}B\{^{1}H\}$ NMR spectrum of $P(tmg)_3{\cdot}HBF_4$ in MeCN-d_3.

Electrochemical Investigations

Cyclic voltammetry (CV) and differential pulse voltammetry (DPV):

All electrochemical investigations were carried out using dry and degassed MeCN as solvent with 0.1 M solution of [*n*-BuN_4][PF_6] (**1**, **2**·2MeCN, 1,10-phenahtroline) or [*n*-BuN_4][$B(C_6H_3(CF_3)_2)_4$] (**1**·$HB(C_6F_5)_4$) as electrolyte. The voltammograms were referenced internally against the decamethylferrocene/decamethylferrocenium (Fc^*/Fc^{*+}) redox pair but are reported and depicted against ferrocene/ferrocenium (Fc/Fc^+).[13] Fc* needed to be used to avoid signal overlapping of the substance with Fc/Fc^+.

A three-electrode setup was used: Glassy Carbon (GC) as working electrode, Pt wire as counter electrode, Ag wire as pseudo-reference electrode.

CV measurements were carried out at scan rates of 25, 50, 100, 250, 500 and 1000 $mV \cdot s^{-1}$ with a step size of 2 mV. Selected voltammograms are stacked and depicted below. DPV measurements were carried out with a step size of 5 mV, a pulse size of 25 mV and a pulse time of 0.1 s.

The *Gamry Interface 1010B* potentiostat was employed and operated using the *Gamry Framework* (v. 7.8.4 Build 8183) software for data collection. The collected data were processed using the *Gamry Echem Analyst* (v. 7.8.4) and *OriginPro 2020* (64-bit, v.9.7.0.185) software.

For a more accurate comparison, CV measurements of freshly sublimed 1,10-phenanthroline (phen) were performed under the same conditions using the same experimental setup as for **1**, **1**·HBF_4 and **2**·2MeCN. Since a full scan showed no fully reversible redox events, the first oxidation potential was used as reference point in **1**, **1**·HBF_4 and **2**·2MeCN. The oxidation and reduction potentials of all compounds are listed in Table S1 for a scan rate of 100 $mV \cdot s^{-1}$ and the respective voltammograms are depicted in Figure S62.

Table S1: Oxidation E^{ox} and reduction E^{red} potentials taken from the cyclic voltammograms measured with a scan rate of 100 $mV \cdot s^{-1}$.

Compound	$E^{ox}_{1^{st}}$	$E^{ox}_{2^{nd}}$	$E^{ox}_{3^{rd}}$	$E^{red}_{1^{st}}$	$E^{red}_{2^{nd}}$
phen	--	--	--	–2.63 V	–2.82 V
1	–0.03 V	0.38 V	0.57	–3.03 V	–3.18 V
1·$HB(C_6F_5)_4$	0.53 V	--	--	–2.19 V	--
2·2MeCN	0.75 V	1.28 V	2.17 V	–2.64 V	--

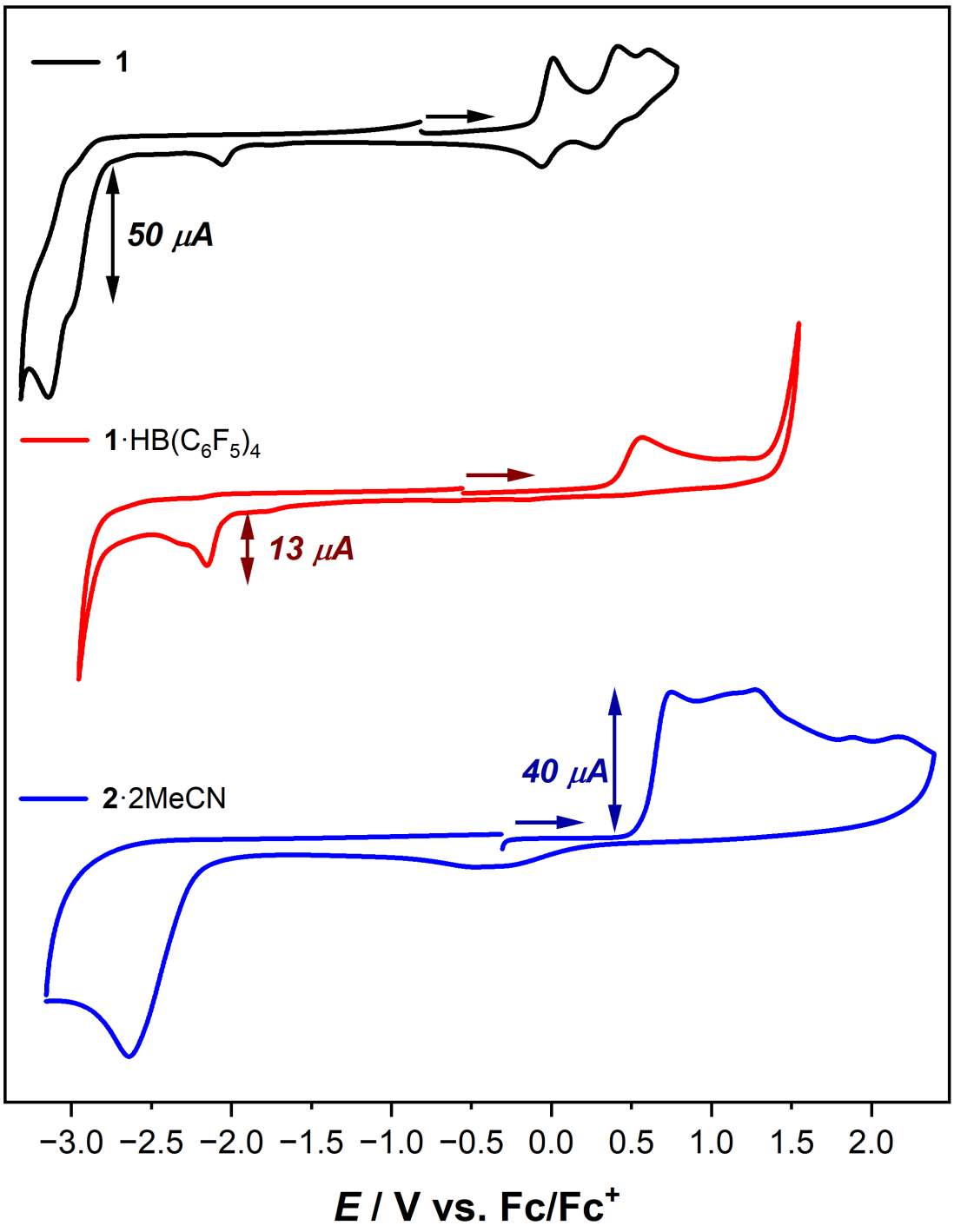

Figure S62: Stacked cyclic voltammograms of **1**, **1**·HB(C_6F_5)$_4$ and **2**·2MeCN at 100 mV·s^{-1}.

Cyclic voltammetry studies of 1,10-phenanthroline

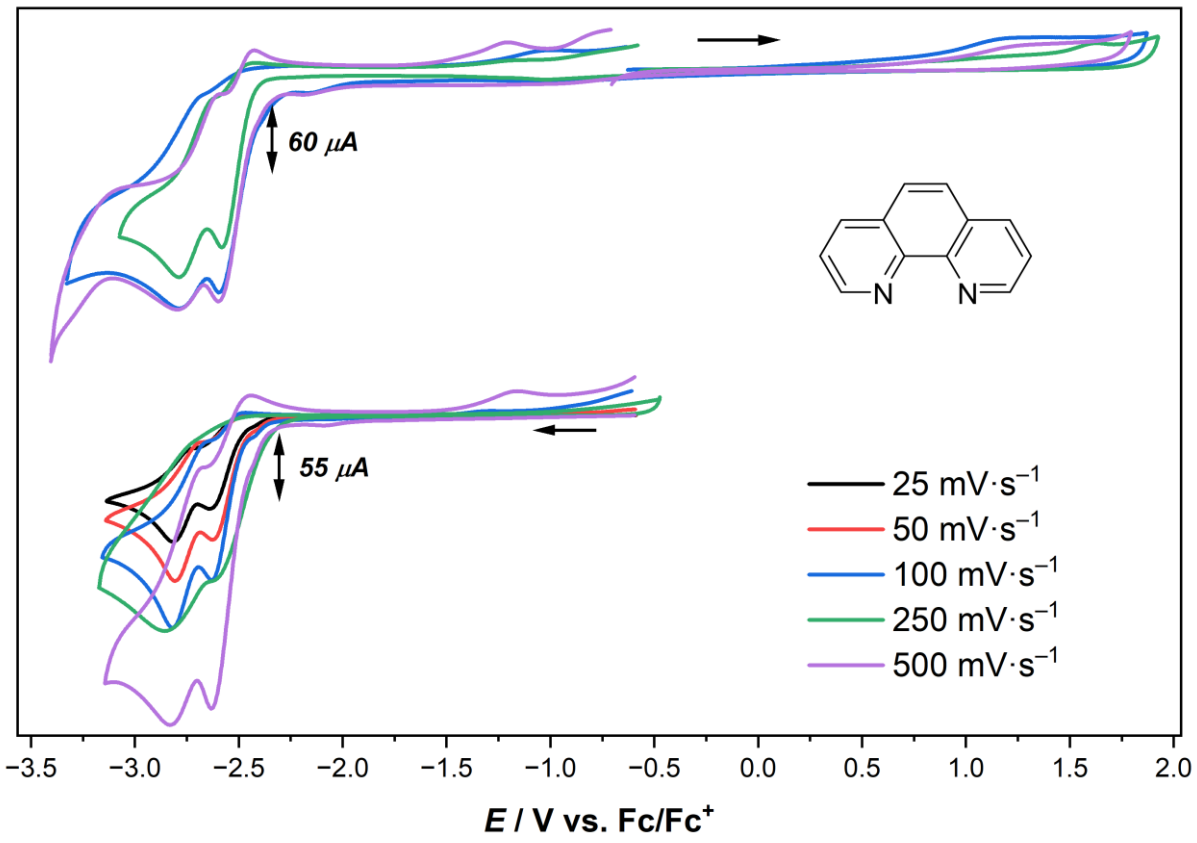

Figure S63: Cyclic voltammogram of 1,10-phenanthroline at different scan rates. Full scan (top) and negative potentials only (bottom).

Cyclic voltammetry studies of **1**

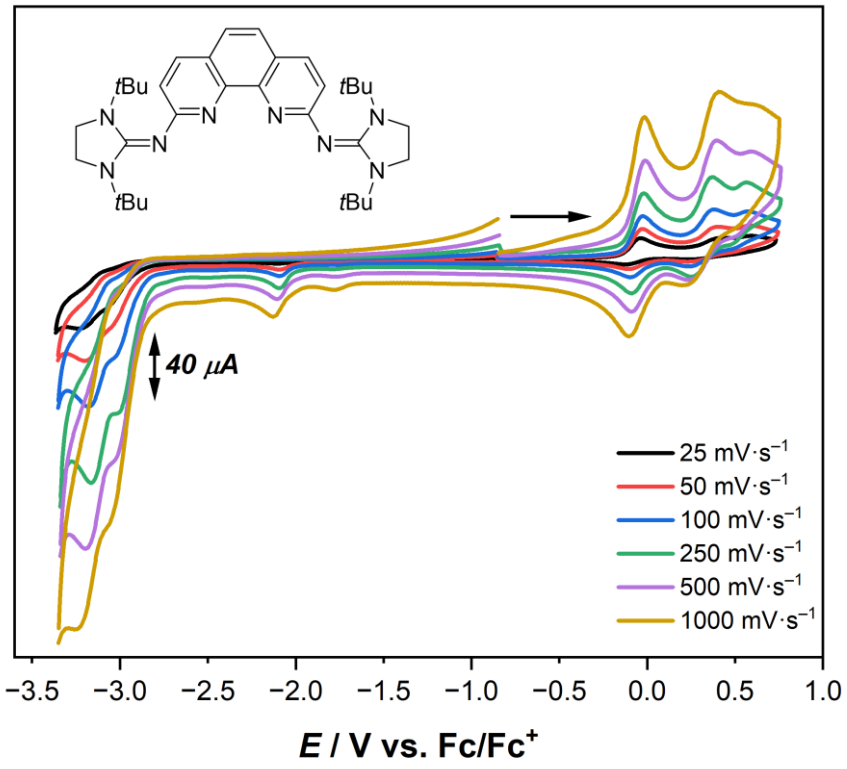

Figure S64: Cyclic voltammogram of **1** at different scan rates.

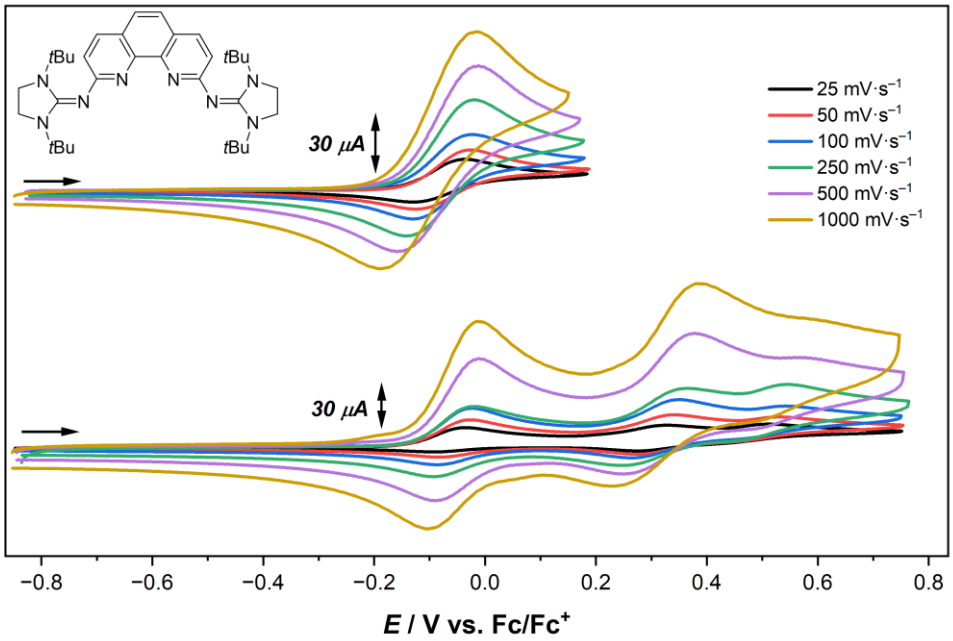

Figure S65: Cyclic voltammogram of the first oxidation event only (top) and all oxidation events (bottom) of **1** at different scan rates.

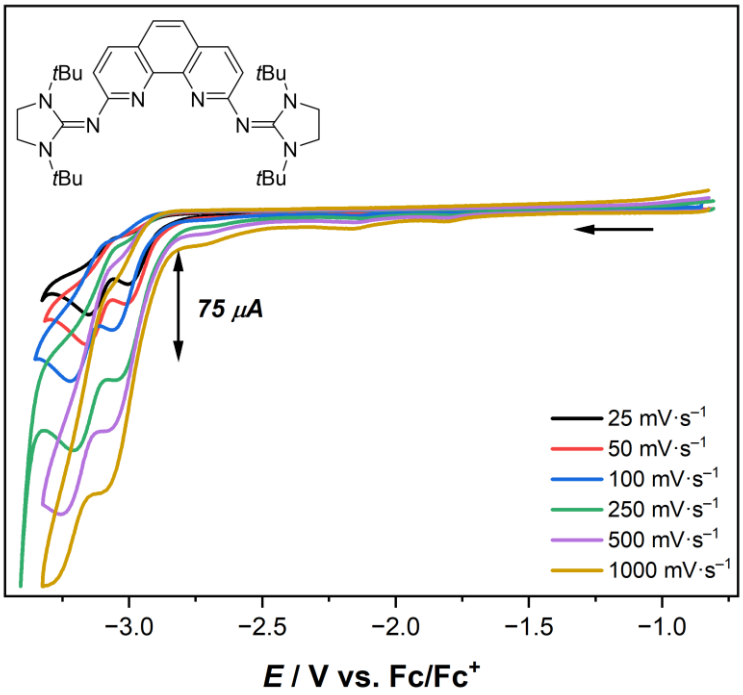

Figure S66: Cyclic voltammogram of **1** for negative potentials at different scan rates.

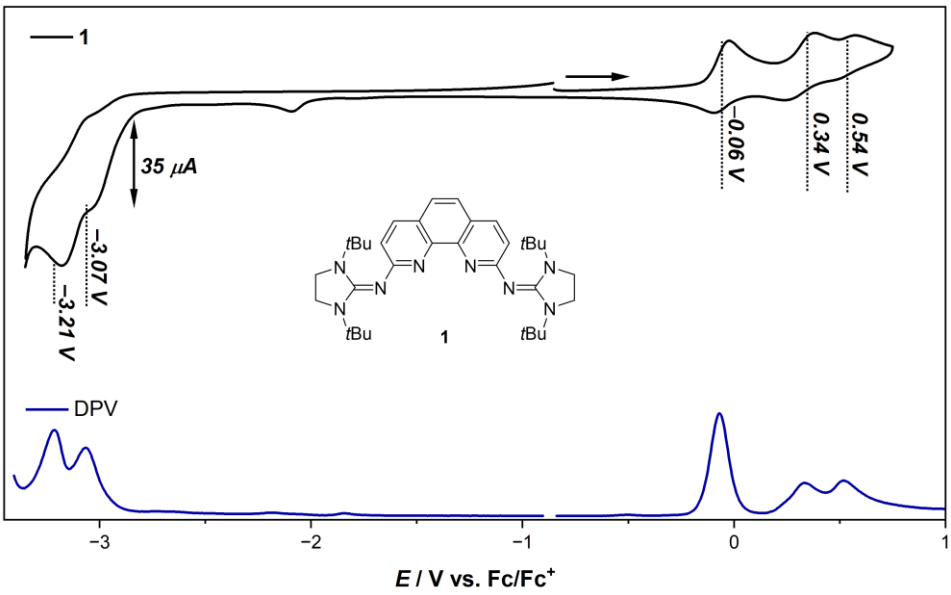

Figure S67: Stacked cyclic voltammogram of **1** at 100 mV·s^{-1} and the corresponding differential pulse voltammogram.

Oxidation events of **1**:

DFT calculations of **1** at the B3LYP/6-31G(d,p) level of theory revealed that the HOMO and HOMO–1 are mostly of π character and mainly distributed across the phenanthroline moiety and imine N atoms (see chapter below for computational details). Therefore, we reasoned that the first oxidation occurs at the HOMO and results in the formation of a radical cation. The positive charge is stabilized through the resonance structures involving the NHI groups similar to the proposed mechanism reported by Henkel.[14] We assume that the second oxidation process occurs at an orbital similar to that of HOMO–1 resulting in the formation of a dication. Again, both positive charges are stabilized through resonance structures involving the NHI groups. For both intermediate species, (partial) reversibility is observed in the CV study. In contrast to Henkel though, a third irreversible oxidation process is observed for **1**, indicating the formation of an unstable tricationic species (see Figure S68).

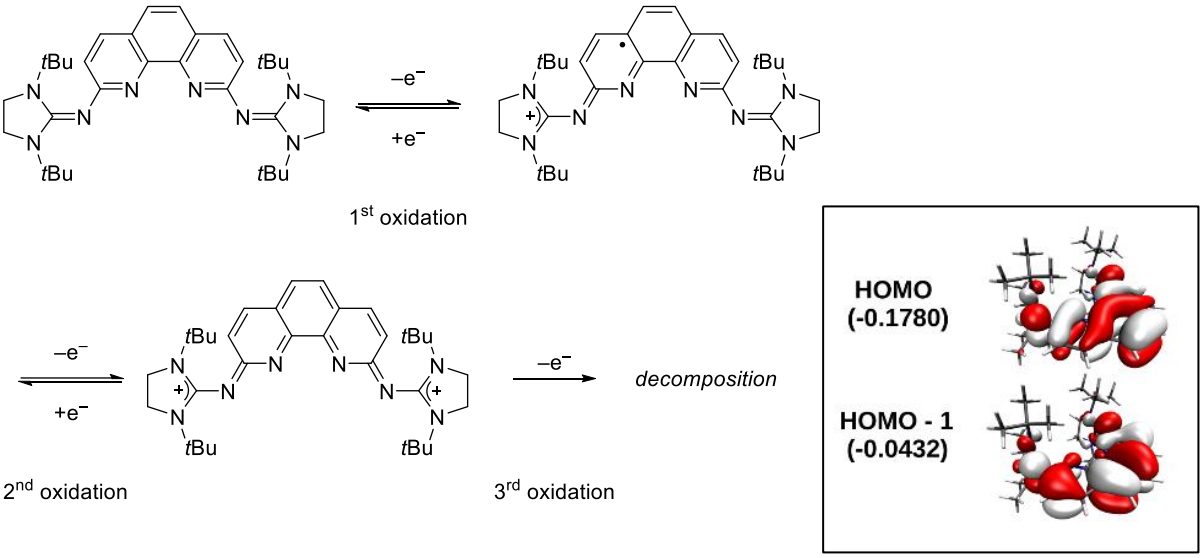

Figure S68: Stepwise oxidation of **1** and chosen resonance structures showing the resonance stabilization involving the NHI substituents (left). HOMO and HOMO–1 plots of **1** (right).

We propose that this is due to the different substitution pattern of the two phenanthroline ligands. In case of the substitution in the 5,6-positions, a Lewis structure can be drawn that depicts the resonance stabilization of the two positive charges within the guanidyl moieties as well as an aromatic bipyridine subunit that follows the Hückel's rule (Figure S69).[14] In contrast, a similar resonance structure cannot be drawn for **1** and the Hückel's rule is not fulfilled. Following this premise, the missing aromaticity in the intermediate $\mathbf{1}^{2+}$ renders it easier to be irreversibly oxidized a third time, eventually leading to decomposition of the transient $\mathbf{1}^{3+}$.

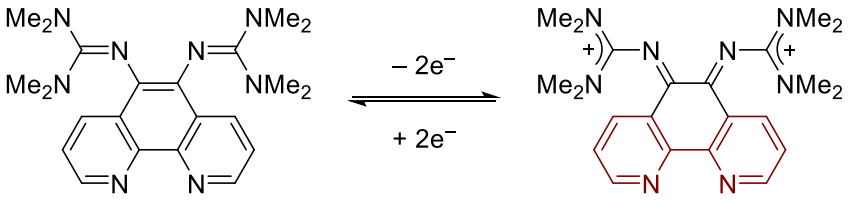

Figure S69: Resonance stabilized dication of the bisguanidyl-substituted phenanthroline ligand reported by Henkel after two-fold oxidation in the CV study. The aromatic bipyridine subunit following the Hückel's rule is highlighted in red.

Cyclic voltammetry studies of **1**·HB(C_6F_5)$_4$

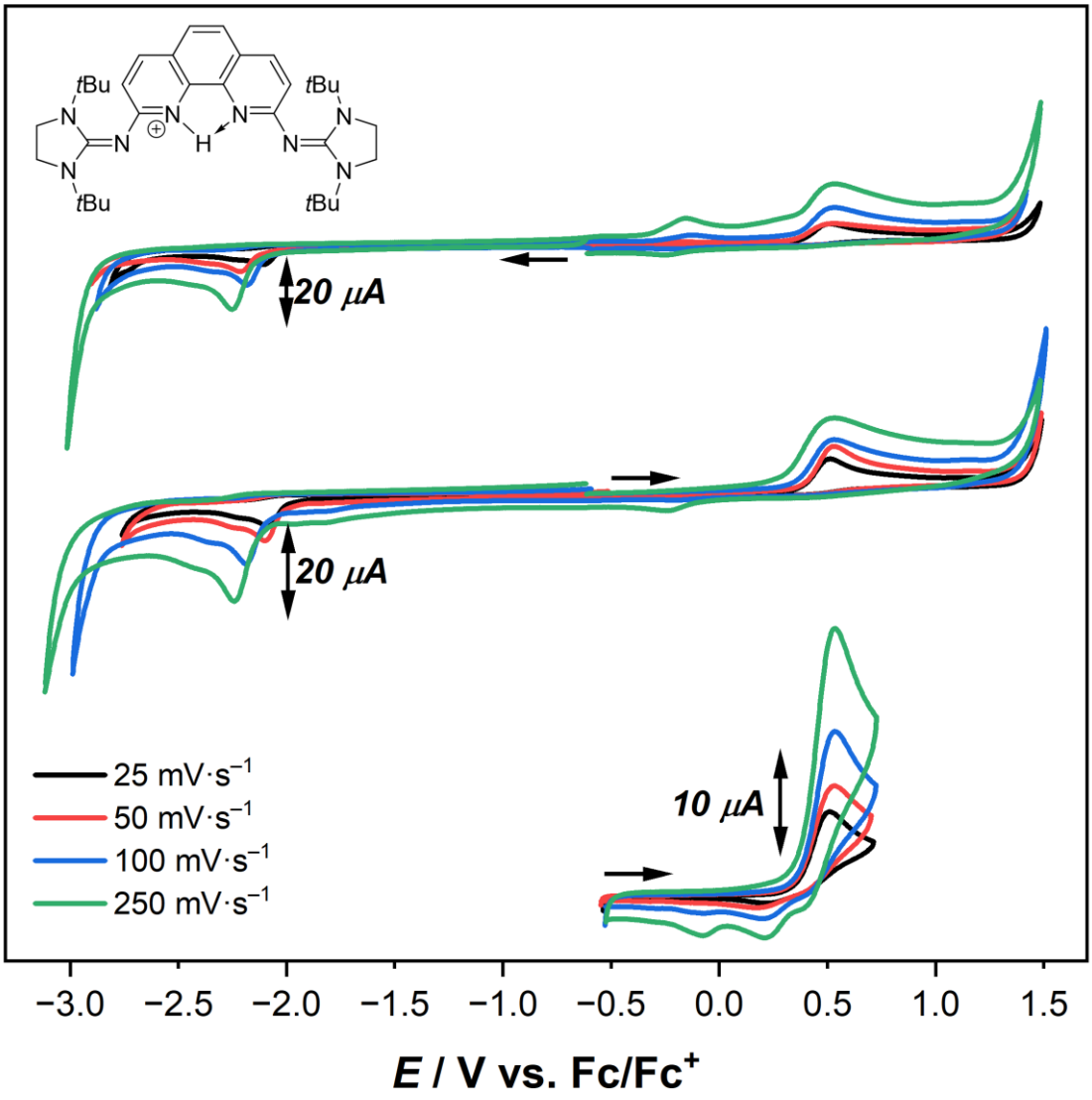

Figure S70: Cyclic voltammogram of **1**·HB(C_6F_5)$_4$ at different scan rates. Full scans (top and middle) and of the first oxidation event only (bottom).

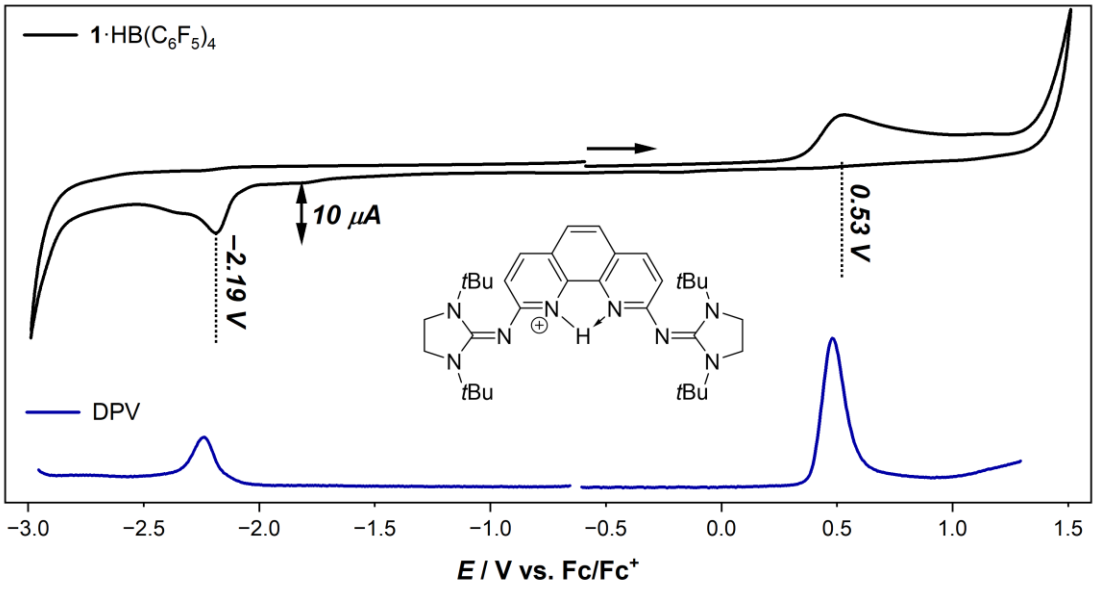

Figure S71: Stacked cyclic voltammogram of **1**·HB(C_6F_5)$_4$ at 100 mV·s^{-1} and the corresponding differential pulse voltammogram.

Cyclic voltammetry studies of **2**·2MeCN

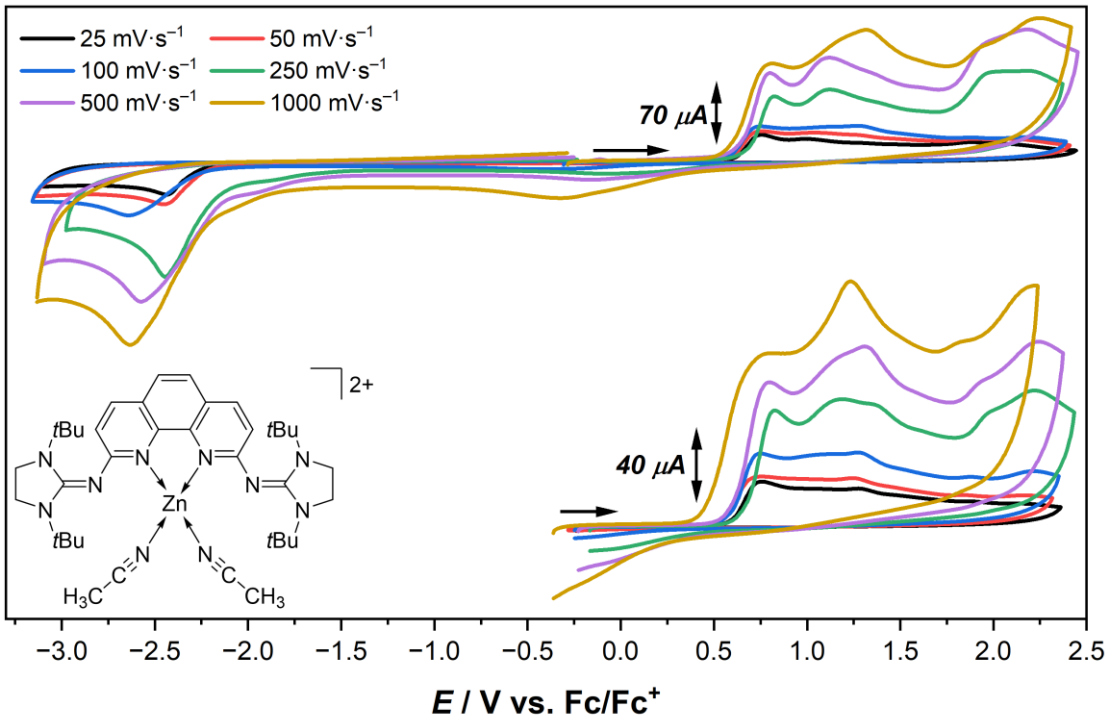

Figure S72: Cylcic voltammograms of **2**·2MeCN. Full scan (top) and for positive potentials only (bottom).

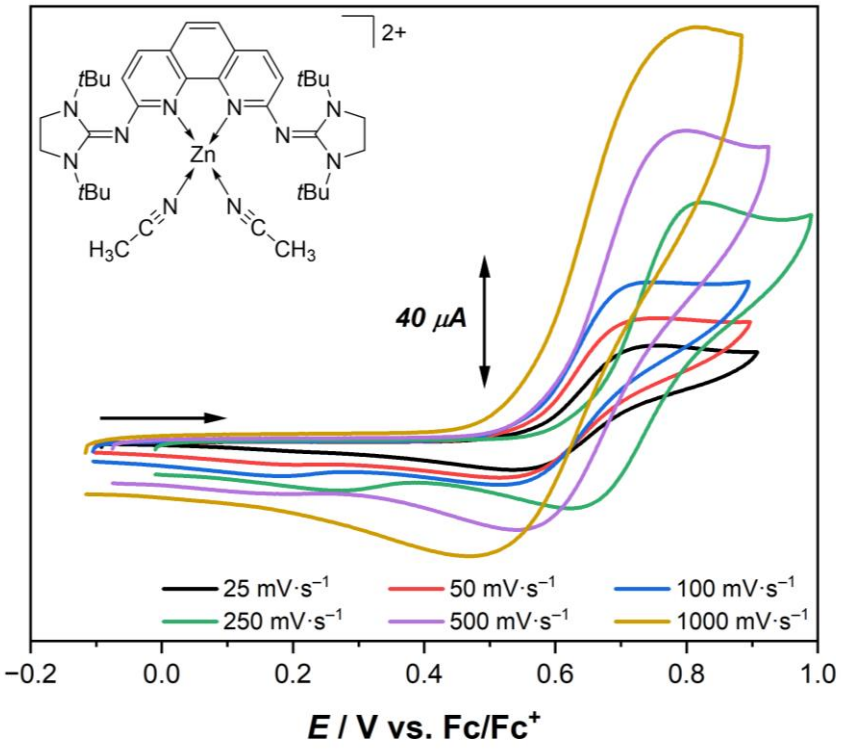

Figure S73: Cyclic voltammogram of **2**·2MeCN of the first oxidation event.

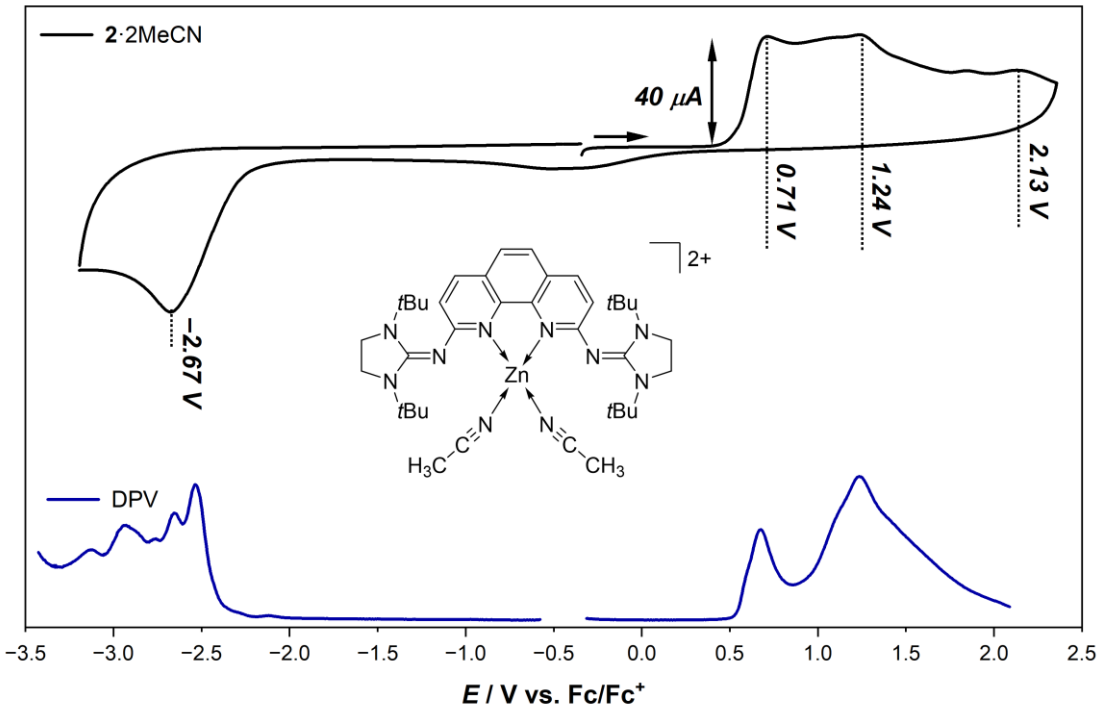

Figure S74: Stacked cyclic voltammogram of **2**·2MeCN and the corresponding differential pulse voltammogram.

Broad signals (CV and DPV) are likely due to dynamic processes of **2**·2MeCN involving dissociation and association processes during the measurement.

Photophysical Investigation

General Information: Absorption spectra were recorded using a *Hewlett-Packard* 4853 diode array spectrometer. Photoluminescence (PL) spectra were recorded using a *Photon Technology International Quanta Master* spectrofluorometer. Excited state lifetime measurements were performed using time-correlated single-photon counting (TCSPC) with an *IBH Fluorocube* apparatus interfaced with a *Horiba FluoroHub+* controller. Quantum yield (QY) measurements were performed using a *Hamamatsu C9920* integrating sphere with a xenon lamp excitation source. Samples for PL, TCSPC, and QY measurements were prepared in a custom-made long glass cuvette that allowed the solutions to be sparged with N_2 and sealed with a PTFE valve.

The IBH Fluorocube apparatus shows a time resolution of FWHM = about 1 nanosecond.

For short lifetimes a FluoTime 300 (PicoQuant GmbH, Germany), with a PDL 820 laser pulse driver and FWHM < 70 picoseconds was used. The photons were collected by using a PMA-C-192 photomultiplier (PMT) single-photon-counting detector. The data was acquired by using the commercially available software EasyTau (Pico-Quant GmbH, Germany), whereas data analysis was performed by using the commercially available software FluoFit (PicoQuant GmbH, Germany).

Compound **1**

Lifetime measurements of **1**:

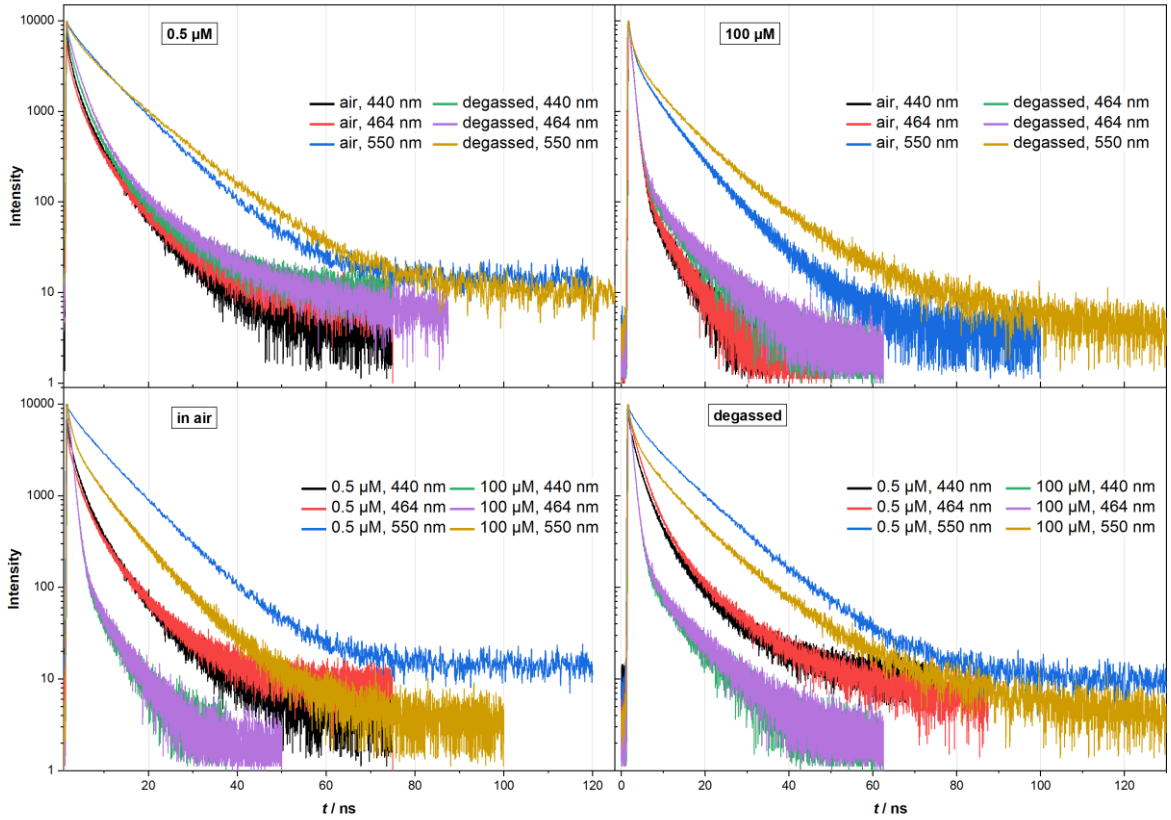

Figure S75: Excited state lifetimes of **1** in THF at **ambient temperature** for the same concentrations of 0.5 or 100 µM, respectively (top) and comparison of different concentrations under identical conditions (bottom). The excitation wavelength is set at 375 nm.

Table S2: Fitted lifetime data for **1** in air or degassed condition at a 0.5 or 100 µM solution in THF at **298 K**.

Conditions	Lifetime τ (ns)		
	emission at λ = 440 nm	emission at λ = 464 nm	emission at λ = 550 nm
0.5 µM-air	τ_1 = 6.78±0.14 (40.4%) τ_2 = 1.901±0.077 (47.54%) τ_3 = 0.156±0.022 (12.01%)	τ_1 = 7.448±0.067 (42.73%) τ_2 = 2.124±0.040 (48.51%) τ_3 = 0.220±0.015 (8.76%)	τ_1 = 8.772±0.054 (90.3%) τ_2 = 2.31±0.33 (8.16%) τ_3 = 0.112±0.056 (1.57%)
0.5 µM-degassed	τ_1 = 8.44±0.11 (29.27%) τ_2 = 2.157±0.025 (61.68%) τ_3 = 0.188±0.011 (9.06%)	τ_1 = 9.40±0.13 (35.13%) τ_2 = 2.523±0.064 (58.59%) τ_3 = 0.266±0.058 (6.28%)	τ_1 = 10.823±0.079 (80.55%) τ_2 = 3.41±0.20 (17.33%) τ_3 = 0.29±0.11 (2.12%)
100 µM-air	τ_1 = 5.439±0.097 (9.33%) τ_2 = 0.7942±0.0072 (86.25%) τ_3 = 0.162±0.026 (4.43%)	τ_1 = 5.739±0.037 (10.302%) τ_2 = 0.7977±0.0033 (84.72%) τ_3 = 0.158±0.035 (4.98%)	τ_1 = 8.937±0.090 (48.9%) τ_2 = 4.21±0.14 (34.3%) τ_3 = 0.689±0.023 (16.79%)
100 µM-degassed	τ_1 = 8.242±0.077 (13.323%) τ_2 = 0.947±0.0062 (63%) τ_3 = 0.51±0.12 (24%)	τ_1 = 8.24±0.11 (15.22%) τ_2 = 0.864±0.024 (77.8%) τ_3 = 0.217±0.084 (7.0%)	τ_1 = 14.17±0.59 (32.8%) τ_2 = 6.29±0.24 (52.5%) τ_3 = 0.805±0.019 (14.72%)

The exact evaluation of all lifetime curves of Figure S75 are given in Table S2. In every case, simulation of the curves by three exponential functions reflecting three different lifetimes gave appropriate fittings. The lifetimes range from 0.11±0.05 ns to 14.17±0.59 ns.

Further lifetime measurements using the IBH Fluorocube gave lifetimes of τ_{465nm} = 0.9 (64%) and 8.0 ns (36%) and τ_{550nm} = 1.2 (28%) and 10.2 ns (72%) (Figure S76).

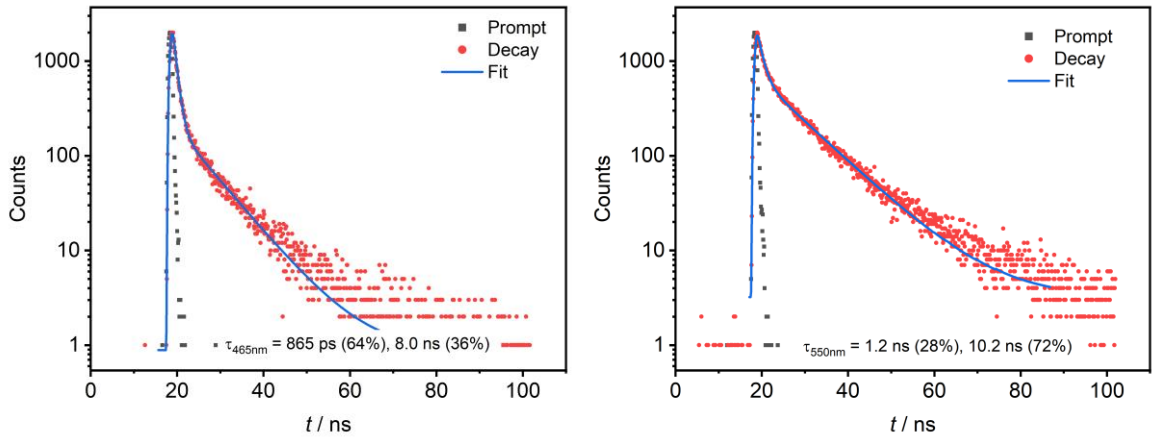

Figure S76: Excited state lifetimes of **1** in THF at **ambient temperature**.

<u>Emission / excitation spectra of **1**</u>:

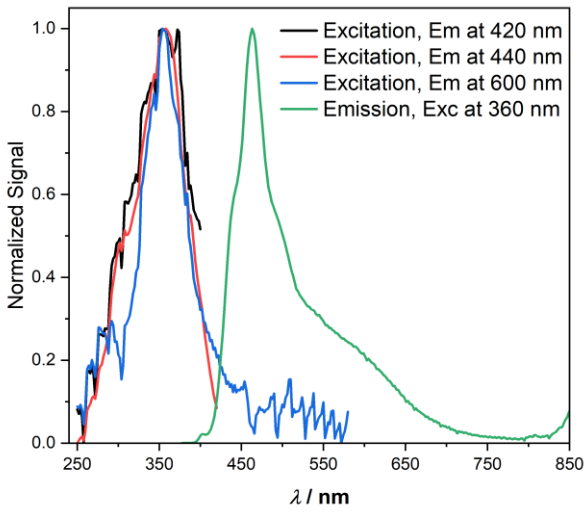

Figure S77: Excitation and emission spectra of a 10 μM solution of 1 in THF at ambient temperature. The excitation spectra are shown for emissions at 420, 440, and 600 nm, respectively. The emission spectrum has been taken for an excitation at 360 nm.

Emission / excitation spectra and lifetime measurements of **1** at **77 K**:

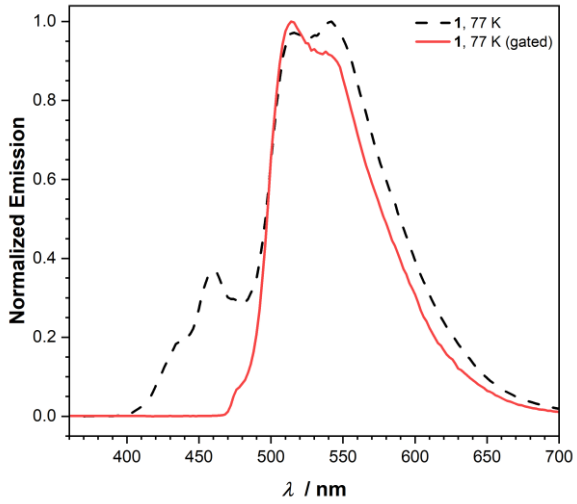

Figure S78: Emission spectra of a 10 µM solution of **1** in glassy 2-methyl-THF at **77 K**. The excitation wavelength was 360 nm. The dashed line contains both fluorescence and phosphorescence, whereas in the gated spectrum the fluorescence was suppressed. These spectra are independent of concentration.

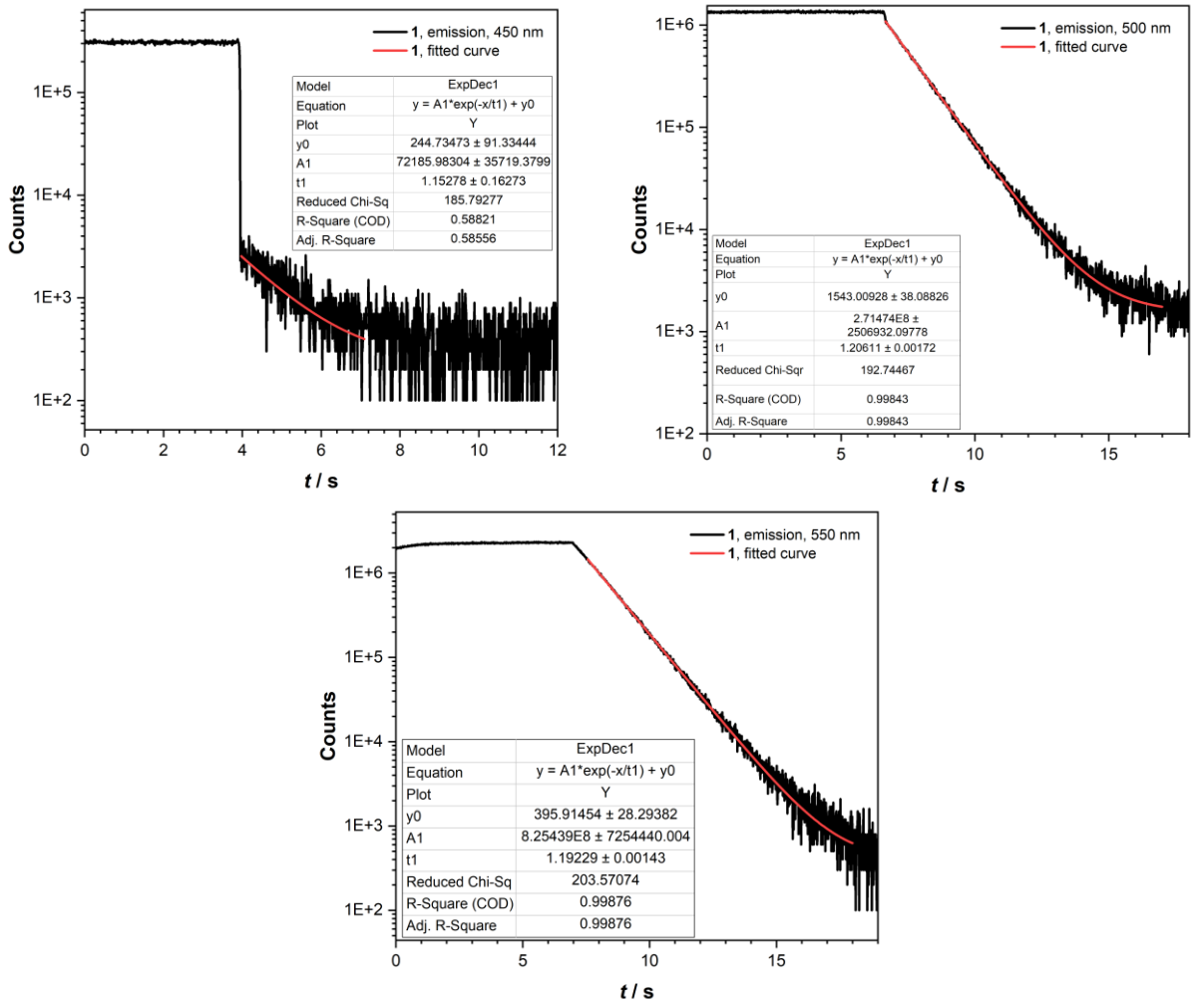

Figure S79: Long-persistent excited state lifetime of a 10 µM solution of **1** in glassy 2-methyl-THF at **77 K**. The emission was measured at 450 nm (left, above), 500 nm (right, above), 550 nm (middle, below). The excitation wavelength was 360 nm.

Beer's law plot of **1**:

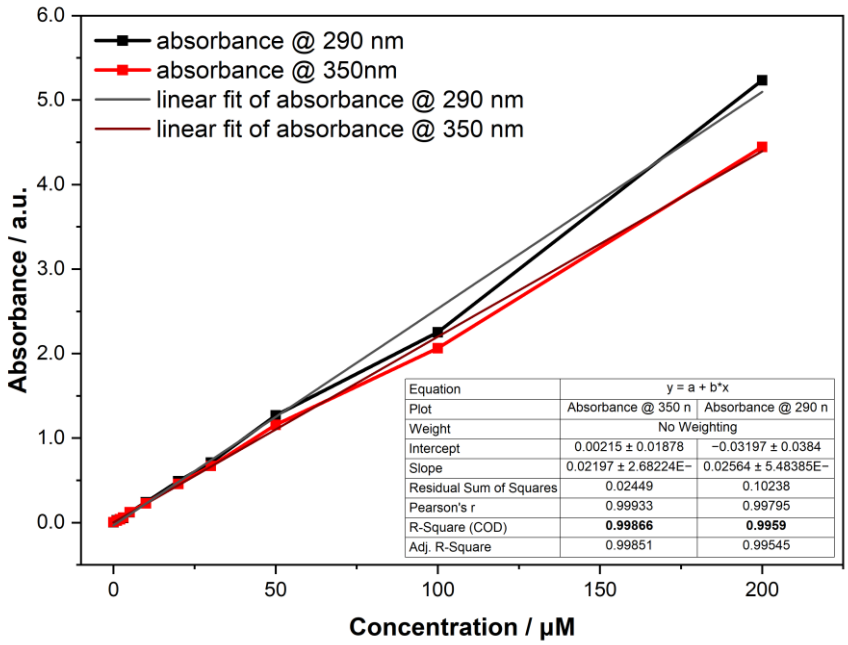

Equation	y = a + b*x	
Plot	Absorbance @ 350 n	Absorbance @ 290 n
Weight	No Weighting	
Intercept	0.00215 ± 0.01878	−0.03197 ± 0.0384
Slope	0.02197 ± 2.68224E−	0.02564 ± 5.48385E−
Residual Sum of Squares	0.02449	0.10238
Pearson's r	0.99933	0.99795
R-Square (COD)	**0.99866**	**0.9959**
Adj. R-Square	0.99851	0.99545

Figure S80: Plot and linear fit of absorbance versus concentration of **1** at different wavelengths measured in THF at **ambient temperature**.

Emission / excitation spectra and lifetime measurements of **1** in a polystyrene (PS) matrix:

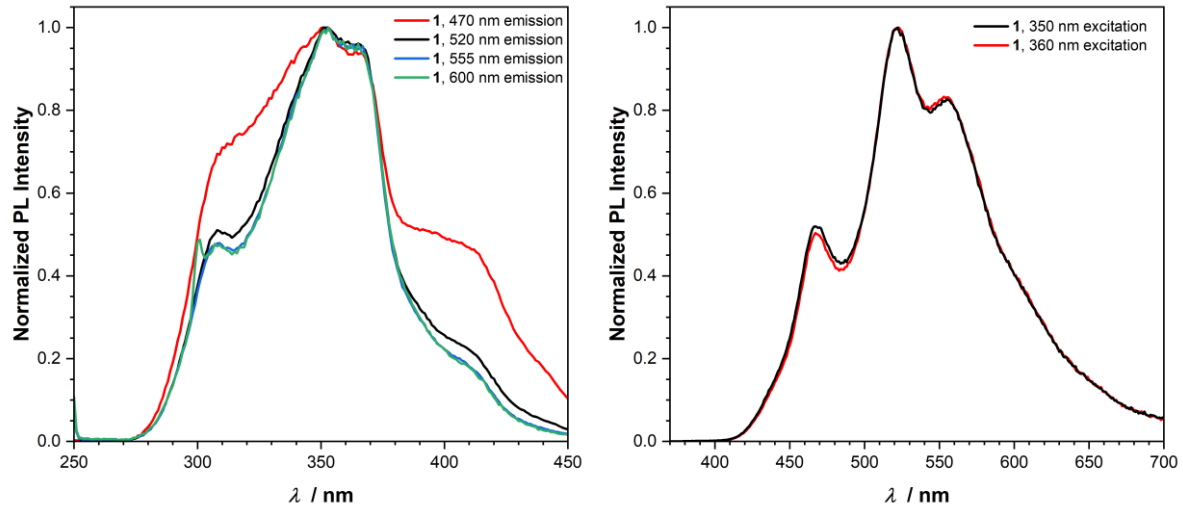

Figure S81: Emission and excitation spectra of **1** in a polystyrene (PS) matrix measured at ambient temperature.

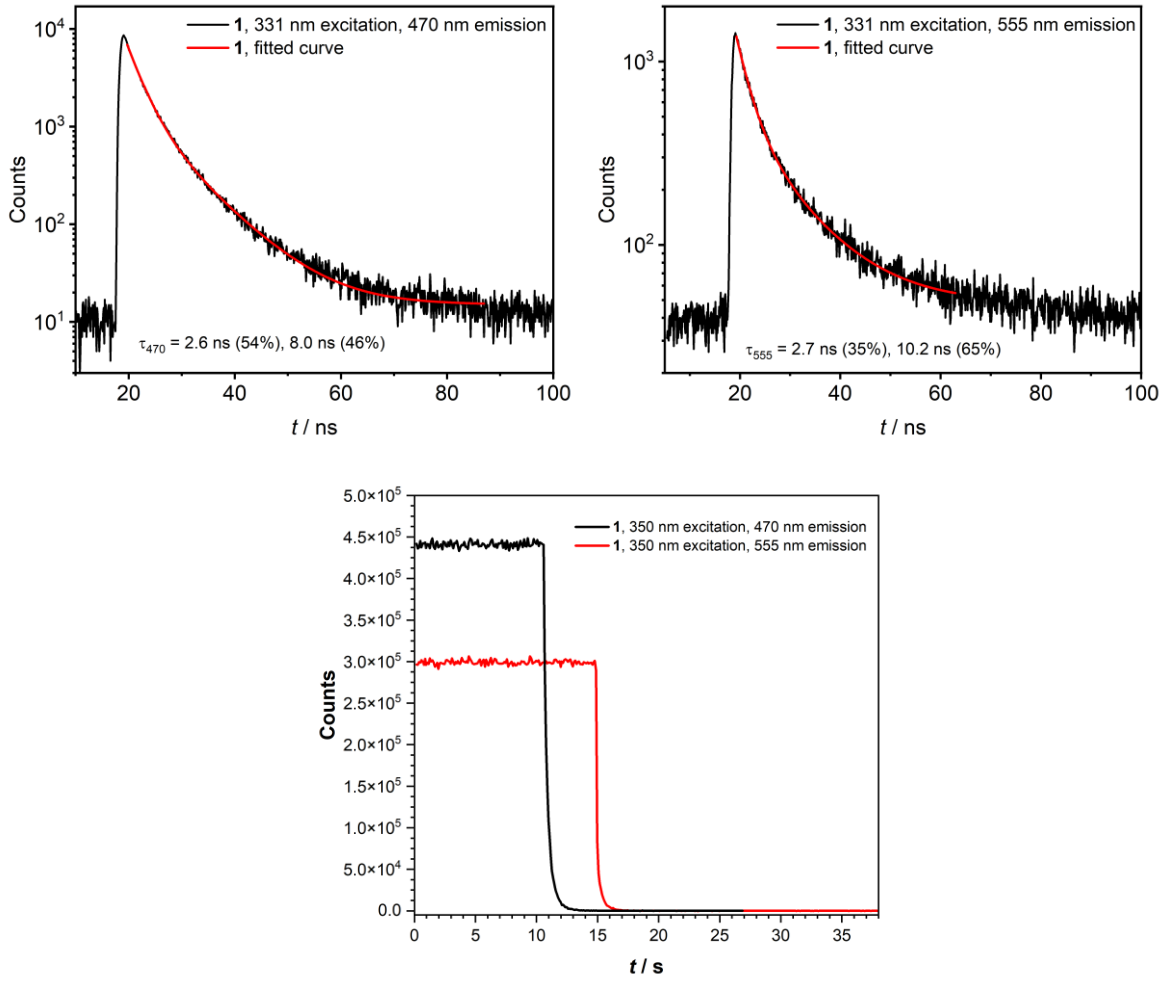

Figure S82: Lifetime measurements of **1** in a polystyrene (PS) matrix measured at ambient temperature.

Compound **1**·HBF_4

Lifetime measurements of **1**·HBF_4:

Table S3: Luminescence lifetimes of a 10 µM solution of **1**·HBF_4 in degassed 2-methyl-THF at **298 K**.

Conditions	Lifetime τ (ns)		
	emission at λ = 450 nm	emission at λ = 500 nm	emission at λ = 550 nm
10 µM-air	τ = 2.04 (77%), 8.17 (23%)	τ = 30.8	τ = 30.9
10 µM-degassed	τ = 3.5 (68%), 15.8 (32%)	τ = 30.3	τ = 30.5

Emission / excitation spectra and lifetime measurements of **1**·HBF_4 at **77 K**:

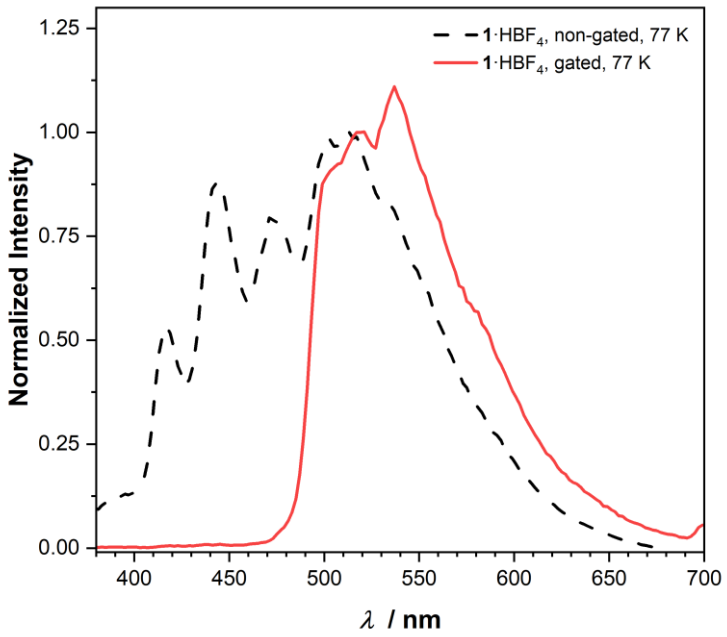

Figure S83: Emission spectra of a 10 µM solution of **1**·HBF_4 in glassy 2-methyl-THF at **77 K**. The excitation wavelength was 360 nm. The dashed line contains both fluorescence and phosphorescence, whereas in the gated spectrum the fluorescence was suppressed. These spectra are independent of concentration.

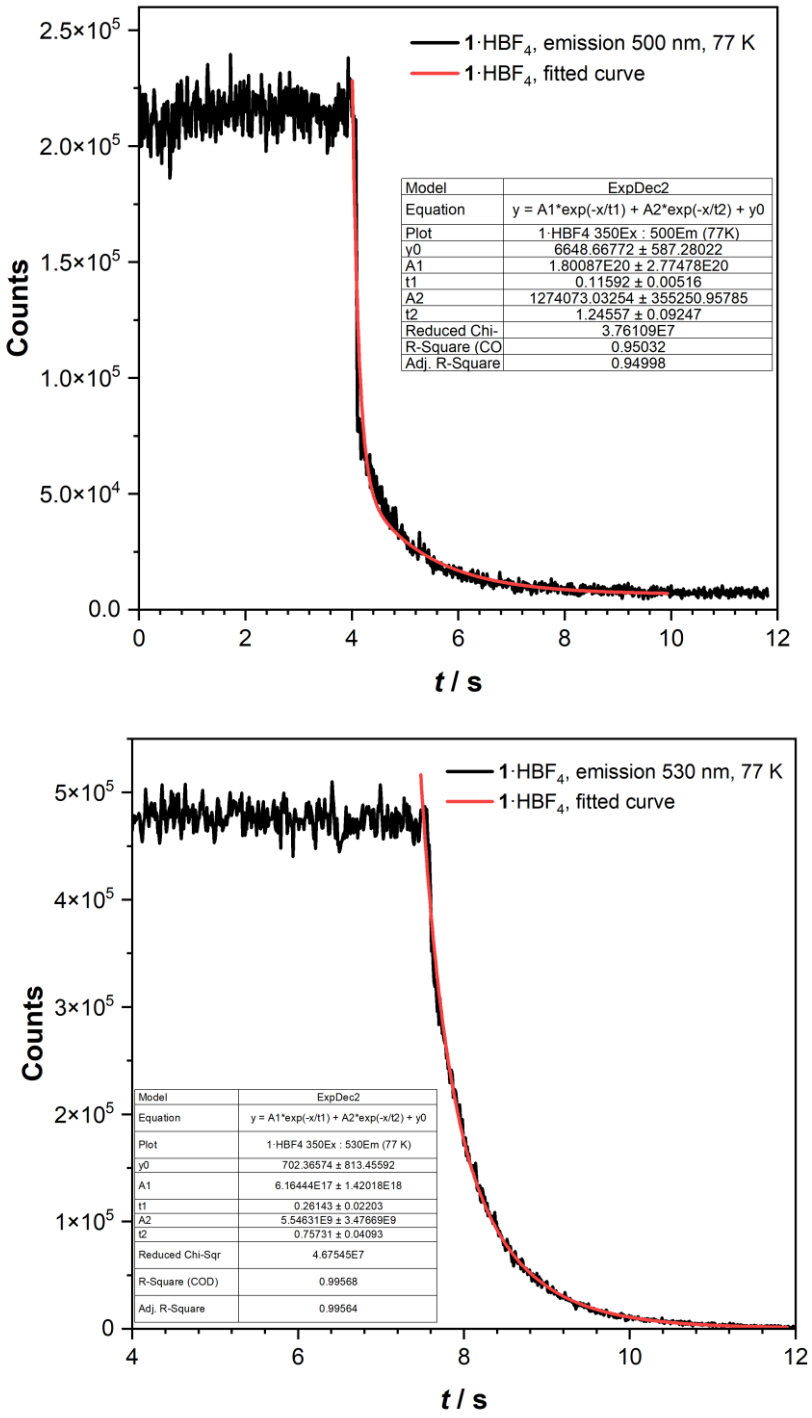

Figure S84: Long-persistent excited state lifetimes of a 10 µM solution of **1**·HBF_4 in glassy 2-methyl-THF at **77 K**. The emissions were measured at 500 nm (top) and 530 nm (bottom). Excitation wavelength was set to 350 nm.

Beer's law plot of **1**·HBF_4:

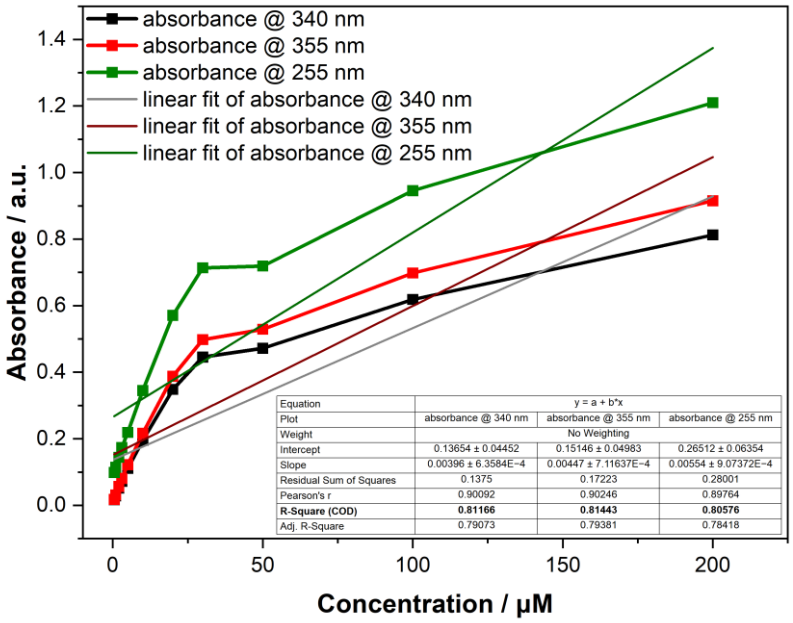

Equation	y = a + b*x		
Plot	absorbance @ 340 nm	absorbance @ 355 nm	absorbance @ 255 nm
Weight	No Weighting		
Intercept	0.13654 ± 0.04452	0.15146 ± 0.04983	0.26512 ± 0.06354
Slope	0.00396 ± 6.3584E−4	0.00447 ± 7.11637E−4	0.00554 ± 9.07372E−4
Residual Sum of Squares	0.1375	0.17223	0.28001
Pearson's r	0.90092	0.90246	0.89764
R-Square (COD)	**0.81166**	**0.81443**	**0.80576**
Adj. R-Square	0.79073	0.79381	0.78418

Figure S85: Plot and linear fit of absorbance versus concentration of **1**·HBF_4 at different wavelengths measured in DMF at **ambient temperature**.

Compound **2**·2MeCN

Lifetime measurements of **2**·2MeCN:

Table S4: Luminescence lifetimes of a 10 µM solution of **2**·2MeCN in degassed THF at **298 K**.

Lifetime τ			
emission at λ = 400 nm	emission at λ = 450 nm	emission at λ = 500 nm	emission at λ = 550 nm
3.1 ns (83%) 7.7 ns (17%)	3.4 ns (90%) 9.9 ns (10%)	3.5 ns (87%) 10.4 ns (13%)	3.7 ns (78%) 11.8 ns (22%)

Emission / excitation spectra and lifetime measurements of **2**·2MeCN at **77 K**:

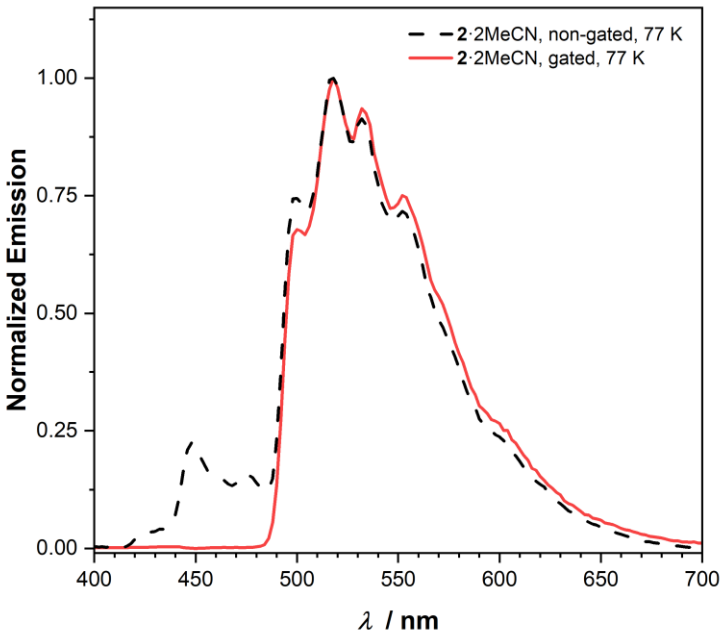

Figure S86: Emission spectra of a 10 µM solution of **2**·2MeCN in glassy 2-methyl-THF at **77 K**. The excitation wavelength was 360 nm. The dashed line contains both fluorescence and phosphorescence, whereas in the gated spectrum the fluorescence was suppressed. These spectra are independent of concentration.

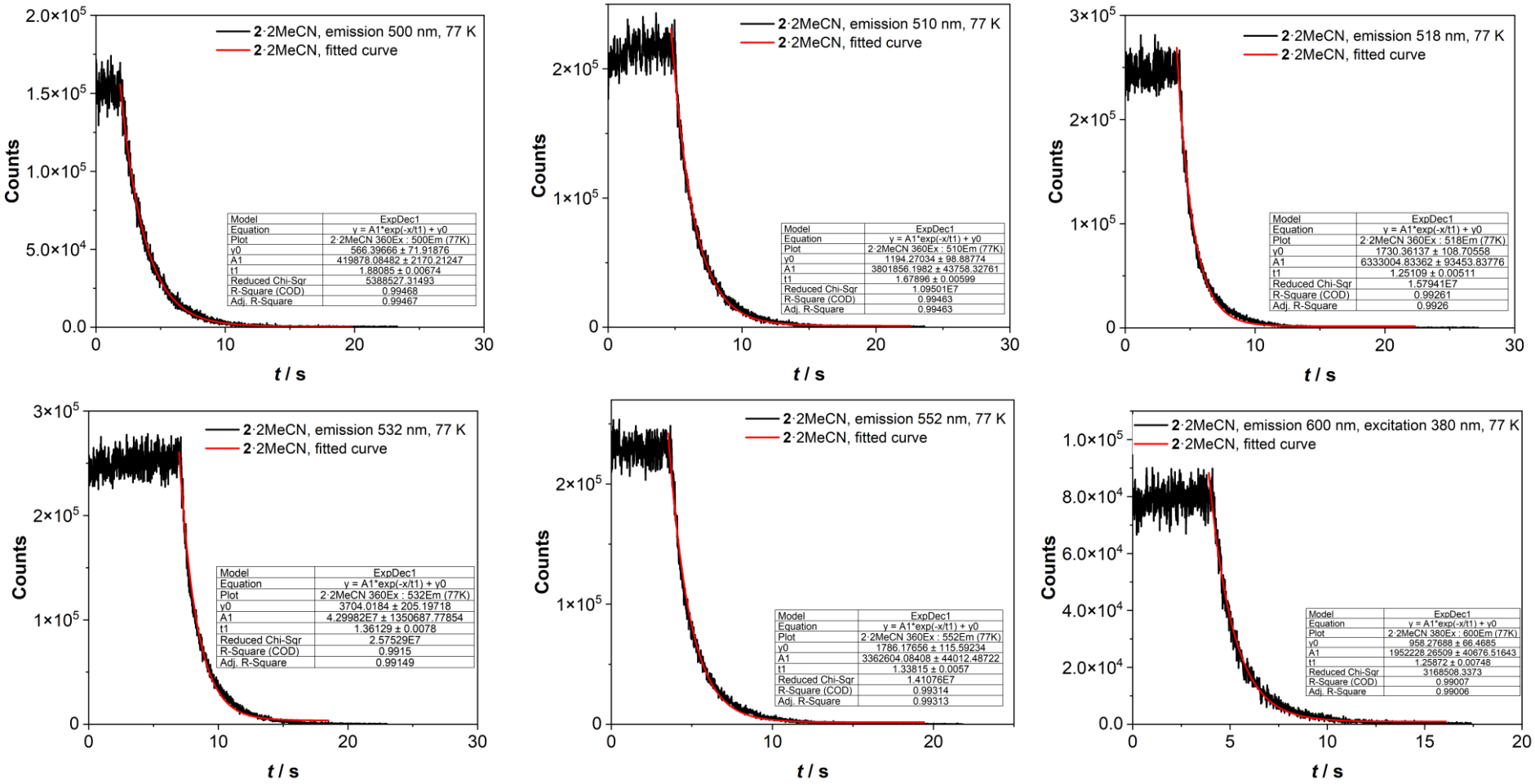

Figure S87: Long-persistent excited state lifetimes of a 10 µM solution of **2**·2MeCN in glassy 2-methyl-THF at **77 K**. The emissions were measured at 500 nm (top, left). 510 nm (top, middle), 518 nm (top, right), 532 nm, (bottom, left), 552 nm (bottom, middle) and 600 nm (bottom, right). Excitation wavelength was set to 380 nm (bottom, right) and 360 nm for all other.

Beer's law plot of **2**·2MeCN:

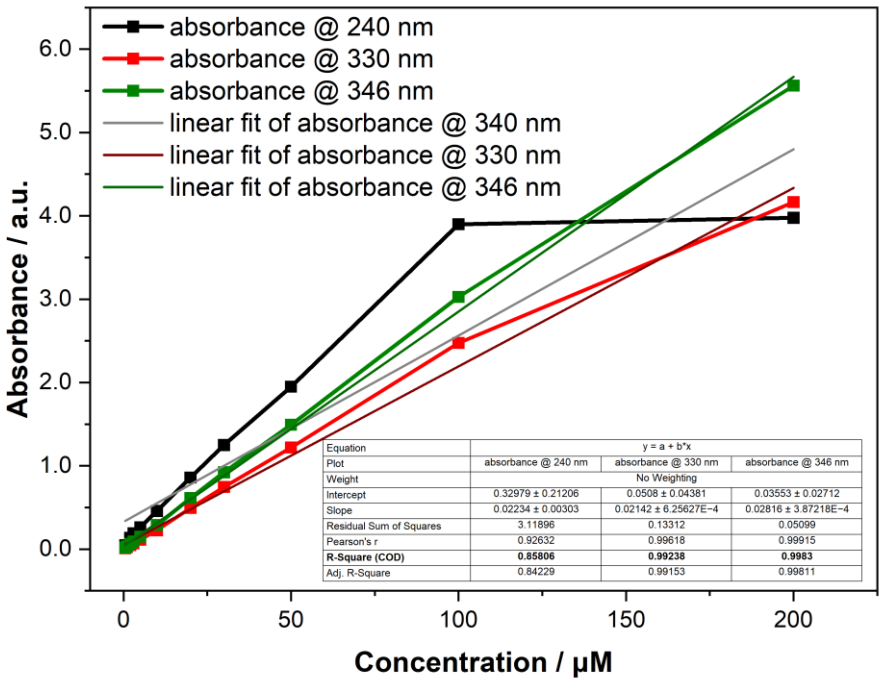

Equation	y = a + b*x		
Plot	absorbance @ 240 nm	absorbance @ 330 nm	absorbance @ 346 nm
Weight	No Weighting		
Intercept	0.32979 ± 0.21206	0.0508 ± 0.04381	0.03553 ± 0.02712
Slope	0.02234 ± 0.00303	0.02142 ± 6.25627E−4	0.02816 ± 3.87218E−4
Residual Sum of Squares	3.11896	0.13312	0.05099
Pearson's r	0.92632	0.99618	0.99915
R-Square (COD)	**0.85806**	**0.99238**	**0.9983**
Adj. R-Square	0.84229	0.99153	0.99811

Figure S88: Plot and linear fit of absorbance versus concentration of **2**·2MeCN at different wavelengths measured in DMF at **ambient temperatures**.

Jablonski Diagrams of **1**, **1**·HBF_4 and **2**·2MeCN

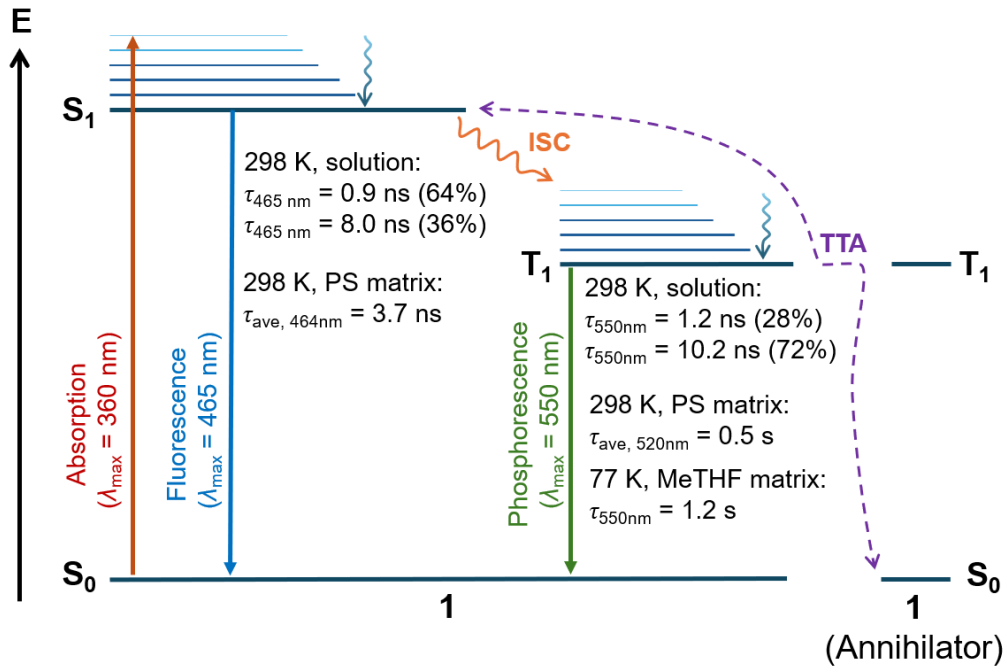

Figure S89: Jablonski diagram of compound **1** including the intermolecular TTA process with a second molecule of **1** acting as annihilator (ISC = intersystem crossing, TTA = triplet-triplet annihilation, PS = polystyrene).

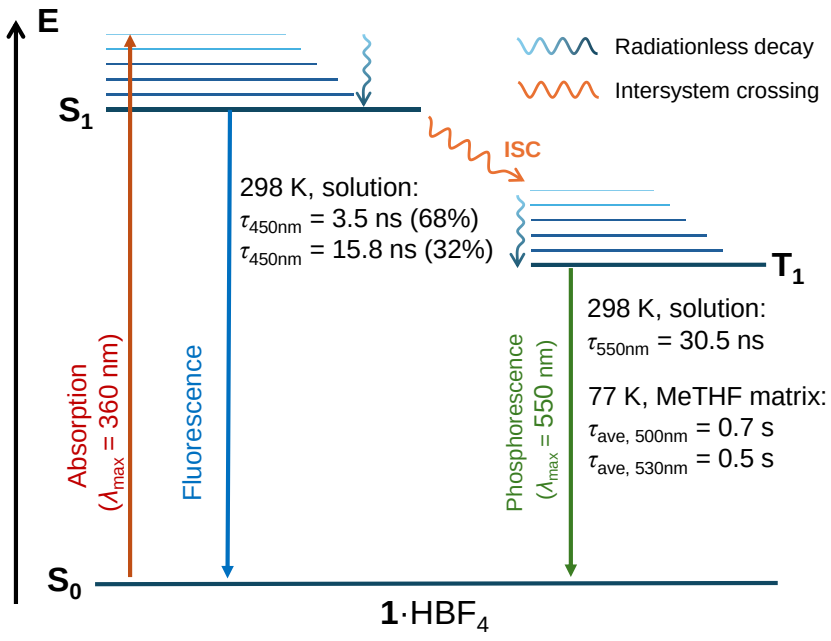

Figure S90: Jablonski diagram of **1**·HBF_4.

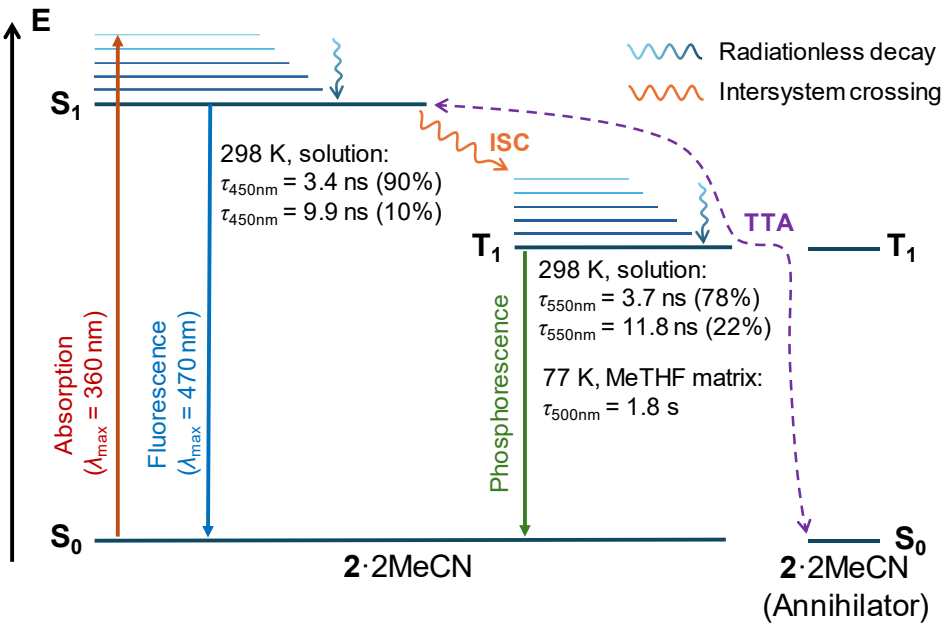

Figure S91: Jablonski diagram of **2**·2MeCN (TTA = triplet-triplet annihilation).

Protonation Experiments of **1**

1 (50 mg, 87.6 µmol) was dissolved in DCM (6 mL) and protonated successively under inert conditions by adding a stock solution of HOTf (c_{HOTf} = 285 mM) in steps of 0.5 equivalents (150 µL) with a 1 mL syringe until 2.0 equivalents of HOTf were added. Then, a total of 3.0 and 4.0 equivalents of HOTf in steps of 1.0 equivalents, and ultimately an excess of 10 equivalents to a total of 14 equivalents were added. After each addition of acid, the Schlenk flask was vigorously shaken to ensure homogeneity of the solution. Pictures of each protonation step described are shown in Figure S92.

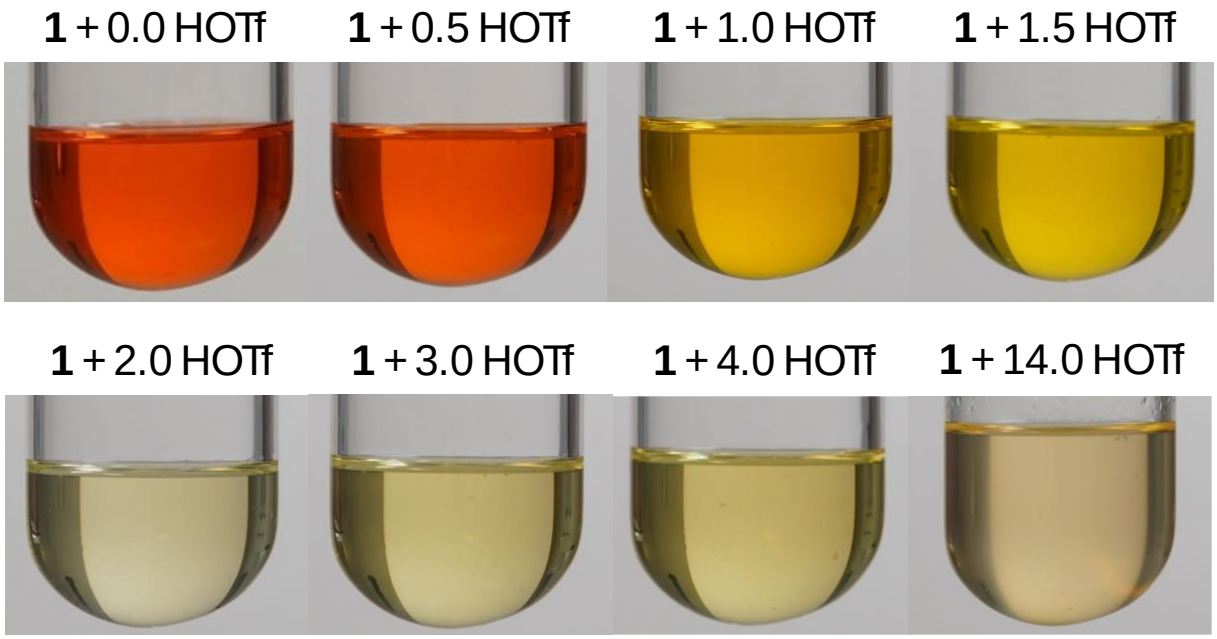

Figure S92: Protonation experiments of **1** with HOTf in DCM under inert conditions.

Protonation of **1** and assessment of the pK_{BH^+} value for **1**

Protonation of 1

To further investigate the protonation of compound **1**, energy minimizations at B3LYP/6-31G(d,p) level were carried out, considering a number of different protonation states. In the mono-protonated case, two potential acceptor atoms can be identified, namely *i*) a nitrogen atom of the phenanthroline moiety and *ii*) a nitrogen atom of an imine group. Based on the associated free energies *G,* protonation at the *N*-atom of phenanthroline is favored by -52.0 kJ mol^{-1} over protonation at one of the imine groups.

In case of the second protonation step, three potential states were considered, namely **I**) both nitrogen atoms of phenanthroline, **II**) a phenanthroline nitrogen atom in addition to the adjacent imine nitrogen atom and **III**) a phenanthroline nitrogen atom in addition to the distant imine nitrogen atom. From the resulting free energies *G*, the latter case was found to be the most stable state. Protonation of both nitrogen atoms of the phenanthroline moiety was found to be less favorable by 12.6 kJ mol^{-1}, indicating a potential competition between these two states. In contrast, protonation at the N-atom of phenanthroline and the imine on the same side of the molecule results in a free energy difference of 63.8 kJ mol^{-1}, clearly showing that this protonation state is the least favorable one.

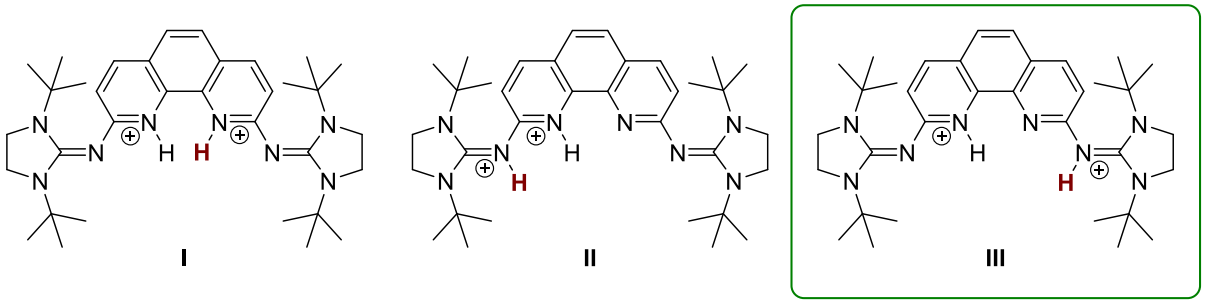

Figure S93: The three potential protonation states **I**–**III** considered for the calculation of the second protonation. The most favorable configuration according to the calculations is highlighted in the green frame.

pK_{BH^+}(ACN) value of 1

DFT calculations at the B3LYP/6-31G(d,p)/SMD(ACN) level of theory were carried out in conjunction with (de)protonation experiments to assess the pK_{BH^+}(ACN) value of **1**. ACN was chosen as solvent for the experiments and as implicit solvent for the DFT calculations. H_2O and THF were not considered as suitable solvents since **1** and **1**·HBF_4 are either insoluble or only weakly soluble in these solvents. The pK_{BH^+}(ACN) value of **1** and of [**1**·H]$^+$ were calculated using pyridine/pyridinium as reference system following the equilibrium reaction (1).

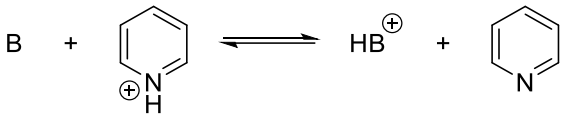

(1)

Previously, DFT calculations revealed that the first protonation of **1** is energetically favored to occur at one of the phenanthroline N atoms over the imine N atom. The second protonation at the opposite imine N atom was energetically slightly favored over the second phenanthroline N atom (see **I** and **III** in Figure S93). The second protonation at the imine N atom on the same side (see **II** in Figure S93) was energetically significantly disfavored by 63.8 kJ mol^{-1}. Consequently, for the calculation of their respective pK_{BH^+}(ACN) value, only the structures **I** and **III** were taken into consideration. The pK_{BH^+}(ACN) values of 1,10-phenanthroline, **1** and [**1**·H]$^+$ were calculated at the B3LYP/6-31G(d,p)/SMD(ACN) level of theory and are listed in Table S5. The calculations reveal that the basicity of **1** lies in the range of amidine superbases such as DBU (pK_{BH^+}(ACN) = 24.1)[15] and the basicity of [**1**·H]$^+$ lies in the range of pyridine (pK_{BH^+}(ACN) = 12.5).[15]

Table S5: $pK_{BH^+,calc}$(ACN) value of 1,10-phenanthroline, **1** and [**1**·H]$^+$ (**I** and **III**) calculated at the B3LYP/6-31G(d,p)/SMD(ACN) level of theory. The value in parentheses for 1,10-phenanthroline is reported in literature.

1,10-phenanthroline	**1**	[**1**·H]$^+$ (**I**)	[**1**·H]$^+$ (**III**)
13.8 (13.7)[16]	25.0	11.5	13.1

To experimentally gauge the pK_{BH^+}(ACN) value of **1** (see experimental procedures), **1** was employed as base to deprotonate the HBF_4 salts of

- PPh_3 (pK_{BH^+}(ACN) = 8.0),[15]
- NEt_3 (pK_{BH^+}(ACN) = 17.8),[15]
- DBU (pK_{BH^+}(ACN) = 24.1),[15]
- TBD (pK_{BH^+}(ACN) = 26.0)[15] and
- $P(tmg)_3$ (pK_{BH^+}(ACN) = 32.7, tmg = tetramethylguanidyl)[12]

In a similar vein, the deprotonation of **1**·HBF_4 using the commercially available phosphazene base *tert*-butylimino-tri(pyrrolidino)phosphoran [P_1-*t*Bu(pyrr)$_3$] (pK_{BH^+}(ACN) = 28.4)[17] or the superbasic phosphine P(NI*i*Pr)$_2$(*i*Pr) (pK_{BH^+}(ACN) = 29.5)[5] was investigated. All reactions were performed on an NMR scale in MeCN-d_3 and analyzed by NMR spectroscopy. The analysis of the NMR spectra (*vide infra*) revealed that addition of 1.0 eq. of **1** to the HBF_4 salts of PPh_3 and NEt_3 led to a complete proton transfer forming [**1**·H]$^+$ within 1 h. In the case of DBU and TBD, the addition of 1.0 eq. of **1** did not lead to a complete proton transfer according to ^{1}H

NMR analysis. Instead, the shifts of the resonances of the reaction mixture indicate that both the free ligand **1** and the protonated ligand **1**·HBF_4 are present in the equilibrium state.
Moreover, no indication of deprotonation was observed according to NMR analysis after combining $P(tmg)_3$·HBF_4 with **1**. Combining **1**·HBF_4 with 1.0 eq. of P_1-*t*Bu$(pyrr)_3$ or P(NI*i*Pr)$_2$(*i*Pr) in MeCN-d_3, led to complete proton transfer to the phosphazene base or superbasic phosphine within 1 h, respectively.
Collectively, these experiments show that **1** is a significantly weaker base than P(NI*i*Pr)$_2$(*i*Pr) and P_1-*t*Bu$(pyrr)_3$. Moreover, an equilibrium mixture is obtained with DBU·HBF_4 and TBD·HBF_4 indicating similar basicity to both. Therefore, the $\mathrm{pK_{BH^+}}$(ACN) value of **1** is estimated to be in the range of $\mathrm{pK_{BH^+}}$(ACN) = 25.

Experimental procedures

General procedure for the use of **1** as base:

1 (15 mg, 26 µmol, 1.0 eq.) was added to an MeCN-d_3 solution containing 1.0 eq. of the HBF_4 salt of PPh_3, NEt_3, DBU, TBD and $P(tmg)_3$, respectively. The resulting reaction mixture was shaken vigorously and subjected to NMR analysis after 1 h. ^1H NMR spectra and ^{31}P NMR spectra (if applicable) were recorded and used to analyze the proton transfer.

Experiment with **1**·HBF_4 and P_1-*t*Bu(pyrr)$_3$ as base:

1·HBF_4 (21.5 mg, 33 µmol, 1.0 eq.) was dissolved in MeCN-d_3 and P_1-*t*Bu(pyrr)$_3$ (10 µL, 33 µmol, 1.0 eq.) was added using a Hamilton® syringe. The resulting reaction mixture was subjected to ^1H NMR and ^{31}P NMR analysis after 1 h.

Experiments with **1**·HBF_4 and P(NI*i*Pr)$_2$(*i*Pr) as base:

1·HBF_4 (15 mg, 23 µmol, 1.0 eq.) was dissolved in MeCN-d_3 and P(NI*i*Pr)$_2$(*i*Pr) (10.5 mg, 23 µmol, 1.0 eq.) was added. The resulting reaction mixture was subjected to ^1H NMR and ^{31}P NMR analysis after 1 h.

NMR analysis of **1** + $PPh_3 \cdot HBF_4$:

The characteristic P–H coupling which is observed in the ^1H NMR spectrum (Figure S94) at δ = 8.72 ppm with a coupling constant of $^1J_{PH}$ = 527.5 Hz and in the $^{31}P\{\}$ NMR spectrum (Figure S95) at δ = 4.9 ppm with a coupling constant of $^1J_{PH}$ = 528 Hz vanishes after the addition of **1** indicating that the $[PPh_3 \cdot H]^+$ cation is deprotonated. This is further supported by the observed new resonance attributed to PPh_3 at δ = –5.9 ppm in the resulting $^{31}P\{\}$ NMR spectrum.

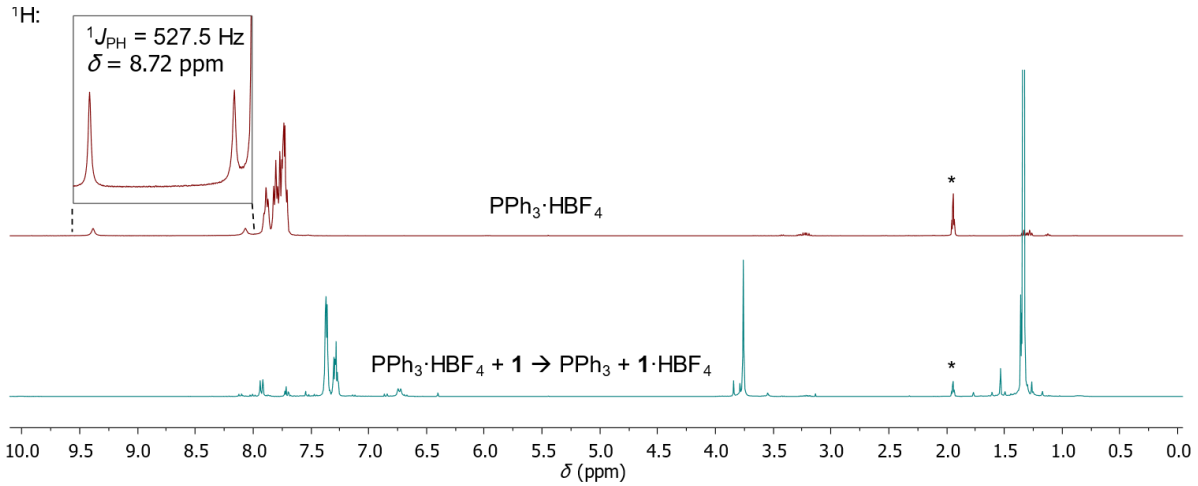

Figure S94: Stacked ^1H NMR spectra of $PPh_3 \cdot HBF_4$ before (top) and after the addition of **1** (bottom) measured in MeCN-d_3 (* = residual solvent signal).

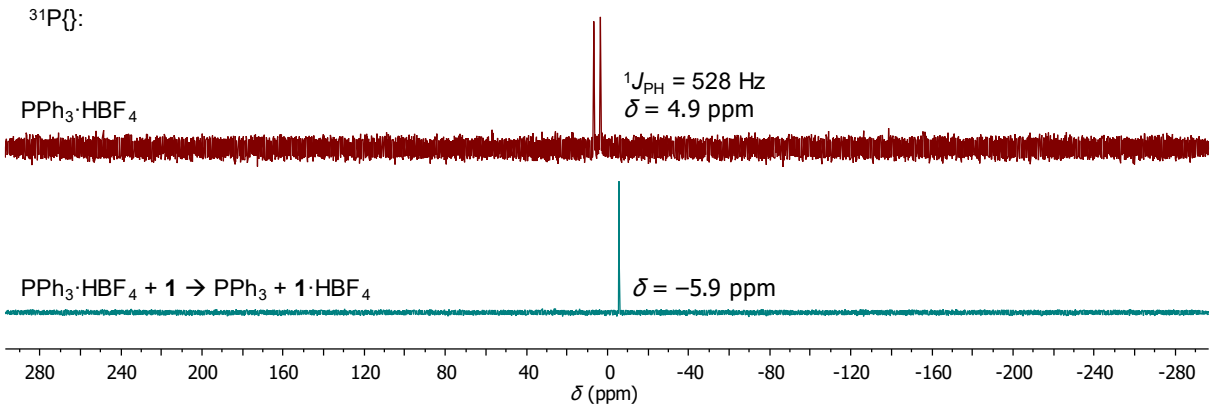

Figure S95: Stacked $^{31}P\{\}$ NMR spectra of $PPh_3 \cdot HBF_4$ before (top) and after the addition of **1** (bottom) measured in MeCN-d_3.

NMR analysis of **1** + $NEt_3 \cdot HBF_4$:

The ^1H NMR resonance of the acidic proton in the spectrum of $NEt_3 \cdot HBF_4$ (Figure S96, top) disappears after the addition of **1** and is observed instead at δ = 9.38 ppm (Figure S96, middle) which is slightly shifted compared to the reference ^1H NMR spectrum of the pure **1**$\cdot HBF_4$ (Figure S96, bottom) at δ = 10.04 ppm. The slight difference in the shifts of the acidic proton resonance could be due to interactions with NEt_3 in solution. All other signals in the aromatic and aliphatic region of the reaction mixture nicely overlap with the reference spectrum of **1**$\cdot HBF_4$ and the two other aliphatic signals are attributed to free NEt_3.

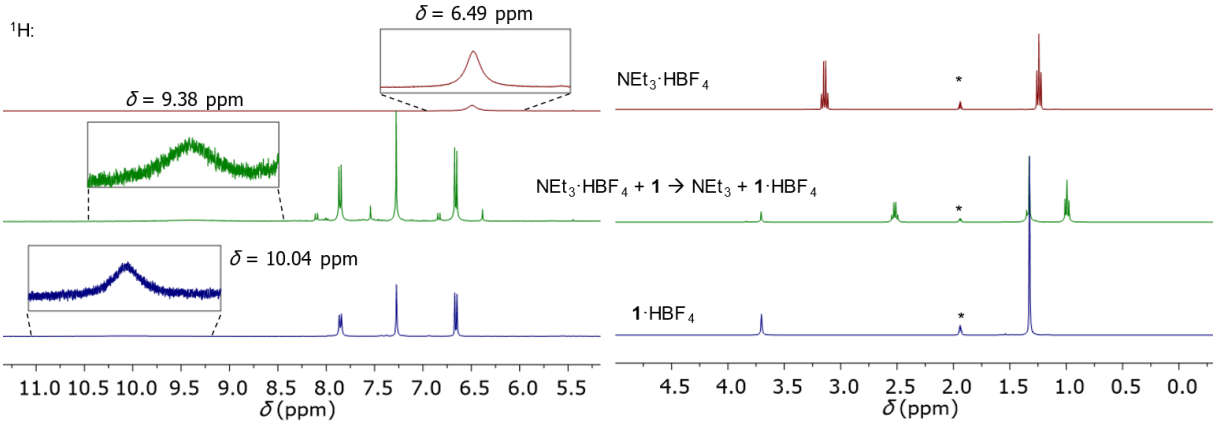

Figure S96: Stacked ^1H NMR spectra of $NEt_3 \cdot HBF_4$ before (top), after the addition of **1** (middle) and of a reference spectrum of **1**$\cdot HBF_4$ (bottom) measured in MeCN-d_3 (* = residual solvent signal). The aromatic ^1H signals (left) are depicted with a 20-fold scaling for better visibility of the signals.

NMR analysis of **1** + DBU·HBF_4:

Like for NEt_3·HBF_4, the ^{1}H NMR resonance of the acidic proton in the spectrum of DBU·HBF_4 is shifted after the addition of **1** and is observed at δ = 10.90 ppm which is also shifted compared to the reference ^{1}H NMR spectrum of the pure **1**·HBF_4 at δ = 10.04 ppm (Figure S97). Yet, the aromatic and aliphatic resonances of the reaction mixture do not align with the refence measurements and are shifted up to $\Delta\delta$ = 0.14 ppm from the reference **1**·HBF_4 ^{1}H NMR spectrum. The resonances of DBU are shifted as well upon addition of **1**. The highlighted ^{1}H resonances of the reaction mixture are in the between that of **1** and **1**·HBF_4 (Figure S97, bottom two) and in between free DBU and DBU·HBF_4 (Figure S97, top two). This indicates that the proton transfer from DBU·HBF_4 to **1** is not complete and the equilibrium is not clearly on one side of the reaction.

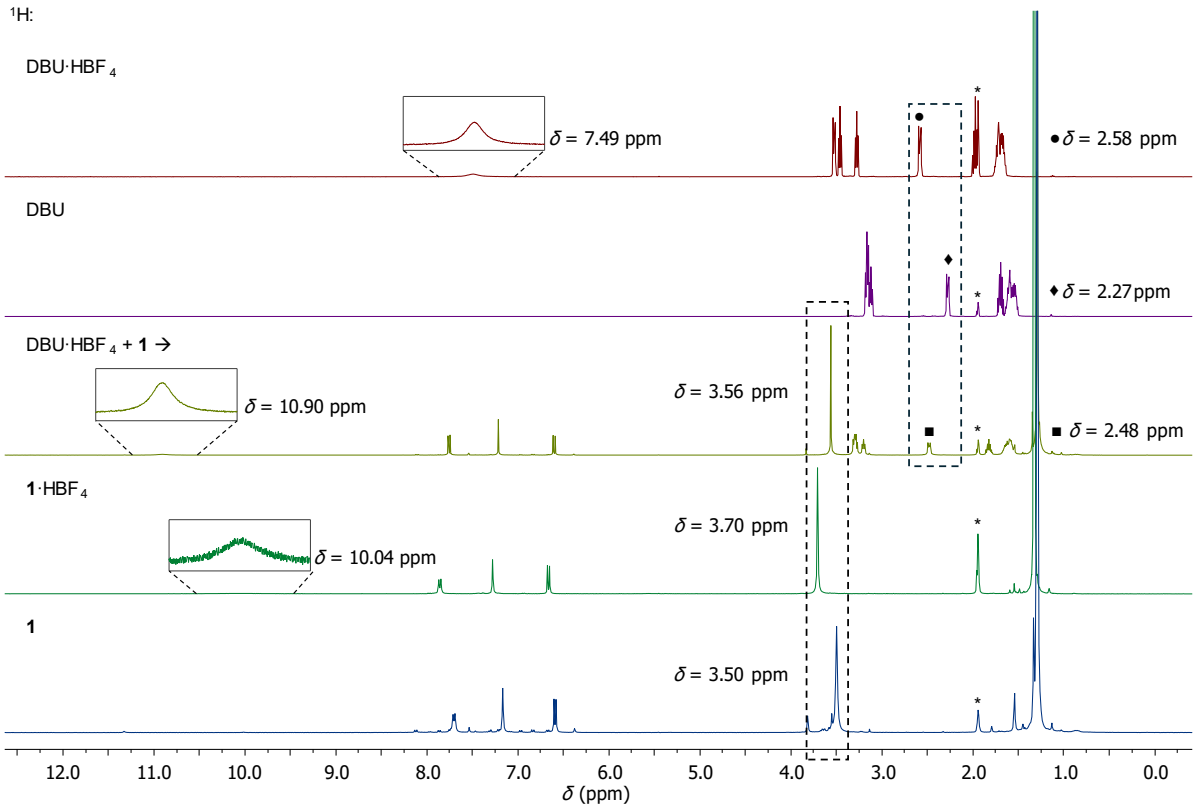

Figure S97: Stacked ^{1}H NMR spectra of DBU·HBF_4, free DBU, the reaction mixture of DBU·HBF_4 and **1**, **1**·HBF_4 and the free ligand **1** measured in MeCN-d_3 (* = residual solvent signal).

NMR analysis of **1** + TBD·HBF_4:

Like for NEt_3·HBF_4, the ^{1}H NMR resonance of the acidic proton in the spectrum of TBD·HBF_4 is shifted after the addition of **1** and is observed at δ = 9.31 ppm which is also shifted compared to the reference ^{1}H NMR spectrum of the pure **1**·HBF_4 at δ = 10.04 ppm (Figure S98). Yet, the aromatic and aliphatic resonances of the reaction mixture do not align with the refence measurements and are shifted up to $\Delta\delta$ = 0.17 ppm. The resonances of TBD are shifted as well upon addition of **1**. The highlighted ^{1}H resonances of the reaction mixture are in the between that of **1** and **1**·HBF_4 (Figure S98, bottom two) and in between free TBD and TBD·HBF_4 (Figure S98, top two). This indicates that the proton transfer from TBD·HBF_4 to **1** is not complete and the equilibrium is not clearly on one side of the reaction.

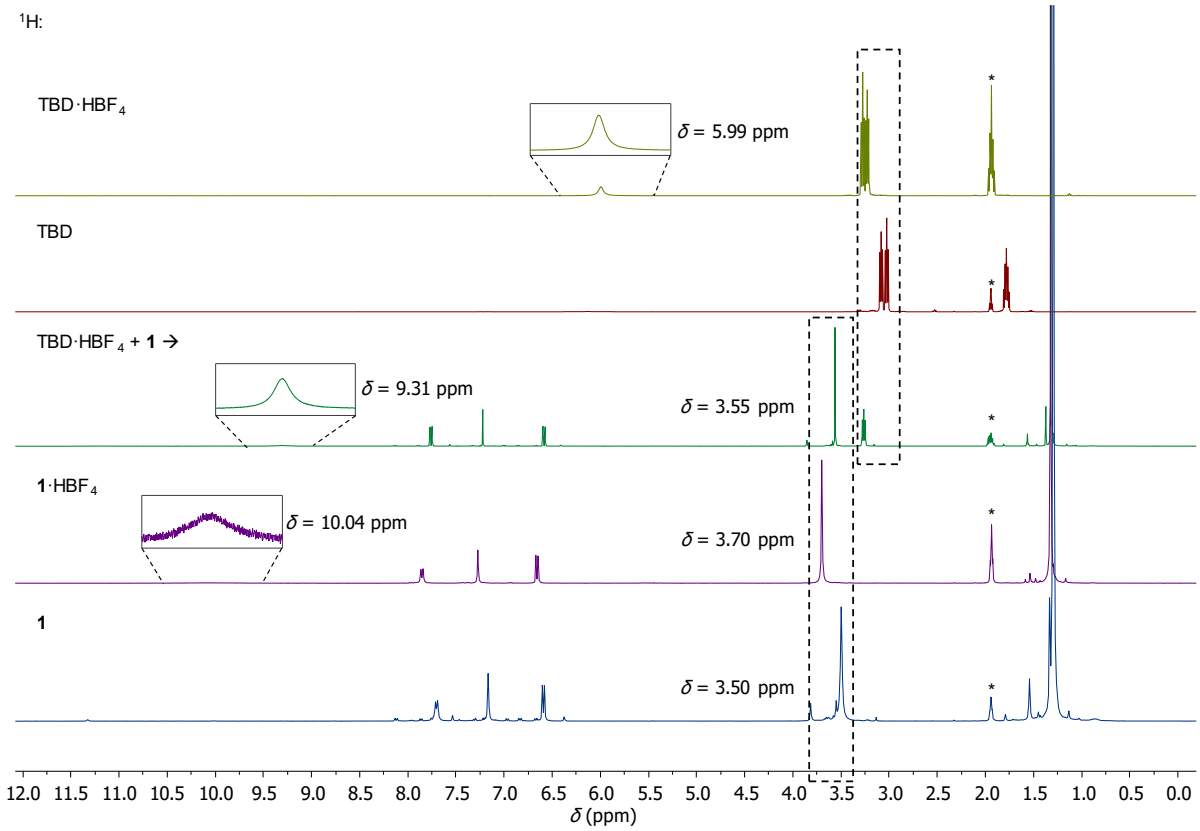

Figure S98: S Stacked ^{1}H NMR spectra of TBD·HBF_4, free TBD, the reaction mixture of TBD·HBF_4 and **1**, **1**·HBF_4 and the free ligand **1** measured in MeCN-d_3 (* = residual solvent signal).

NMR analysis of **1** + $P(tmg)_3 \cdot HBF_4$:

After the addition of **1** to the solution of $P(tmg)_3 \cdot HBF_4$ in MeCN-d_3, ^1H and ^{31}P NMR analysis revealed that no deprotonation and formation of the $[\mathbf{1} \cdot H]^+$ cation occurs. The characteristic P–H coupling observed in the ^1H NMR spectrum (Figure S99) at δ = 7.86 ppm with a coupling constant of $^1J_{PH}$ = 539.4 Hz and in the ^{31}P NMR spectrum (Figure S100) at δ = –16.7 ppm with a coupling constant of $^1J_{PH}$ = 539 Hz remain unchanged.

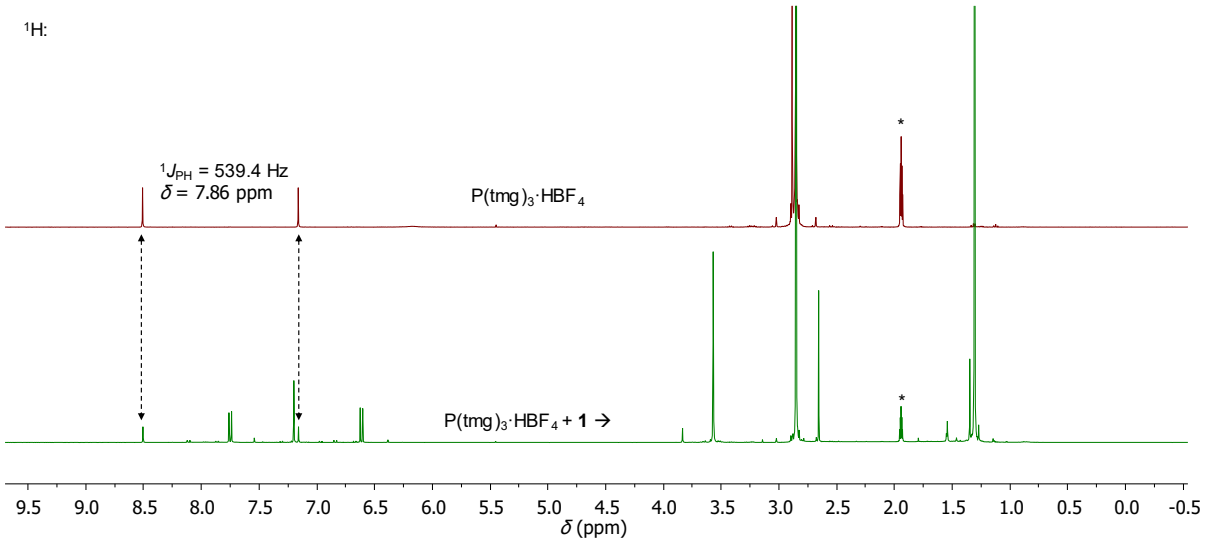

Figure S99: Stacked ^1H NMR spectra of $P(tmg)_3 \cdot HBF_4$ before (top) and after the addition of **1** (bottom) measured in MeCN-d_3 (* = residual solvent signal).

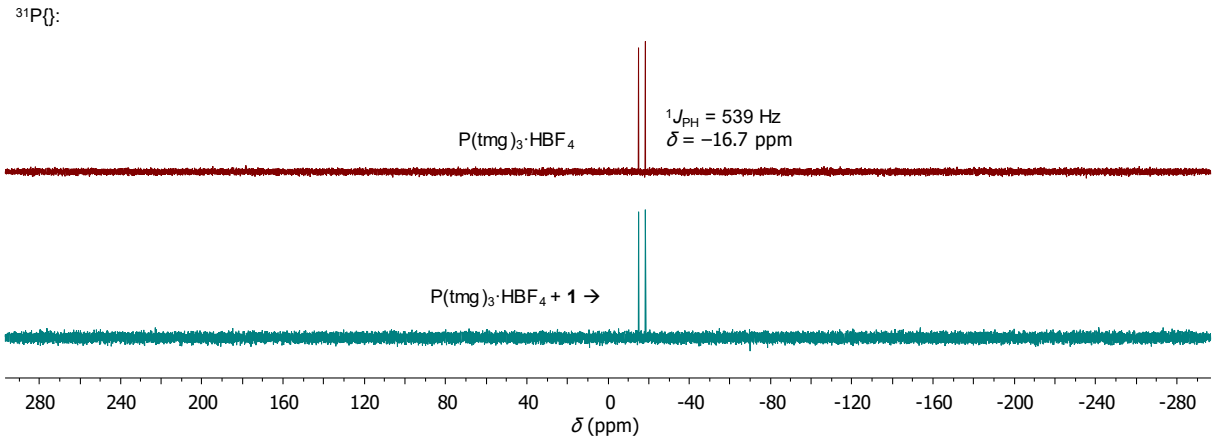

Figure S100: Stacked $^{31}P\{\}$ NMR spectra of $P(tmg)_3 \cdot HBF_4$ before (top) and after the addition of **1** (bottom) measured in MeCN-d_3.

NMR analysis of **1**·HBF_4 + P(NI*i*Pr)$_2$(*i*Pr):

After the addition of P(NI*i*Pr)$_2$(*i*Pr) to the solution of **1**·HBF_4 in MeCN-d_3, ^{1}H and ^{31}P NMR analysis revealed that complete deprotonation of **1**·HBF_4 occurs releasing the free ligand **1**, and P(NI*i*Pr)$_2$(*i*Pr)·HBF_4 is formed in the process. This is evidenced by the characteristic P–H coupling in the ^{1}H NMR spectrum (Figure S101) at δ = 7.54 ppm with a coupling constant of $^1J_{PH}$ = 467.3 Hz and in the ^{31}P NMR spectrum (Figure S102) at δ = 0.2 ppm with a coupling constant of $^1J_{PH}$ = 469 Hz. Furthermore, the acidic proton resonance of **1**·HBF_4 disappears after addition of the phosphine.

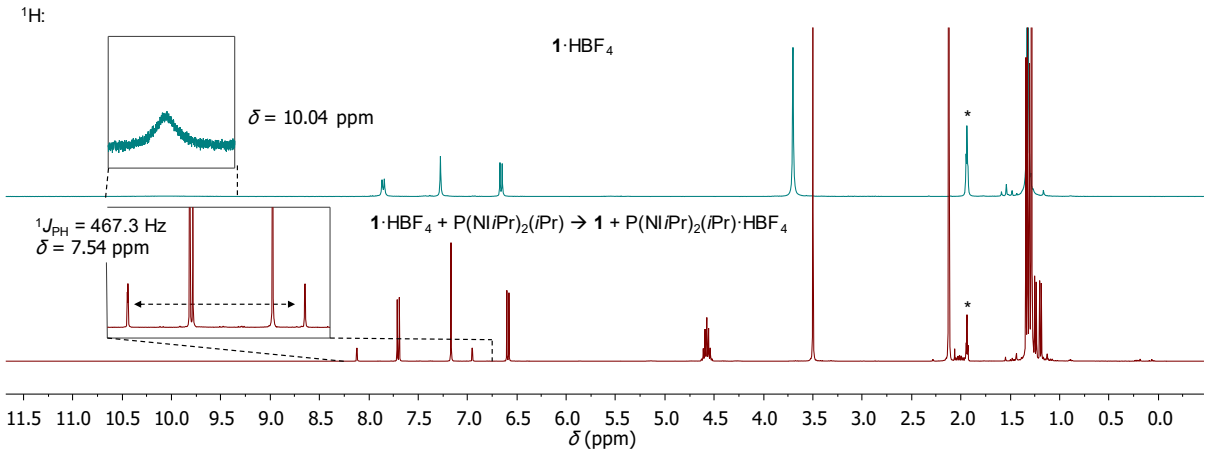

Figure S101: Stacked ^{1}H NMR spectra of **1**·HBF_4 before (top) and after the addition of P(NI*i*Pr)$_2$(*i*Pr) (bottom) measured in MeCN-d_3 (* = residual solvent signal).

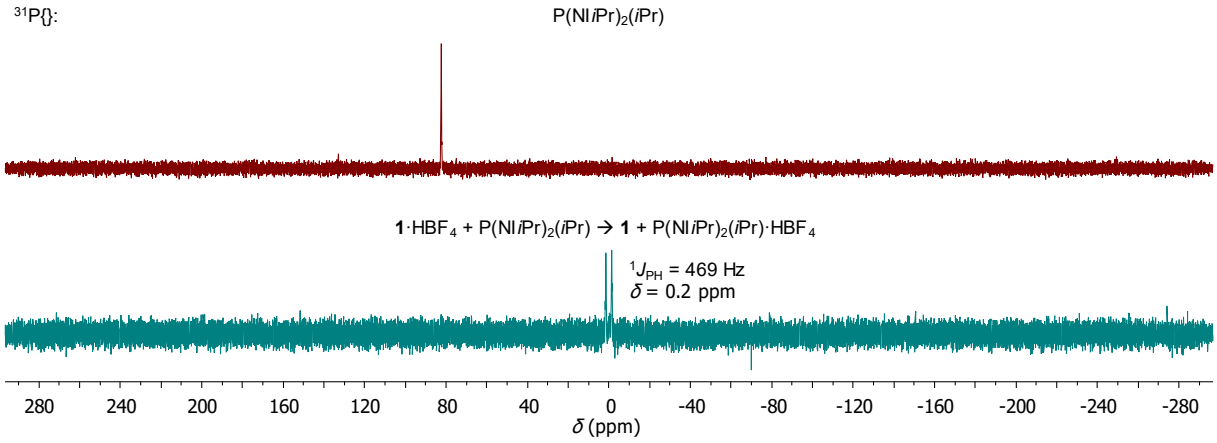

Figure S102: Stacked ^{31}P{} NMR spectra of a reference spectrum of P(NI*i*Pr)$_2$(*i*Pr) (top) and of the reaction mixture with **1**·HBF_4 (bottom) measured in MeCN-d_3.

NMR analysis of **1**·HBF_4 + P_1-*t*Bu(pyrr)$_3$:

After the addition of P_1-*t*Bu(pyrr)$_3$ to the solution of **1**·HBF_4 in MeCN-d_3, ^{1}H and ^{31}P NMR analysis revealed that complete deprotonation of **1**·HBF_4 occurs releasing the free ligand **1**, and P_1-*t*Bu(pyrr)$_3$·HBF_4 is formed in the process. The resonance of the acidic proton of **1**·HBF_4 in the ^{1}H NMR spectrum (Figure S103) at δ = 10.4 ppm disappears upon addition of the phosphazene base and the resonance of the ^{31}P resonance (Figure S104) is shifted from δ = –6.9 ppm to δ = 21.3 ppm. The N–H proton resonance of P_1-*t*Bu(pyrr)$_3$·HBF_4 is broadened and partially overlapping with a resonance of **1** (see cutout in Figure S103, bottom).

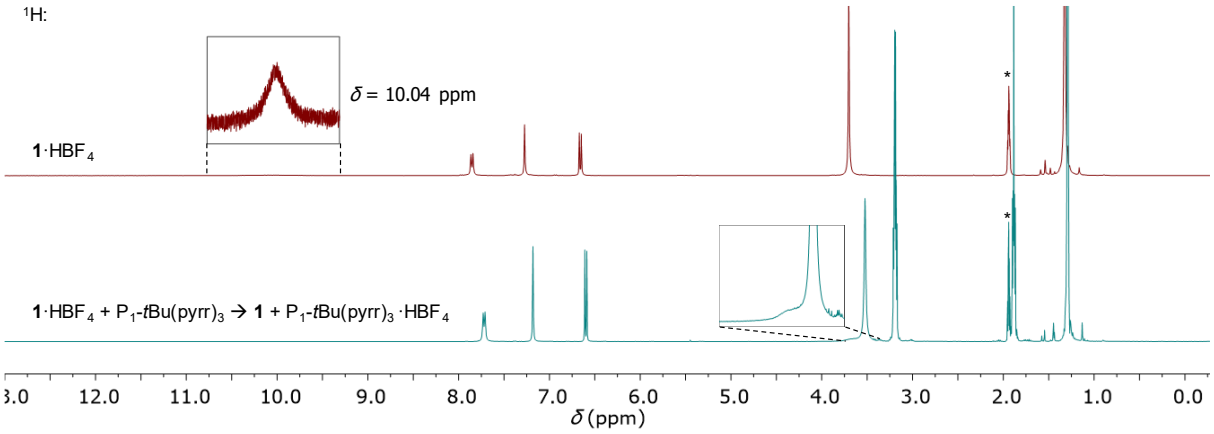

Figure S103: Stacked ^{1}H NMR spectra of **1**·HBF_4 before (top) and after the addition of P_1-*t*Bu(pyrr)$_3$ (bottom) measured in MeCN-d_3 (* = residual solvent signal).

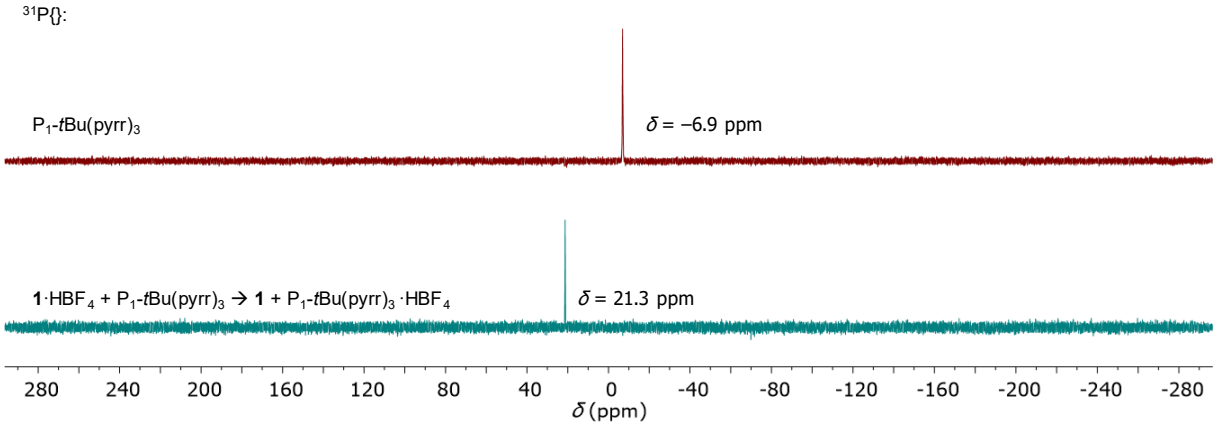

Figure S104: Stacked ^{31}P{} NMR spectra of a reference spectrum of P_1-*t*Bu(pyrr)$_3$ (top) and of the reaction mixture with **1**·HBF_4 (bottom) measured in MeCN-d_3.

Computational Details

In addition to experimental measurements, theoretical calculations at density functional theory (DFT) level were carried out to characterize the associated UV/Vis excitations and to investigate the preferred protonation sites of compound **1**.

All calculations were executed employing the B3LYP[18] functional in conjunction with 6-31G(d,p) basis sets[19–21] using Gaussian16.[22] The influence of solvent effects in dichloromethane (relative permittivity $\varepsilon = 8.93$) or acetonitrile (relative permittivity $\varepsilon = 35.688$) was accounted for using the implicit solvent model density (SMD) approach.[23]

In addition to the neutral form of compound **1** the respective protonated and two-fold protonated states were investigated. For each of these molecular systems an energy minimization employing tight convergence criteria of $\leq 10^{-8}$ E_h and $\leq 1.5 \times 10^{-5}$ E_h $bohr^{-1}$ was carried out. To validate that the optimized structures correspond to minima on the potential energy surface and to estimate the contributions to the free energy *G*, a thermochemical analysis based on harmonic vibrational frequencies was carried out according to the method outlined by Ochterski.[24,25]

In addition, UV/Vis excitations have been calculated for compound **1** using time-dependent density functional theory (TD DFT) calculations[26] employing the settings outlined above. To match the thermal broadening of the experimental spectrum, a weighted kernel density estimation based on Gaussian distributions was applied, setting the peak half-width at half height to 0.185 eV.

UV/Vis Spectrum

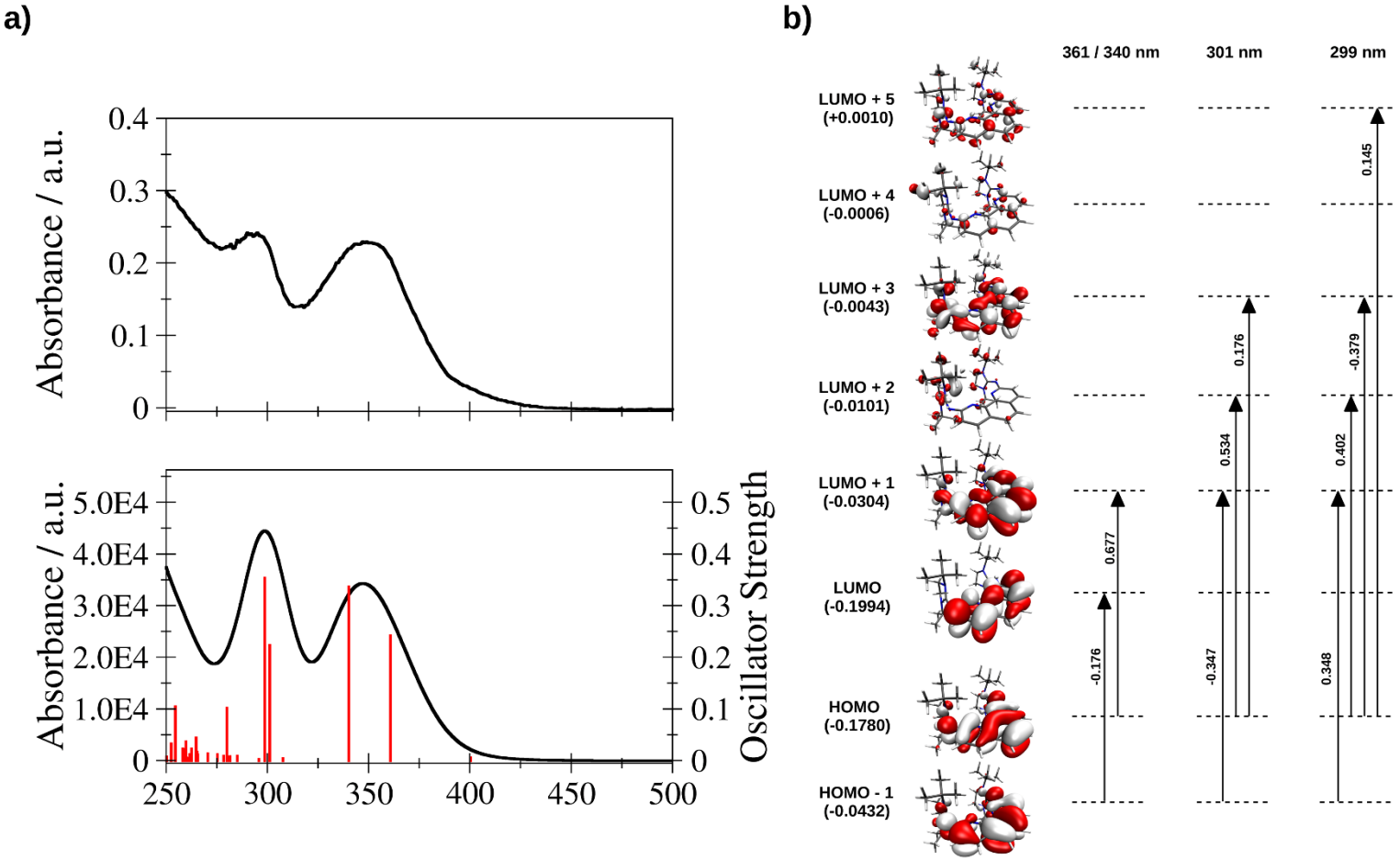

Figure S105: a) A comparison of the experimental UV/Vis absorption spectrum of compound **1** (10 µM, top) and the corresponding theoretical prediction obtained via TD-DFT calculation at B3LYP/6-31G(d,p) level of theory in implicit dichloromethane (bottom). b) Orbital contributions of the three main excitations obtained from the TD-DFT calculation. The eigenenergies of the individual canonical molecular orbitals (MOs) are given in parentheses in units of E_h, the labels assigned to the individual excitations correspond to the most dominant MO coefficient

Theoretical calculations of the UV/Vis excitations have shown that three main transition near 350 and 300 nm can be identified, that can be classified to be exclusively $\pi \rightarrow \pi^*$ transitions. Based on the free energy differences of different protonation states, the nitrogen atoms of phenanthroline were found to be preferred over the imine group. In case of the second protonation step, the imine group opposite to the initial protonation site was found to be preferred, albeit a competition with the two-fold protonation of the phenanthroline moiety can be expected.

XYZ Coordinates

Table S6: XYZ coordinates of the optimized geometry for **1** obtained at the B3LYP/6-31G(d,p)/SMD(DCM) level of theory.

Atom	X	Y	Z	Atom	X	Y	Z
N	1.369951	1.593310	0.015228	H	-2.524484	1.191729	-2.538057
N	-1.411128	1.559109	-0.061876	H	-1.860005	0.539513	-4.030508
N	-3.455014	0.378092	-0.067278	C	-4.155821	-0.879793	-3.135019
N	-2.540986	-1.490961	-1.329988	H	-4.669150	-0.152725	-2.499456
N	-3.443614	-1.827413	0.718849	H	-4.667160	-1.844200	-3.042883
N	3.430152	0.447757	-0.091882	H	-4.250595	-0.548775	-4.174590
N	3.312580	-1.827422	-0.652365	C	-1.968843	-2.006802	-3.676975
N	2.922766	-1.317030	1.503232	H	-0.914858	-2.129259	-3.406566
C	0.697092	2.772789	-0.031294	H	-2.010495	-1.626401	-4.701272
C	-0.764820	2.753696	-0.079230	H	-2.447780	-2.988947	-3.676492
C	-2.751747	1.533238	-0.154018	C	-5.188666	-0.749834	2.132714
C	-3.515955	2.746916	-0.260436	H	-5.963550	-1.316278	1.604540
H	-4.597023	2.679265	-0.331188	H	-5.087465	0.223687	1.655188
C	-2.868603	3.950234	-0.263222	H	-5.519473	-0.604472	3.166555
H	-3.427105	4.880658	-0.339346	C	-4.100373	-2.859701	2.862263
C	-1.450519	4.000707	-0.170995	H	-4.869373	-3.461508	2.367239
C	-0.741102	5.239793	-0.180176	H	-4.451081	-2.638104	3.874337
H	-1.310409	6.164394	-0.239442	H	-3.190286	-3.459464	2.954701
C	0.624038	5.256997	-0.123882	C	-2.755429	-0.747609	2.866889
H	1.173699	6.195129	-0.137352	H	-1.829487	-1.330398	2.901242
C	1.359507	4.034628	-0.062196	H	-3.065210	-0.547440	3.898327
C	2.781313	4.015917	-0.050373	H	-2.541549	0.205821	2.381077
H	3.322678	4.959317	-0.067421	C	5.370423	-1.277461	-1.952772
C	3.454655	2.826676	-0.032860	H	5.955782	-2.010629	-1.386409
H	4.539152	2.782697	-0.041066	H	5.475009	-0.301916	-1.473265
C	2.713312	1.594492	-0.003383	H	5.795972	-1.215407	-2.960236
C	-3.119193	-0.876399	-0.225186	C	3.076936	-0.688820	-2.863478
C	-2.622712	-2.950775	-1.135427	H	3.191121	0.329678	-2.497198
H	-1.725800	-3.456471	-1.493980	H	2.012634	-0.945563	-2.847770
H	-3.493637	-3.362081	-1.663729	H	3.420885	-0.723970	-3.902780
C	-2.795244	-3.093273	0.368827	C	3.788030	-3.064471	-2.728849
H	-3.407326	-3.957916	0.625840	H	4.388392	-3.835120	-2.236837
H	-1.824287	-3.188166	0.875382	H	4.163768	-2.960351	-3.750742
C	-2.668354	-0.991659	-2.750164	H	2.750951	-3.411193	-2.786925
C	-3.858571	-1.527192	2.128277	C	3.484055	0.645831	2.966927
C	3.176381	-0.789815	0.250790	H	4.540157	0.422025	2.786692
C	3.363318	-3.100955	0.069614	H	3.384497	0.986264	4.002332
H	4.401709	-3.409191	0.263167	H	3.188311	1.473319	2.326140
H	2.858148	-3.899352	-0.473146	C	1.113090	-0.260182	2.847277
C	2.641515	-2.752988	1.364393	H	0.507290	-1.172164	2.829165
H	1.560487	-2.934498	1.281649	H	0.819255	0.364476	2.000683
H	3.028887	-3.328001	2.203263	H	0.885936	0.272387	3.777540
C	3.888918	-1.696155	-2.028093	C	2.952785	-1.559834	3.953955
C	2.610639	-0.609951	2.785504	H	2.303587	-2.438677	3.988270
C	-1.962521	0.358132	-2.955587	H	2.812111	-1.019392	4.894141
H	-0.966274	0.354353	-2.507491	H	3.995292	-1.893046	3.908341

Table S7: XYZ coordinates of the optimized geometry for **[1·H]$^+$**, protonation at one phenanthroline N atom obtained at the B3LYP/6-31G(d,p)/SMD(DCM) level of theory.

Atom	X	Y	Z	Atom	X	Y	Z
N	1.415508	1.627949	0.000677	H	-3.189927	1.418814	-1.972411
N	-1.307350	1.578205	0.289032	H	-3.013093	0.944375	-3.658142
N	-3.348112	0.403254	0.456945	C	-4.942568	-0.627520	-2.273520
N	-2.861124	-1.359426	-1.106754	H	-5.240044	0.024775	-1.448367
N	-2.953948	-1.837005	1.094611	H	-5.400082	-1.611275	-2.123452
N	3.418227	0.380906	-0.282908	H	-5.344246	-0.208973	-3.202128
N	2.481164	-1.584658	-1.288920	C	-3.024185	-1.640898	-3.550951
N	3.184304	-1.685405	0.847044	H	-1.938096	-1.759628	-3.626030
C	0.733572	2.824336	0.119497	H	-3.374145	-1.171564	-4.474285
C	-0.688807	2.789272	0.284966	H	-3.482824	-2.631227	-3.494983
C	-2.649200	1.543783	0.434979	C	-4.122005	-0.890247	3.086196
C	-3.401330	2.769305	0.610051	H	-5.033596	-1.426795	2.802579
H	-4.475894	2.691812	0.738465	H	-4.180439	0.120934	2.686155
C	-2.769332	3.976267	0.597788	H	-4.086901	-0.833921	4.178958
H	-3.330739	4.899446	0.717044	C	-2.866978	-3.028240	3.254822
C	-1.353908	4.037963	0.423543	H	-3.767779	-3.601995	3.015814
C	-0.626702	5.259673	0.382995	H	-2.842540	-2.883064	4.338339
H	-1.172749	6.192880	0.491668	H	-1.988895	-3.620885	2.982691
C	0.734468	5.264881	0.204316	C	-1.582384	-0.899735	2.954693
H	1.292456	6.195386	0.165092	H	-0.705122	-1.472844	2.634741
C	1.440055	4.036079	0.067146	H	-1.522922	-0.775335	4.040947
C	2.856832	3.958276	-0.134153	H	-1.532158	0.087954	2.492729
H	3.425940	4.882398	-0.186776	C	4.076137	-1.178053	-3.159035
C	3.493807	2.761816	-0.260768	H	4.541891	-2.155450	-2.994791
H	4.563872	2.695044	-0.416372	H	4.635193	-0.425074	-2.596801
C	2.767409	1.517522	-0.183763	H	4.160063	-0.940172	-4.224230
C	-3.019861	-0.839953	0.161635	C	1.941887	0.174689	-3.010574
C	-2.873336	-2.831288	-1.008730	H	2.543687	1.006074	-2.646332
H	-2.155188	-3.287448	-1.689944	H	0.944941	0.231244	-2.563506
H	-3.873501	-3.220121	-1.240721	H	1.832515	0.303483	-4.091567
C	-2.515371	-3.081221	0.451313	C	1.828878	-2.240770	-3.571639
H	-3.029412	-3.954428	0.851702	H	2.272104	-3.237490	-3.506361
H	-1.433808	-3.222363	0.581950	H	1.857446	-1.939359	-4.621838
C	-3.409220	-0.733940	-2.366070	H	0.779121	-2.300780	-3.266166
C	-2.877347	-1.643642	2.581571	C	4.980198	-0.539494	2.151923
C	2.999826	-0.887735	-0.233874	H	5.730099	-1.181979	1.679193
C	2.485964	-3.020056	-0.938545	H	5.315787	-0.317530	3.169676
H	3.359208	-3.511561	-1.385047	H	4.927693	0.395827	1.595961
H	1.583410	-3.519738	-1.287519	C	2.547486	-0.368738	2.872555
C	2.576746	-3.000504	0.584296	H	1.583655	-0.886554	2.914607
H	1.585657	-3.058957	1.051072	H	2.411748	0.571517	2.335101
H	3.191232	-3.814306	0.965018	H	2.842716	-0.125756	3.898178
C	2.594251	-1.191996	-2.743575	C	3.804537	-2.521397	3.086211
C	3.621439	-1.259316	2.224033	H	2.871278	-3.075430	3.220846
C	-2.788749	0.648401	-2.628560	H	4.147553	-2.209596	4.076275
H	-1.701901	0.620750	-2.511449	H	4.559705	-3.194100	2.668485
				H	0.823081	0.801118	0.043218

Table S8: XYZ coordinates of the optimized geometry for **[1·H]$^+$**, protonation at one NHI N atom obtained at the B3LYP/6-31G(d,p)/SMD(DCM) level of theory.

Atom	X	Y	Z	Atom	X	Y	Z
N	1.701925	1.475713	0.245074	H	-1.721842	1.111232	-2.729822
N	-1.054279	1.675959	-0.170475	H	-0.842406	0.203657	-3.951476
N	-3.199122	0.707927	-0.412670	C	-3.481601	-0.772757	-3.487707
N	-2.388596	-1.405550	-1.326479	H	-3.996423	0.081283	-3.038524
N	-3.749928	-1.371757	0.485385	H	-4.146719	-1.641762	-3.444590
N	3.600472	0.124287	0.586075	H	-3.301812	-0.542817	-4.543094
N	3.111028	-1.975584	-0.435334	C	-1.432266	-2.239294	-3.443416
N	2.055018	-1.481027	1.478602	H	-0.493724	-2.476714	-2.930702
C	1.137571	2.703078	0.070048	H	-1.192504	-1.968162	-4.475072
C	-0.296453	2.801188	-0.180935	H	-2.048686	-3.140562	-3.480483
C	-2.362962	1.765327	-0.473953	C	-5.624317	0.054117	1.292303
C	-2.967978	3.031668	-0.797971	H	-6.312846	-0.477289	0.626450
H	-4.025122	3.054037	-1.041324	H	-5.268470	0.947378	0.780464
C	-2.211983	4.167257	-0.777545	H	-6.181437	0.358165	2.184643
H	-2.652709	5.134371	-1.006887	C	-5.062361	-2.067564	2.459168
C	-0.827837	4.093970	-0.458425	H	-5.776638	-2.619936	1.840663
C	-0.006455	5.259820	-0.425828	H	-5.601885	-1.690724	3.332649
H	-0.469316	6.222466	-0.628369	H	-4.297848	-2.761978	2.819822
C	1.328123	5.171233	-0.152088	C	-3.485940	-0.135659	2.648591
H	1.959099	6.055180	-0.127024	H	-2.686201	-0.807767	2.975500
C	1.923406	3.894501	0.084638	H	-4.021050	0.207638	3.540377
C	3.314872	3.759956	0.317602	H	-3.035372	0.732864	2.166104
H	3.936393	4.650870	0.344362	C	5.507174	-2.165987	-1.089869
C	3.869474	2.518443	0.503656	H	5.577597	-3.123057	-0.563639
H	4.930702	2.384183	0.687763	H	5.854364	-1.378349	-0.412710
C	3.000629	1.400819	0.443014	H	6.196947	-2.193173	-1.938958
C	-3.067126	-0.591128	-0.418870	C	3.961837	-0.585560	-2.358928
C	-2.806671	-2.800367	-1.075358	H	4.415292	0.257728	-1.836491
H	-1.977196	-3.497648	-1.195138	H	2.917062	-0.344204	-2.574062
H	-3.610271	-3.090845	-1.764675	H	4.488911	-0.688964	-3.311678
C	-3.321060	-2.764722	0.355164	C	3.697419	-3.046280	-2.580195
H	-4.140905	-3.466935	0.505533	H	3.795952	-4.039964	-2.135547
H	-2.525449	-3.000214	1.076087	H	4.383045	-2.998569	-3.429897
C	-2.143237	-1.044901	-2.774994	H	2.679449	-2.924515	-2.962342
C	-4.460436	-0.866324	1.706783	C	2.549939	0.217180	3.321110
C	2.931400	-1.072928	0.550504	H	3.629803	0.092799	3.218542
C	2.393574	-3.214207	-0.057955	H	2.332303	0.380199	4.380435
H	3.089575	-3.934963	0.388390	H	2.232573	1.109219	2.783544
H	1.909578	-3.666719	-0.919530	C	0.262755	-0.765813	2.995612
C	1.374790	-2.682061	0.943214	H	-0.318116	-1.676309	2.821158
H	0.447774	-2.372379	0.448681	H	-0.044874	-0.010054	2.268273
H	1.143627	-3.398458	1.727067	H	0.023576	-0.406369	4.000753
C	4.073408	-1.921486	-1.598772	C	2.191065	-2.184235	3.835699
C	1.772692	-1.034272	2.893749	H	1.636095	-3.107782	3.655101
C	-1.212022	0.168646	-2.921607	H	1.992085	-1.883705	4.868462
H	4.561707	0.086205	0.274672	H	3.261159	-2.395094	3.742084
H	-0.356997	0.096793	-2.245423				

Table S9: XYZ coordinates of the optimized geometry for **[1·2H]$^+$**, protonation at both phenanthroline N atoms (**I**) obtained at the B3LYP/6-31G(d,p)/(SMD)Dichloromethane level of theory.

Atom	X	Y	Z	Atom	X	Y	Z
N	-1.459727	1.581893	0.043862	H	3.306767	1.213597	2.209296
N	1.457295	1.576767	-0.119675	H	3.058143	0.603402	3.836694
N	3.522758	0.415018	-0.245831	C	5.077504	-0.828234	2.419085
N	3.062144	-1.497287	1.112640	H	5.399634	-0.104718	1.665254
N	3.090762	-1.745843	-1.124300	H	5.554758	-1.790855	2.208993
N	-3.529620	0.423991	0.157934	H	5.431462	-0.483045	3.395549
N	-2.803295	-1.592650	1.226212	C	3.125393	-1.969374	3.529200
N	-3.285082	-1.644155	-0.972978	H	2.039868	-2.112977	3.546094
C	-0.709727	2.753469	-0.018193	H	3.427426	-1.572518	4.501653
C	0.706769	2.750316	-0.122497	H	3.607181	-2.942604	3.409433
C	2.827659	1.518486	-0.258145	C	4.308907	-0.612729	-2.992000
C	3.508501	2.781604	-0.413885	H	5.220076	-1.151017	-2.712933
H	4.584842	2.746457	-0.527939	H	4.335048	0.372995	-2.528958
C	2.819405	3.948381	-0.395118	H	4.311242	-0.480398	-4.078091
H	3.343167	4.893937	-0.497861	C	3.093591	-2.747008	-3.381884
C	1.390834	3.980132	-0.246287	H	3.999202	-3.322697	-3.169721
C	0.679752	5.202244	-0.223915	H	3.091755	-2.509210	-4.448657
H	1.236225	6.129008	-0.317825	H	2.219595	-3.373063	-3.181938
C	-0.686070	5.206531	-0.080159	C	1.765392	-0.672346	-2.945644
H	-1.244073	6.136687	-0.051318	H	0.885919	-1.258328	-2.656282
C	-1.395992	3.987696	0.019837	H	1.715670	-0.508290	-4.026431
C	-2.826240	3.962504	0.151041	H	1.710745	0.304434	-2.460733
H	-3.351958	4.911632	0.193053	C	-4.549796	-1.076434	2.930861
C	-3.516474	2.797724	0.216129	H	-5.061519	-2.020917	2.719710
H	-4.594829	2.768583	0.311395	H	-4.998866	-0.289856	2.318543
C	-2.833695	1.528306	0.141338	H	-4.721668	-0.828878	3.983026
C	3.185846	-0.874191	-0.093780	C	-2.322571	0.124875	3.005967
C	3.082443	-2.957231	0.877988	H	-2.836981	0.999466	2.609100
H	2.369598	-3.474675	1.517927	H	-1.291171	0.119797	2.639558
H	4.087316	-3.350384	1.072866	H	-2.290167	0.235680	4.093615
C	2.715214	-3.071191	-0.598863	C	-2.436710	-2.293235	3.560349
H	3.264703	-3.870296	-1.092615	H	-2.935222	-3.257599	3.437749
H	1.640876	-3.243400	-0.740395	H	-2.560043	-1.992812	4.603900
C	3.545050	-0.962709	2.442502	H	-1.365569	-2.422528	3.371950
C	3.062113	-1.423771	-2.596580	C	-4.940254	-0.459047	-2.415113
C	-3.173082	-0.869491	0.129208	H	-5.736855	-1.108698	-2.038965
C	-2.862500	-3.026023	0.865237	H	-5.174623	-0.197935	-3.451486
H	-3.807568	-3.458465	1.214533	H	-4.933742	0.457010	-1.824553
H	-2.035505	-3.583219	1.302826	C	-2.450552	-0.300724	-2.910852
C	-2.794418	-2.998519	-0.658691	H	-1.488888	-0.823630	-2.862266
H	-1.767208	-3.120134	-1.024608	H	-2.369429	0.638484	-2.361329
H	-3.418802	-3.769156	-1.106697	H	-2.642058	-0.052827	-3.959327
C	-3.038820	-1.193414	2.666949	C	-3.694823	-2.435727	-3.278877
C	-3.587373	-1.191542	-2.380086	H	-2.758799	-3.000115	-3.325018
C	2.886414	0.385690	2.778608	H	-3.928158	-2.101341	-4.292967
H	1.804463	0.350801	2.617019	H	-4.498465	-3.103762	-2.956781
H	1.001964	0.694551	0.072788	H	-0.992273	0.689574	-0.044285

Table S10: XYZ coordinates of the optimized geometry for **[1·2H]$^+$**, protonation at one phenanthroline N atom and adjacent NHI N atom (**II**) obtained at the B3LYP/6-31G(d,p)/SMD(DCM) level of theory.

Atom	X	Y	Z	Atom	X	Y	Z
N	1.661834	1.465488	-0.270666	H	-2.991421	1.689856	-1.875226
N	-1.006421	1.681188	0.232037	H	-3.103552	1.180073	-3.555082
N	-3.144213	0.736706	0.585980	C	-5.153864	0.048478	-1.928514
N	-3.145174	-1.090536	-0.973378	H	-5.221449	0.747896	-1.091457
N	-3.041217	-1.530593	1.235498	H	-5.783777	-0.820182	-1.709520
N	3.462675	-0.021071	-0.672547	H	-5.558717	0.540348	-2.818846
N	2.131338	-1.947581	-1.198447	C	-3.640577	-1.345419	-3.376252
N	2.960974	-1.776994	0.885771	H	-2.617059	-1.680504	-3.574796
C	1.118432	2.724275	-0.120177	H	-3.998116	-0.819822	-4.265756
C	-0.279760	2.825073	0.165790	H	-4.277218	-2.222667	-3.238463
C	-2.329625	1.784517	0.502459	C	-3.799497	-0.393443	3.325081
C	-2.928444	3.084506	0.742232	H	-4.814089	-0.767981	3.154625
H	-3.988042	3.115274	0.972255	H	-3.732459	0.614543	2.918179
C	-2.184420	4.221452	0.661522	H	-3.632263	-0.345081	4.405795
H	-2.635135	5.196215	0.826563	C	-2.903633	-2.710597	3.400999
C	-0.793074	4.135536	0.352490	H	-3.909096	-3.126141	3.284221
C	0.050060	5.276098	0.231935	H	-2.724910	-2.566307	4.470002
H	-0.389452	6.258541	0.380065	H	-2.175198	-3.443048	3.041432
C	1.382793	5.153292	-0.069303	C	-1.328825	-0.829760	2.906543
H	2.023459	6.023172	-0.167790	H	-0.603470	-1.544194	2.498789
C	1.946404	3.858032	-0.251378	H	-1.123718	-0.717332	3.976072
C	3.313196	3.629867	-0.564427	H	-1.170502	0.136876	2.424235
H	3.975888	4.482116	-0.681016	C	3.444655	-2.388487	-3.255718
C	3.813916	2.360100	-0.712378	H	3.619769	-3.416066	-2.922109
H	4.858309	2.181624	-0.941602	H	4.286585	-1.765625	-2.937030
C	2.956468	1.245671	-0.544801	H	3.420257	-2.388003	-4.349580
C	-3.054271	-0.544776	0.290500	C	1.868180	-0.406939	-3.196630
C	-3.439116	-2.530065	-0.828691	H	2.738032	0.235962	-3.065189
H	-2.927820	-3.126200	-1.583591	H	1.004492	0.041309	-2.696938
H	-4.519359	-2.707406	-0.912316	H	1.650669	-0.442033	-4.267388
C	-2.942595	-2.839525	0.578049	C	0.942834	-2.715585	-3.217925
H	-3.558174	-3.592125	1.069091	H	1.080184	-3.776642	-2.996940
H	-1.902013	-3.192100	0.570234	H	0.886197	-2.613213	-4.304212
C	-3.695022	-0.372823	-2.182299	H	-0.010510	-2.382240	-2.796386
C	-2.764447	-1.346981	2.700250	C	4.912008	-0.494975	1.853988
C	2.847748	-1.233172	-0.325541	H	5.566286	-1.101977	1.220434
C	1.754574	-3.223309	-0.542147	H	5.427145	-0.337653	2.805251
H	2.346438	-4.034231	-0.976500	H	4.773930	0.486194	1.400453
H	0.697131	-3.436607	-0.688175	C	2.581527	-0.284410	2.835503
C	2.100881	-2.983738	0.932411	H	1.645650	-0.806090	3.053772
H	1.215822	-2.762537	1.538309	H	2.359325	0.592112	2.222823
H	2.631301	-3.826600	1.369429	H	3.001456	0.064431	3.783523
C	2.109957	-1.846586	-2.718202	C	3.900215	-2.414553	3.070311
C	3.589138	-1.219758	2.151116	H	2.999316	-2.942786	3.391403
C	-2.834301	0.848396	-2.547556	H	4.392033	-2.030392	3.967038
H	-1.770347	0.593662	-2.547466	H	4.580340	-3.124850	2.590177
H	0.974758	0.713001	-0.175659	H	4.455435	-0.073175	-0.880322

Table S11: XYZ coordinates of the optimized geometry for **[1·2H]$^+$**, protonation at one phenanthroline N atom and opposite NHI N atom (**III**) obtained at the B3LYP/6-31G(d,p)/SMD(DCM) level of theory.

Atom	X	Y	Z	Atom	X	Y	Z
N	-1.123204	1.709437	0.125073	C	4.431128	-1.731928	2.681866
N	1.633653	1.452093	-0.105335	H	5.117101	-1.234571	1.989544
N	3.557710	0.099210	-0.211796	H	4.495158	-2.813433	2.525719
N	2.511073	-1.604802	1.110337	H	4.767597	-1.520148	3.701338
N	2.768990	-1.977845	-1.094083	C	2.052993	-1.890687	3.518894
N	-3.261923	0.672586	0.246188	H	1.019566	-1.555414	3.387366
N	-2.784492	-1.518306	1.072406	H	2.372962	-1.600984	4.522904
N	-3.239351	-1.264475	-1.117591	H	2.082713	-2.981188	3.469480
C	-0.327707	2.839431	0.076246	C	4.092377	-0.871583	-2.957165
C	1.090274	2.704755	-0.065154	H	4.997557	-1.251667	-2.471465
C	2.944266	1.357302	-0.221743	H	3.970773	0.188625	-2.730582
C	3.814234	2.480302	-0.345158	H	4.242883	-0.949500	-4.037078
H	4.883628	2.326202	-0.447270	C	2.994478	-3.076147	-3.287733
C	3.268273	3.734432	-0.311153	H	3.894903	-3.605813	-2.961326
H	3.899084	4.614816	-0.391322	H	3.078651	-2.897781	-4.362406
C	1.865621	3.894614	-0.152574	H	2.126971	-3.720975	-3.130300
C	1.245382	5.173691	-0.077197	C	1.561648	-1.015450	-3.028720
H	1.868224	6.060582	-0.142883	H	0.688892	-1.641808	-2.819029
C	-0.110524	5.276057	0.084884	H	1.593471	-0.832609	-4.107051
H	-0.592958	6.245906	0.154336	H	1.437698	-0.056354	-2.518507
C	-0.920637	4.108090	0.162983	C	-4.466569	-0.977038	2.831305
C	-2.343311	4.165227	0.334406	H	-5.084848	-1.828764	2.529307
H	-2.816856	5.138659	0.421935	H	-4.816340	-0.085621	2.304242
C	-3.094756	3.034875	0.383885	H	-4.613719	-0.818163	3.904241
H	-4.170252	3.063890	0.509049	C	-2.109893	-0.064201	3.008959
C	-2.492366	1.729183	0.247785	H	-2.513195	0.899610	2.701080
C	2.932038	-1.131287	-0.071807	H	-1.085818	-0.157576	2.633591
C	2.003408	-2.982931	0.908955	H	-2.069395	-0.065319	4.102234
H	0.988919	-3.079881	1.295823	C	-2.522211	-2.495731	3.320290
H	2.649105	-3.688305	1.436381	H	-3.134786	-3.373951	3.102707
C	2.072886	-3.190042	-0.609954	H	-2.613699	-2.290152	4.389955
H	2.626941	-4.088389	-0.881109	H	-1.474570	-2.737629	3.113507
H	1.078948	-3.238517	-1.062372	C	-4.757896	0.267248	-2.378093
C	2.992973	-1.216102	2.503395	H	-5.618751	-0.305311	-2.018651
C	2.857298	-1.712840	-2.585319	H	-4.990880	0.637002	-3.381203
C	-3.048598	-0.633892	0.066022	H	-4.616842	1.126018	-1.722371
C	-3.017909	-2.883006	0.556389	C	-2.278860	0.164702	-2.932548
H	-4.013455	-3.231189	0.858045	H	-1.399519	-0.483149	-3.009144
H	-2.271788	-3.584677	0.926827	H	-2.041433	0.997542	-2.268783
C	-2.927911	-2.695395	-0.956162	H	-2.475370	0.579478	-3.926130
H	-1.920155	-2.909333	-1.333598	C	-3.794822	-1.745907	-3.477492
H	-3.639422	-3.326696	-1.484520	H	-2.947980	-2.426390	-3.603083
C	-2.978553	-1.245958	2.545771	H	-3.987829	-1.277498	-4.446081
C	-3.508646	-0.629190	-2.457925	H	-4.680891	-2.328018	-3.207868
C	2.930107	0.297531	2.748465	H	-0.632030	0.821738	0.061445
H	1.950110	0.703738	2.488018	H	4.468414	0.064502	-0.652754
H	3.701243	0.844737	2.207985	H	3.094788	0.469692	3.815809

Table S12: XYZ coordinates of the optimized geometry for **1** obtained at the B3LYP/6-31G(d,p)/SMD(ACN) level of theory.

Atom	X	Y	Z	Atom	X	Y	Z
N	-1.408325	1.540231	0.138070	H	3.018615	1.495649	2.111097
N	1.354359	1.565819	-0.150850	H	2.705224	1.007314	3.771967
N	3.398875	0.417720	-0.392658	C	4.765255	-0.524491	2.542514
N	2.796125	-1.300333	1.214210	H	5.117957	0.126928	1.737961
N	3.210463	-1.857515	-0.939491	H	5.251721	-1.500408	2.439245
N	-3.416246	0.348493	0.458761	H	5.083235	-0.090282	3.496183
N	-2.923043	-1.914852	0.908262	C	2.767245	-1.561679	3.670534
N	-3.111125	-1.332966	-1.252406	H	1.681315	-1.701696	3.655445
C	-0.761755	2.735563	0.099631	H	3.030440	-1.075364	4.613832
C	0.689901	2.748890	-0.073810	H	3.247322	-2.543032	3.665308
C	2.693527	1.567102	-0.277954	C	4.503395	-0.920348	-2.856869
C	3.430589	2.798955	-0.376211	H	5.407772	-1.412688	-2.482763
H	4.508173	2.755230	-0.499971	H	4.487384	0.101882	-2.481641
C	2.763890	3.989224	-0.298481	H	4.558250	-0.895528	-3.950275
H	3.303398	4.931953	-0.357394	C	3.350903	-3.109392	-3.061168
C	1.350996	4.010479	-0.130961	H	4.239668	-3.645100	-2.712454
C	0.624830	5.234502	-0.015777	H	3.433047	-2.995359	-4.145862
H	1.173694	6.171697	-0.068475	H	2.468766	-3.723901	-2.860927
C	-0.729806	5.220905	0.168867	C	1.963446	-1.027001	-2.934408
H	-1.290692	6.146957	0.269859	H	1.085028	-1.619184	-2.657562
C	-1.437876	3.982741	0.235474	H	1.984114	-0.945241	-4.026435
C	-2.843809	3.932139	0.449700	H	1.847086	-0.025175	-2.516280
H	-3.394292	4.863228	0.565308	C	-4.642146	-1.613096	2.688226
C	-3.488885	2.729243	0.513299	H	-5.266397	-2.400362	2.251183
H	-4.558578	2.663421	0.685788	H	-4.963152	-0.649290	2.286648
C	-2.740012	1.511995	0.337423	H	-4.812026	-1.611081	3.770273
C	3.107606	-0.814757	-0.048584	C	-2.271324	-0.779541	3.034686
C	2.841799	-2.775155	1.161169	H	-2.594049	0.224159	2.763370
H	2.049544	-3.225070	1.759698	H	-1.226040	-0.902804	2.733052
H	3.810306	-3.141894	1.525738	H	-2.325813	-0.875839	4.124146
C	2.678355	-3.075973	-0.320493	C	-2.737479	-3.220179	2.989215
H	3.233417	-3.966019	-0.616417	H	-3.352606	-4.046865	2.622828
H	1.621837	-3.215863	-0.587712	H	-2.865097	-3.171600	4.074320
C	3.231298	-0.657243	2.510811	H	-1.686031	-3.446555	2.783868
C	3.249704	-1.707376	-2.431644	C	-4.287093	0.544053	-2.434803
C	-3.114434	-0.863586	0.042122	H	-5.231719	0.143740	-2.053224
C	-2.998422	-3.179850	0.168148	H	-4.468893	0.933415	-3.441495
H	-4.008900	-3.609229	0.225354	H	-3.987037	1.381856	-1.808671
H	-2.284575	-3.913486	0.540408	C	-1.848615	0.025458	-2.920174
C	-2.663970	-2.734369	-1.250457	H	-1.122911	-0.774774	-3.098316
H	-1.585019	-2.798684	-1.448225	H	-1.458542	0.673051	-2.131861
H	-3.190984	-3.332558	-1.990914	H	-1.937709	0.607775	-3.843883
C	-3.152030	-1.864485	2.387768	C	-3.676330	-1.530006	-3.642114
C	-3.217956	-0.561388	-2.531870	H	-2.932870	-2.301276	-3.859802
C	2.572456	0.715201	2.725391	H	-3.828074	-0.956739	-4.560889
H	1.501424	0.675008	2.511772	H	-4.623856	-2.015700	-3.385683

Table S13: optimized geometry for **[1·H]$^+$**, protonation at one phenanthroline N atom obtained at the B3LYP/6-31G(d,p)/SMD(ACN) level of theory.

Atom	X	Y	Z	Atom	X	Y	Z
N	-1.382569	1.629948	0.098454	H	3.209044	0.968565	3.578473
N	1.328250	1.565787	-0.290839	C	5.000941	-0.714878	2.147439
N	3.352362	0.375598	-0.537475	H	5.302489	-0.086526	1.305005
N	2.846713	-1.350893	1.060635	H	5.401753	-1.722446	1.993870
N	2.849151	-1.857154	-1.135434	H	5.454826	-0.307716	3.056900
N	-3.386724	0.394428	0.421397	C	3.077592	-1.612437	3.502197
N	-2.451381	-1.645759	1.259791	H	1.990039	-1.673353	3.614624
N	-3.192781	-1.590111	-0.862415	H	3.483698	-1.151251	4.406534
C	-0.696536	2.822375	-0.030678	H	3.481780	-2.625878	3.442517
C	0.717948	2.780097	-0.254785	C	3.961046	-0.958380	-3.183238
C	2.662923	1.522133	-0.492650	H	4.872592	-1.507895	-2.924918
C	3.413777	2.743333	-0.701291	H	4.053512	0.058299	-2.804016
H	4.481074	2.660771	-0.879206	H	3.885286	-0.920425	-4.274709
C	2.790841	3.954557	-0.655410	C	2.659808	-3.071695	-3.275067
H	3.352166	4.874641	-0.797455	H	3.552834	-3.663667	-3.051496
C	1.385308	4.025214	-0.414804	H	2.609089	-2.938906	-4.359332
C	0.669557	5.251630	-0.331740	H	1.775436	-3.638448	-2.970957
H	1.216989	6.181933	-0.457711	C	1.428477	-0.914766	-2.952714
C	-0.682243	5.263966	-0.090568	H	0.556294	-1.459300	-2.575393
H	-1.231667	6.197554	-0.017123	H	1.320643	-0.816849	-4.038028
C	-1.390270	4.038630	0.065171	H	1.423584	0.085361	-2.514818
C	-2.798389	3.969438	0.325801	C	-3.950635	-1.233324	3.207782
H	-3.356294	4.897436	0.416390	H	-4.490274	-2.165489	3.010212
C	-3.439781	2.776441	0.458733	H	-4.473172	-0.413784	2.707512
H	-4.503596	2.716599	0.655311	H	-3.978287	-1.048732	4.286475
C	-2.729158	1.526866	0.325603	C	-1.722641	-0.035625	3.044980
C	2.985710	-0.855667	-0.217704	H	-2.259295	0.856520	2.724771
C	2.779706	-2.823542	0.982554	H	-0.733573	-0.045115	2.576706
H	2.057274	-3.232350	1.688597	H	-1.583299	0.039459	4.127705
H	3.764516	-3.259756	1.192954	C	-1.782866	-2.479115	3.481369
C	2.369428	-3.072488	-0.463362	H	-2.300528	-3.435104	3.369651
H	2.830545	-3.973003	-0.867053	H	-1.767031	-2.236558	4.547162
H	1.279564	-3.159954	-0.564253	H	-0.747366	-2.596919	3.146327
C	3.468210	-0.740282	2.293453	C	-5.019075	-0.351317	-2.032323
C	2.722162	-1.679256	-2.620922	H	-5.756885	-1.017047	-1.572716
C	-2.979771	-0.873346	0.268342	H	-5.387464	-0.067269	-3.022965
C	-2.474195	-3.053367	0.812723	H	-4.940548	0.549549	-1.424532
H	-3.345020	-3.567200	1.237894	C	-2.611541	-0.147972	-2.822724
H	-1.570038	-3.582286	1.110414	H	-1.652894	-0.665602	-2.928006
C	-2.588804	-2.925012	-0.703241	H	-2.453290	0.757700	-2.234425
H	-1.606251	-2.954202	-1.189805	H	-2.941492	0.157052	-3.821032
H	-3.215592	-3.706300	-1.128484	C	-3.888725	-2.275891	-3.129155
C	-2.489199	-1.332328	2.735659	H	-2.963842	-2.824845	-3.327050
C	-3.668818	-1.072810	-2.194102	H	-4.259945	-1.898582	-4.085698
C	2.931064	0.675528	2.561193	H	-4.635433	-2.969401	-2.730792
H	1.840560	0.704035	2.484979	H	-0.803030	0.796325	0.021134
H	3.348261	1.417197	1.881928				

Table S14: optimized geometry for **[1·2H]$^+$**, protonation at both phenanthroline N atoms (**I**) obtained at the B3LYP/6-31G(d,p)/SMD(ACN) level of theory.

Atom	X	Y	Z	Atom	X	Y	Z
N	-1.468698	1.573833	0.069847	H	3.017806	0.586204	3.819121
N	1.443217	1.582905	-0.127982	C	5.041019	-0.820463	2.387143
N	3.513722	0.428896	-0.271807	H	5.358811	-0.088092	1.639986
N	3.030382	-1.487315	1.074766	H	5.523063	-1.778506	2.166841
N	3.072835	-1.726600	-1.161975	H	5.392994	-0.482450	3.366999
N	-3.529262	0.404527	0.244895	C	3.098721	-1.984849	3.486642
N	-2.721490	-1.639893	1.193939	H	2.014179	-2.133776	3.505123
N	-3.286912	-1.610290	-0.983722	H	3.402400	-1.595059	4.461657
C	-0.725549	2.748481	0.018866	H	3.585784	-2.954028	3.354756
C	0.690092	2.752523	-0.108576	C	4.256771	-0.559896	-3.031897
C	2.811767	1.529739	-0.273540	H	5.180088	-1.079888	-2.757147
C	3.486642	2.797149	-0.424795	H	4.265357	0.426989	-2.570715
H	4.562191	2.767884	-0.549111	H	4.250381	-0.429211	-4.118339
C	2.794046	3.961651	-0.388198	C	3.077482	-2.713064	-3.423077
H	3.313515	4.910183	-0.486420	H	3.988462	-3.279802	-3.208503
C	1.367502	3.986788	-0.221360	H	3.077253	-2.468701	-4.488535
C	0.652875	5.206143	-0.165130	H	2.209442	-3.349242	-3.229963
H	1.205398	6.136055	-0.252299	C	1.715589	-0.664410	-2.964725
C	-0.709562	5.202851	0.007752	H	0.851437	-1.268869	-2.669629
H	-1.270029	6.130080	0.068709	H	1.654599	-0.494059	-4.044210
C	-1.413502	3.979500	0.099524	H	1.647078	0.306727	-2.469878
C	-2.838899	3.946235	0.274179	C	-4.402276	-1.242106	2.988900
H	-3.366154	4.892392	0.351475	H	-4.901162	-2.187052	2.750227
C	-3.521386	2.777097	0.342916	H	-4.892779	-0.437155	2.434754
H	-4.595616	2.741905	0.476834	H	-4.535378	-1.049866	4.058271
C	-2.836802	1.512193	0.218492	C	-2.200550	0.008148	3.025721
C	3.167426	-0.860958	-0.126482	H	-2.738506	0.885697	2.669137
C	3.016828	-2.945980	0.834001	H	-1.177341	0.031596	2.638569
H	2.285469	-3.447500	1.465606	H	-2.148568	0.081771	4.116028
H	4.010186	-3.364776	1.034269	C	-2.237854	-2.432927	3.476721
C	2.657638	-3.044021	-0.645582	H	-2.719069	-3.402816	3.329491
H	3.190108	-3.854947	-1.138696	H	-2.325163	-2.180809	4.536761
H	1.580160	-3.183276	-0.795666	H	-1.173196	-2.526350	3.238648
C	3.509151	-0.964499	2.409315	C	-4.957517	-0.327996	-2.329561
C	3.027644	-1.394567	-2.630338	H	-5.757374	-0.950704	-1.916155
C	-3.148275	-0.881064	0.146609	H	-5.230601	-0.059497	-3.354648
C	-2.731036	-3.055912	0.768370	H	-4.893533	0.587753	-1.742663
H	-3.639768	-3.548263	1.134282	C	-2.484208	-0.239813	-2.912385
H	-1.860490	-3.590422	1.145193	H	-1.539071	-0.792632	-2.905952
C	-2.725032	-2.954402	-0.753945	H	-2.353979	0.681290	-2.341238
H	-1.708584	-3.009872	-1.162362	H	-2.703232	0.040474	-3.947524
H	-3.333477	-3.730093	-1.214211	C	-3.821473	-2.322604	-3.284771
C	-2.901180	-1.310342	2.658055	H	-2.905938	-2.909700	-3.397006
C	-3.630053	-1.106066	-2.361500	H	-4.102090	-1.955346	-4.275390
C	2.840154	0.375259	2.760433	H	-4.623109	-2.977562	-2.930726
H	1.758001	0.329183	2.604688	H	-0.998987	0.686206	-0.054996
H	3.248030	1.211652	2.194023	H	0.987276	0.696905	0.048148

Table S15: optimized geometry for **[1·2H]**$^{+}$, protonation at one phenanthroline N atom and opposite NHI N atom (**III**) obtained at the B3LYP/6-31G(d,p)/SMD(ACN) level of theory.

Atom	X	Y	Z	Atom	X	Y	Z
N	-1.468698	1.573833	0.069847	H	3.017806	0.586204	3.819121
N	1.443217	1.582905	-0.127982	C	5.041019	-0.820463	2.387143
N	3.513722	0.428896	-0.271807	H	5.358811	-0.088092	1.639986
N	3.030382	-1.487315	1.074766	H	5.523063	-1.778506	2.166841
N	3.072835	-1.726600	-1.161975	H	5.392994	-0.482450	3.366999
N	-3.529262	0.404527	0.244895	C	3.098721	-1.984849	3.486642
N	-2.721490	-1.639893	1.193939	H	2.014179	-2.133776	3.505123
N	-3.286912	-1.610290	-0.983722	H	3.402400	-1.595059	4.461657
C	-0.725549	2.748481	0.018866	H	3.585784	-2.954028	3.354756
C	0.690092	2.752523	-0.108576	C	4.256771	-0.559896	-3.031897
C	2.811767	1.529739	-0.273540	H	5.180088	-1.079888	-2.757147
C	3.486642	2.797149	-0.424795	H	4.265357	0.426989	-2.570715
H	4.562191	2.767884	-0.549111	H	4.250381	-0.429211	-4.118339
C	2.794046	3.961651	-0.388198	C	3.077482	-2.713064	-3.423077
H	3.313515	4.910183	-0.486420	H	3.988462	-3.279802	-3.208503
C	1.367502	3.986788	-0.221360	H	3.077253	-2.468701	-4.488535
C	0.652875	5.206143	-0.165130	H	2.209442	-3.349242	-3.229963
H	1.205398	6.136055	-0.252299	C	1.715589	-0.664410	-2.964725
C	-0.709562	5.202851	0.007752	H	0.851437	-1.268869	-2.669629
H	-1.270029	6.130080	0.068709	H	1.654599	-0.494059	-4.044210
C	-1.413502	3.979500	0.099524	H	1.647078	0.306727	-2.469878
C	-2.838899	3.946235	0.274179	C	-4.402276	-1.242106	2.988900
H	-3.366154	4.892392	0.351475	H	-4.901162	-2.187052	2.750227
C	-3.521386	2.777097	0.342916	H	-4.892779	-0.437155	2.434754
H	-4.595616	2.741905	0.476834	H	-4.535378	-1.049866	4.058271
C	-2.836802	1.512193	0.218492	C	-2.200550	0.008148	3.025721
C	3.167426	-0.860958	-0.126482	H	-2.738506	0.885697	2.669137
C	3.016828	-2.945980	0.834001	H	-1.177341	0.031596	2.638569
H	2.285469	-3.447500	1.465606	H	-2.148568	0.081771	4.116028
H	4.010186	-3.364776	1.034269	C	-2.237854	-2.432927	3.476721
C	2.657638	-3.044021	-0.645582	H	-2.719069	-3.402816	3.329491
H	3.190108	-3.854947	-1.138696	H	-2.325163	-2.180809	4.536761
H	1.580160	-3.183276	-0.795666	H	-1.173196	-2.526350	3.238648
C	3.509151	-0.964499	2.409315	C	-4.957517	-0.327996	-2.329561
C	3.027644	-1.394567	-2.630338	H	-5.757374	-0.950704	-1.916155
C	-3.148275	-0.881064	0.146609	H	-5.230601	-0.059497	-3.354648
C	-2.731036	-3.055912	0.768370	H	-4.893533	0.587753	-1.742663
H	-3.639768	-3.548263	1.134282	C	-2.484208	-0.239813	-2.912385
H	-1.860490	-3.590422	1.145193	H	-1.539071	-0.792632	-2.905952
C	-2.725032	-2.954402	-0.753945	H	-2.353979	0.681290	-2.341238
H	-1.708584	-3.009872	-1.162362	H	-2.703232	0.040474	-3.947524
H	-3.333477	-3.730093	-1.214211	C	-3.821473	-2.322604	-3.284771
C	-2.901180	-1.310342	2.658055	H	-2.905938	-2.909700	-3.397006
C	-3.630053	-1.106066	-2.361500	H	-4.102090	-1.955346	-4.275390
C	2.840154	0.375259	2.760433	H	-4.623109	-2.977562	-2.930726
H	1.758001	0.329183	2.604688	H	-0.998987	0.686206	-0.054996
H	3.248030	1.211652	2.194023	H	0.987276	0.696905	0.048148

Table S16: Optimized geometry for 1,10-phenanthroline, obtained at the B3LYP/6-31G(d,p)/SMD(ACN) level of theory.

Atom	X	Y	Z
C	0.371198	3.485441	0.000000
C	-0.842623	2.829932	0.000000
C	-0.869600	1.416511	0.000000
C	1.549156	2.711764	0.000000
N	1.565327	1.385491	0.000000
C	0.378512	0.729236	0.000000
C	-2.102113	0.680823	0.000000
C	-2.102113	-0.680823	0.000000
C	-0.869600	-1.416511	0.000000
C	0.378512	-0.729236	0.000000
N	1.565327	-1.385491	0.000000
C	1.549156	-2.711764	0.000000
C	-0.842623	-2.829932	0.000000
C	0.371198	-3.485441	0.000000
H	0.431265	-4.568978	0.000000
H	2.519031	-3.207538	0.000000
H	-1.779731	-3.380313	0.000000
H	-3.035028	1.237980	0.000000
H	-3.035028	-1.237980	0.000000
H	0.431265	4.568979	0.000000
H	-1.779731	3.380313	0.000000
H	2.519031	3.207538	0.000000

Table S17: Optimized geometry for the protonated 1,10-phenanthroline, obtained at the B3LYP/6-31G(d,p)/SMD(ACN) level of theory.

Atom	X	Y	Z
C	-3.468103	-0.356023	0.000000
C	-2.810256	0.864606	0.000000
C	-1.398554	0.924287	0.000000
C	-2.720577	-1.533639	0.000000
N	-1.385784	-1.466197	0.000000
C	-0.689617	-0.297797	0.000000
C	-0.651847	2.150056	0.000000
C	0.712389	2.133466	0.000000
C	1.444166	0.897334	0.000000
C	0.746276	-0.336953	0.000000
N	1.346711	-1.549179	0.000000
C	2.671865	-1.574151	0.000000
C	2.857071	0.827634	0.000000
C	3.469984	-0.408847	0.000000
H	4.550868	-0.499901	0.000000
H	3.141737	-2.554966	0.000000
H	3.439141	1.744475	0.000000
H	-1.200632	3.086099	0.000000
H	1.274266	3.062649	0.000000
H	-4.549411	-0.415554	0.000001
H	-3.376636	1.790901	0.000000
H	-3.157454	-2.524330	0.000000
H	-0.825151	-2.321568	0.000000

Table S18: Optimized geometry for pyridine, obtained at the B3LYP/6-31G(d,p)/SMD(ACN) level of theory.

Atom	X	Y	Z
N	0.000001	1.420870	0.000000
C	-1.145888	0.721964	0.000000
C	-1.199860	-0.672703	0.000000
C	-0.000001	-1.385053	0.000000
C	1.199859	-0.672703	0.000000
C	1.145889	0.721962	0.000000
H	-2.158194	-1.182500	0.000000
H	-2.065629	1.304754	0.000000
H	2.158192	-1.182503	0.000000
H	-0.000001	-2.471398	0.000000
H	2.065630	1.304753	0.000000

Table S19: Optimized geometry for the protonated pyridine, obtained at the B3LYP/6-31G(d,p)/SMD(ACN) level of theory.

Atom	X	Y	Z
C	0.667197	1.187620	0.000000
C	-0.716555	1.210414	0.000000
C	-1.414922	-0.000005	0.000000
C	-0.716547	-1.210419	0.000000
C	0.667205	-1.187615	0.000000
N	1.306015	0.000004	0.000000
H	-1.233051	2.162508	0.000000
H	1.290436	2.072736	0.000000
H	-1.233035	-2.162517	0.000000
H	-2.500009	-0.000008	0.000000
H	1.290450	-2.072727	0.000000
H	2.324839	0.000008	0.000000

X-ray Diffraction Studies

General information: Single-crystal X-ray diffraction data were collected on a Bruker D8 quest Photon III diffractometer using Mo-K_α radiation (λ = 0.71073 Å). Crystals were selected under oil, mounted on nylon loops and then immediately placed in a cold stream of N_2 on a diffractometer. Using Olex2[27], the structures were solved with the Olex2.solve[28] or ShelXT[29] using iterative or dual methods. The refinement was done with ShelXL[29] or Olex2.refine[28] using full matrix least squares minimization on F^2.

Crystallographic data have been deposited with the Cambridge Crystallographic Data Centre as supplementary publication no. CCDC-2420826 (**1**), CCDC-2420827 (**1**·HBF_4), CCDC-2420828 (**1**·$2HBF_4$), CCDC-2420829 (**2**). These data can be obtained free of charge via https://www.ccdc.cam.ac.uk/structures (or from the CCDC, 12 Union Road, Cambridge CB2 1EZ, UK; fax: (+44) 1223-336-033; or deposit@ccdc.cam.ac.uk).

Single-crystal X-ray structure analysis of 1:

Yellow single crystals of **1** were obtained by letting a saturated, hot solution of **1** in THF cool down to ambient temperature. The single-crystal X-ray structure analysis revealed that **1** crystallizes in the monoclinic space group $P2_1/c$. The asymmetric unit contains one molecule of **1** and one THF molecule. The THF molecule was heavily disordered. Therefore, a solvent mask was used. 172 electrons were found in a volume of 672 Å^3 in **1** void per unit cell. This is consistent with the presence of one THF molecule per asymmetric unit.

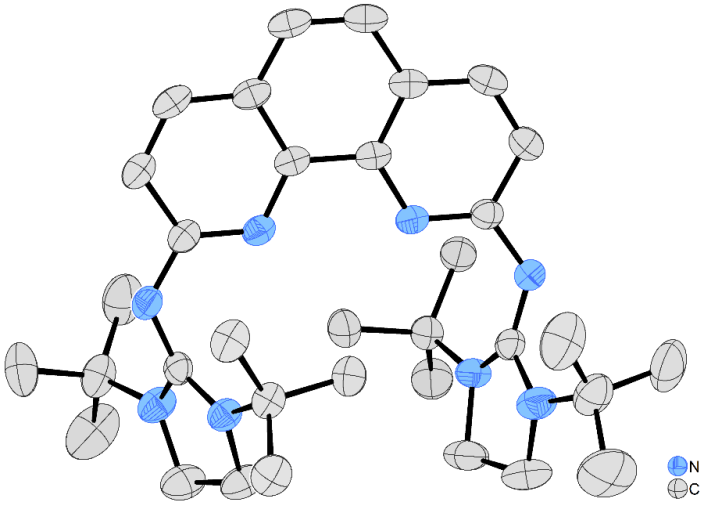

Figure S106: Molecular view of **1** in the solid state with thermal ellipsoid plot at the 50% levels of probability. Hydrogen atoms are omitted for clarity.

Identification code	**2420826**	ρ_{calc}g/cm^3	1.159
Empirical formula	$C_{38}H_{58}N_8O$	μ/mm^{-1}	0.072
Formula weight	642.92	F(000)	1400.0
Temperature/K	173.0	Crystal size/mm^3	0.22 × 0.18 × 0.14
Crystal system	monoclinic	Radiation	MoKα (λ = 0.71073)
Space group	$P2_1/c$	2Θ range for data collection/°	4.138 to 52
a/Å	13.3249(4)	Index ranges	$-16 \le h \le 16$, $-23 \le k \le 23$, $-19 \le l \le 17$
b/Å	18.7866(6)	Reflections collected	64589
c/Å	15.5032(4)	Independent reflections	7233 [R_{int} = 0.0448, R_{sigma} = 0.0218]
α/°	90	Data/restraints/parameters	7233/0/392
β/°	108.3370(10)	Goodness-of-fit on F^2	1.056
γ/°	90	Final R indexes [I>=2σ (I)]	R_1 = 0.0410, wR_2 = 0.1091
Volume/Å^3	3683.85(19)	Final R indexes [all data]	R_1 = 0.0502, wR_2 = 0.1157
Z	4	Largest diff. peak/hole / e Å^{-3}	0.21/–0.20

Single-crystal X-ray structure analysis of 1·HBF_4:

Yellow single crystals of **1**·HBF_4 were obtained by diffusion of Et_2O in a solution of **1**·HBF_4 in DCM/*n*-hexane. The single-crystal X-ray structure analysis revealed that **1**·HBF_4 crystallizes in the monoclinic space group *C*2/*c*. The asymmetric unit contains half of the cation [**1**H]$^+$ and half of the BF_4^- anion. The BF_4^- anion is located on an inversion center showing a disorder over two positions (occupancy 0.25 : 0.25). The cation [**1**H]$^+$ is located on a 2-fold axis showing a disorder over two positions (occupancy 0.92 : 0.08). Due to the location on a 2-fold axis it is not possible to assign the N–H proton to a certain N atom of the phenanthroline unit.

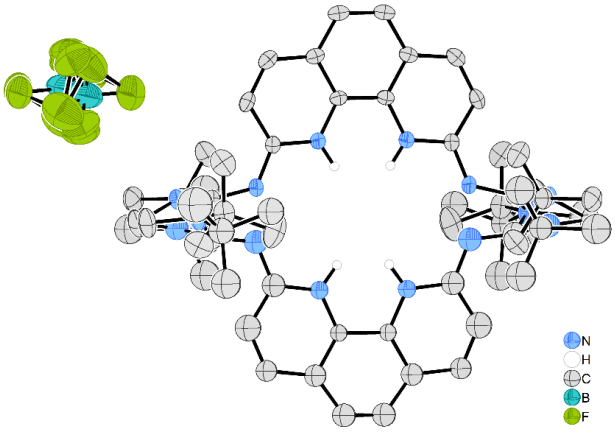

Figure S107: Molecular view of **1**·HBF_4 in the solid state with thermal ellipsoid plot at the 50% levels of probability. Hydrogen atoms are omitted for clarity, except for the phenanthroline N–H protons.

Identification code	**2420827**	ρ_{calc}g/cm^3	1.228
Empirical formula	$C_{34}H_{51}BF_4N_8$	μ/mm^{-1}	0.089
Formula weight	658.63	*F*(000)	1408.0
Temperature/K	150.0	Crystal size/mm^3	0.382 × 0.123 × 0.05
Crystal system	monoclinic	Radiation	MoKα (λ = 0.71073)
Space group	*C*2/*c*	2Θ range for data collection/°	4.882 to 50.778
a/Å	28.9228(12)	Index ranges	$-34 \le h \le 34$, $-8 \le k \le 8$, $-20 \le l \le 20$
b/Å	7.3839(3)	Reflections collected	31038
c/Å	16.6880(7)	Independent reflections	3244 [R_{int} = 0.0459, R_{sigma} = 0.0348]
α/°	90	Data/restraints/parameters	3244/181/365
β/°	90.118(2)	Goodness-of-fit on F^2	1.095
γ/°	90	Final *R* indexes [I>=2σ (I)]	R_1 = 0.0556, wR_2 = 0.1442
Volume/Å^3	3563.9(3)	Final *R* indexes [all data]	R_1 = 0.0680, wR_2 = 0.1529
Z	4	Largest diff. peak/hole / e Å^{-3}	0.23/–0.20

Single-crystal X-ray structure analysis of 1·2HBF_4:

Yellow single crystals of **1**·2HBF$_4$ were obtained by diffusion of Et$_2$O in a MeCN solution of **1**·2HBF$_4$. The single-crystal X-ray structure analysis revealed that **1**·2HBF$_4$ crystallizes in the monoclinic space group $P2_1/c$. The asymmetric unit contains one molecule of the cation [**1**·2H]$^{2+}$, two BF$_4^-$ anions and three MeCN solvent molecules. One *tert*-butyl group is disordered over two positions (occupancy 0.81 : 0.19) and the fluoride atoms of one BF$_4^-$ anions are disordered over two positions (occupancy 0.41 : 0.59)

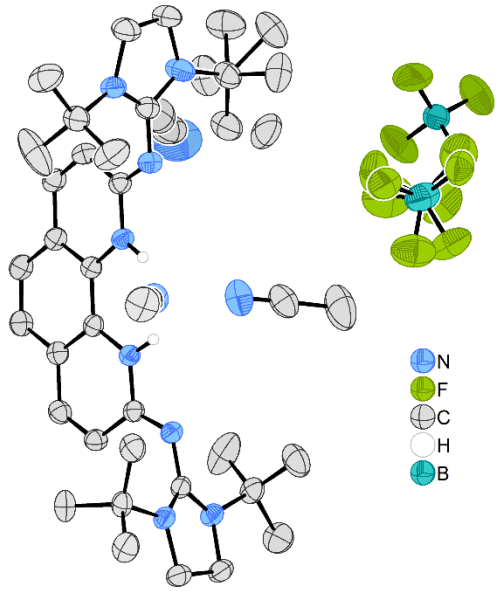

Figure S108: Molecular view of **1**·2HBF$_4$ in the solid state with thermal ellipsoid plot at the 50% levels of probability. Hydrogen atoms are omitted for clarity, except for the phenanthroline N–H protons.

Identification code	**2420828**	ρ_{calc}g/cm^3	1.264
Empirical formula	$C_{40}H_{61}B_2N_{11}F_8$	μ/mm^{-1}	0.100
Formula weight	869.61	F(000)	1840.0
Temperature/K	153.0	Crystal size/mm^3	0.23 × 0.14 × 0.13
Crystal system	monoclinic	Radiation	MoKα (λ = 0.71073)
Space group	$P2_1/c$	2Θ range for data collection/°	4.402 to 56.574
a/Å	17.2435(10)	Index ranges	$-22 \le h \le 22$, $-29 \le k \le 29$, $-16 \le l \le 14$
b/Å	21.9344(13)	Reflections collected	129169
c/Å	12.0847(6)	Independent reflections	11333 [R_{int} = 0.0481, R_{sigma} = 0.0222]
α/°	90	Data/restraints/parameters	11333/102/641
β/°	91.033(2)	Goodness-of-fit on F^2	1.032
γ/°	90	Final R indexes [I>=2σ (I)]	R_1 = 0.0558, wR_2 = 0.1508
Volume/Å^3	4570.0(4)	Final R indexes [all data]	R_1 = 0.0738, wR_2 = 0.1682
Z	4	Largest diff. peak/hole / e Å^{-3}	0.42/–0.45

Single-crystal X-ray structure analysis of 2:

Pale-yellow single crystals of **2** were obtained by diffusion of Et_2O in a MeCN solution of **2**. The single-crystal X-ray structure analysis revealed that **2** crystallizes in the monoclinic space group $P2_1/c$. The asymmetric unit contains one molecule of the cation, two triflate anions and one Et_2O solvent molecule. The latter was heavily disordered. Therefore, was a solvent mask calculated, and 232 electrons were found in a volume of 784 Å^3 in 1 void per unit cell. This is consistent with the presence of one Et_2O molecule per asymmetric unit. Further, both triflate anions are disordered over two positions (occupancy 0.75 : 0.25).

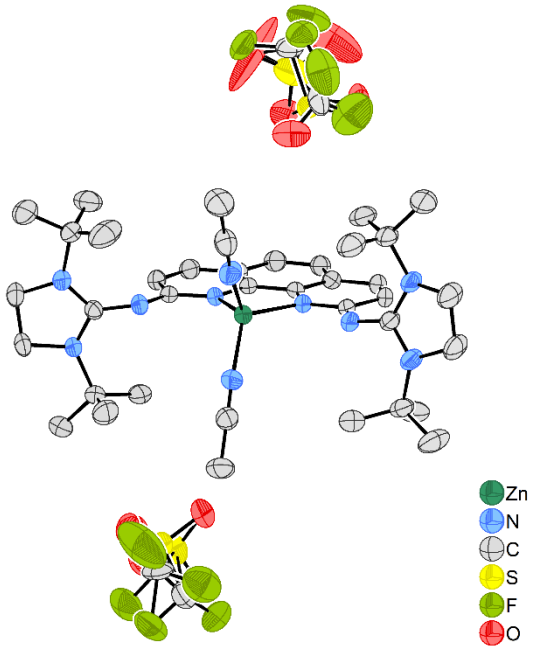

Figure S109: Molecular view of **2** in the solid state with thermal ellipsoid plot at the 50% levels of probability. Hydrogen atoms are omitted for clarity.

Identification code	**2420829**	ρ_{calc}g/cm^3	1.384
Empirical formula	$C_{44}F_6H_{66}N_{10}O_7S_2Zn$	μ/mm^{-1}	0.627
Formula weight	1090.55	F(000)	2288.0
Temperature/K	173.0	Crystal size/mm^3	0.26 × 0.18 × 0.14
Crystal system	monoclinic	Radiation	MoKα (λ = 0.71073)
Space group	$P2_1/c$	2Θ range for data collection/°	3.988 to 51.516
a/Å	17.3341(5)	Index ranges	$-19 \le h \le 21$, $-15 \le k \le 15$, $-29 \le l \le 29$
b/Å	12.3428(4)	Reflections collected	113457
c/Å	24.4948(8)	Independent reflections	9965 [R_{int} = 0.0505, R_{sigma} = 0.0264]
α/°	90	Data/restraints/parameters	9965/0/708

Table continued:

β/°	92.6004(11)	Goodness-of-fit on F^2	1.090
γ/°	90	Final R indexes [I>=2σ (I)]	R_1 = 0.0484, wR_2 = 0.1278
Volume/Å^3	5235.3(3)	Final R indexes [all data]	R_1 = 0.0583, wR_2 = 0.1343
Z	4	Largest diff. peak/hole / e Å^{-3}	0.42/–0.39

References

[1] L. F. B. Wilm; T. Eder; C. Mück-Lichtenfeld; P. Mehlmann; M. Wünsche; F. Buß; F. Dielmann. *Reversible CO2 fixation by N-heterocyclic imines forming water-stable zwitterionic nitrogen-base–CO2 adducts, Green Chem.*, **2019**, *21*, 640–648.

[2] M. D. Böhme; T. Eder; M. B. Röthel; P. D. Dutschke; L. F. B. Wilm; F. E. Hahn; F. Dielmann. *Synthesis of N-Heterocyclic Carbenes and Their Complexes by Chloronium Ion Abstraction from 2-Chloroazolium Salts Using Electron-Rich Phosphines, Angew. Chem., Int. Ed.*, **2022**, *61*, e202202190.

[3] P. Jutzi; C. Müller; A. Stammler; H.-G. Stammler. *Synthesis, Crystal Structure, and Application of the Oxonium Acid [H(OEt2)2]+ [B(C6F5)4]-, Organometallics*, **2000**, *19*, 1442–1444.

[4] M. C. Leech; D. Nagornîi; J. M. Walsh; C. Kiaku; D. L. Poole; J. Mason; I. C. A. Goodall; P. Devo; K. Lam. *eFluorination Using Cheap and Readily Available Tetrafluoroborate Salts, Organic letters*, **2023**, *25*, 1353–1358.

[5] P. Mehlmann; F. Dielmann. *Switching the Electron-Donating Ability of Phosphines through Proton-Responsive Imidazolin-2-ylidenamino Substituents, Chem. Eur. J.*, **2019**, *25*, 2352–2357.

[6] H. Shimada; T. Sakurai; Y. Kitamura; H. Matsuura; T. Ihara. *Metallo-regulation of the bimolecular triplex formation of a peptide nucleic acid, Dalton Trans.*, **2013**, *42*, 16006–16013.

[7] J. Lewis; T. D. O'Donoghue. *Chemistry of polydentate ligands. Part 5. Complexes of 2,9-di-hydrazino-derivatives of 1,10-phenanthroline. Dependence of co-ordination number of a ligand on the anion present, J. Chem. Soc., Dalton Trans.*, **1980**, 736.

[8] M. Yamada; M. Kimura; M. Nishizawa; S. Kuroda; I. Shimao. *Electronic Spectra of Phenanthrolinediones, Phenanthrolinones, Bipyridinediones, and Amino-Substituted Phenanthrolines, Bull. Chem. Soc. Jpn.*, **1991**, *64*, 1821–1827.

[9] B. Lerma-Berlanga; J. P. Cerón-Carrasco; A. Leyva-Pérez. *Diverted Telomerization Reaction with Aryl Boronic Derivatives: Expeditious Synthesis of Aryl-Substituted 1,6- and 1,7-dienes, Organometallics*, **2024**, *43*, 1827–1836.

[10] A. C. Rowett; S. G. Sweeting; D. M. Heard; A. J. J. Lennox. *A Stoichiometric Haloform Coupling for Ester Synthesis with Secondary Alcohols, Angew. Chem. Int. Ed.*, **2024**, *63*, e202400570.

[11] X. Yuan; Z. Liu; Z. Li; Y. Shi; B. Yang; X. Zou; Y. Hu; C. Li; S. Li; K. Guo. *Halide-free pyridinium base binary organocatalyst for the cycloaddition of carbon dioxide to epoxides, New J. Chem.*, **2024**, *48*, 11435–11446.

[12] F. Buß; M. B. Röthel; J. A. Werra; P. Rotering; L. F. B. Wilm; C. G. Daniliuc; P. Löwe; F. Dielmann. *Tris(tetramethylguanidinyl)phosphine: The Simplest Non-ionic Phosphorus Superbase and Strongly Donating Phosphine Ligand, Chem. Eur. J.*, **2022**, *28*, e202104021.

[13] J. R. Aranzaes; M.-C. Daniel; D. Astruc. *Metallocenes as references for the determination of redox potentials by cyclic voltammetry — Permethylated iron and cobalt sandwich complexes, inhibition by polyamine dendrimers, and the role of hydroxy-containing ferrocenes, Can. J. Chem.*, **2006**, *84*, 288–299.

[14] J. Ortmeyer; Y. Vukadinovic; A. Neuba; H. Egold; U. Flörke; G. Henkel. *Combining a Phenanthroline Moiety with Two Peralkylated Guanidine Residues: Janus Head Pro-Ligands, Eur. J. Org. Chem.*, **2017**, *2017*, 6085–6095.

[15] I. Kaljurand; A. Kütt; L. Sooväli; T. Rodima; V. Mäemets; I. Leito; I. A. Koppel. *Extension of the self-consistent spectrophotometric basicity scale in acetonitrile to a full span of 28 pKa units: unification of different basicity scales, The Journal of organic chemistry*, **2005**, *70*, 1019–1028.

[16] S. Tshepelevitsh; A. Kütt; M. Lõkov; I. Kaljurand; J. Saame; A. Heering; P. G. Plieger; R. Vianello; I. Leito. *On the Basicity of Organic Bases in Different Media, Eur. J. Org. Chem.*, **2019**, *2019*, 6735–6748.

[17] A. Kütt; S. Selberg; I. Kaljurand; S. Tshepelevitsh; A. Heering; A. Darnell; K. Kaupmees; M. Piirsalu; I. Leito. *pKa values in organic chemistry – Making maximum use of the available data, Tetrahedron Letters*, **2018**, *59*, 3738–3748.

[18] A. D. Becke. *Density-functional thermochemistry. III. The role of exact exchange, The Journal of Chemical Physics*, **1993**, *98*, 5648–5652.

[19] R. Ditchfield; W. J. Hehre; J. A. Pople. *Self-Consistent Molecular-Orbital Methods. IX. An Extended Gaussian-Type Basis for Molecular-Orbital Studies of Organic Molecules, The Journal of Chemical Physics*, **1971**, *54*, 724–728.

[20] W. J. Hehre; R. Ditchfield; J. A. Pople. *Self—Consistent Molecular Orbital Methods. XII. Further Extensions of Gaussian—Type Basis Sets for Use in Molecular Orbital Studies of Organic Molecules, The Journal of Chemical Physics*, **1972**, *56*, 2257–2261.

[21] P. C. Hariharan; J. A. Pople. *The influence of polarization functions on molecular orbital hydrogenation energies, Theoret. Chim. Acta*, **1973**, *28*, 213–222.

[22] M. J. Frisch, G. W. Trucks, H. B. Schlegel, G. E. Scuseria, M. A. Robb, J. R. Cheeseman, G. Scalmani, V. Barone, G. A. Petersson, H. Nakatsuji, X. Li, M. Caricato, A. V. Marenich, J. Bloino, B. G. Janesko, R. Gomperts, B. Mennucci, H. P. Hratchian, J. V. Ortiz, A. F. Izmaylov, J. L. Sonnenberg, D. Williams-Young, F. Ding, F. Lipparini, F. Egidi, J. Goings, B. Peng, A. Petrone, T. Henderson, D. Ranasinghe, V. G. Zakrzewski, J. Gao, N. Rega, G. Zheng, W. Liang, M. Hada, M. Ehara, K. Toyota, R. Fukuda, J. Hasegawa, M. Ishida, T. Nakajima, Y. Honda, O. Kitao, H. Nakai, T. Vreven, K. Throssell, J. A. Montgomery, Jr., J. E. Peralta, F. Ogliaro, M. J. Bearpark, J. J. Heyd, E. N. Brothers, K. N. Kudin, V. N. Staroverov, T. A. Keith, R. Kobayashi, J. Normand, K. Raghavachari, A. P. Rendell, J. C. Burant, S. S. Iyengar, J. Tomasi, M. Cossi, J. M. Millam, M. Klene, C. Adamo, R. Cammi, J. W. Ochterski, R. L. Martin, K. Morokuma, O. Farkas, J. B. Foresman and D. J. Fox. *Gaussian 16, Revision C.01*, Inc., Wallingford CT, 2016.

[23] A. V. Marenich; C. J. Cramer; D. G. Truhlar. *Universal solvation model based on solute electron density and on a continuum model of the solvent defined by the bulk dielectric*

constant and atomic surface tensions, The journal of physical chemistry. B, **2009**, *113*, 6378–6396.

[24] J. W. Ochterski. *Thermochemistry in Gaussian*, https://gaussian.com/wp-content/uploads/dl/thermo.pdf, accessed: June, 2024.

[25] J. W. Ochterski. *Vibrational Analysis in Gaussian*, https://gaussian.com/wp-content/uploads/dl/vib.pdf, accessed: June, 2024.

[26] E. Runge; E. K. U. Gross. *Density-Functional Theory for Time-Dependent Systems, Phys. Rev. Lett.*, **1984**, *52*, 997–1000.

[27] O. V. Dolomanov; L. J. Bourhis; R. J. Gildea; J. A. K. Howard; H. Puschmann. *OLEX2 : a complete structure solution, refinement and analysis program, J. Appl. Crystallogr.*, **2009**, *42*, 339–341.

[28] L. J. Bourhis; O. V. Dolomanov; R. J. Gildea; J. A. K. Howard; H. Puschmann. *The anatomy of a comprehensive constrained, restrained refinement program for the modern computing environment - Olex2 dissected, Acta crystallogr. A*, **2015**, *71*, 59–75.

[29] G. M. Sheldrick. *SHELXT - integrated space-group and crystal-structure determination, Acta crystallogr. A*, **2015**, *71*, 3–8.